

Oxide surfaces

Hans-Joachim Freund[†], Helmut Kuhlenbeck[†] and Volker Staemmler[‡]

[†] Lehrstuhl für Physikalische Chemie I, Ruhr-Universität Bochum, 44780 Bochum, Germany

[‡] Lehrstuhl für Theoretische Chemie, Ruhr-Universität Bochum, 44780 Bochum, Germany

Abstract

We review the current knowledge of the geometric and electronic structure of oxide surfaces. In particular, material published during the last five years and going beyond the latest book by Henrich and Cox, *Surface Science of Oxide Surfaces*, is documented. In addition to the discussion of effects on and in bulk oxide single crystal samples, and in fact mainly, we also refer to work on thin oxide films epitaxially grown on metallic substrates. Surface states on oxide surfaces as well as band structure effects are discussed. Reconstruction and the local electronic structure are other aspects covered. We review experimental as well as theoretical approaches. Adsorption on oxide surfaces is an important subject covered in this review, and oxide modification by metal adsorption is also mentioned.

This review was received in October 1995

Contents

	Page
1. Introduction	285
2. Oxide surface preparation	285
3. Structural characterization	289
4. Theoretical treatment of oxide surfaces	299
5. Electronic structure of oxide surfaces	311
5.1. Rock salt type structures	314
5.2. Corundum type structures	325
6. Adsorbates on oxides	329
7. Synopsis and perspectives	340
Acknowledgments	341
References	341

1. Introduction

Oxides comprise a very diverse class of compounds with properties covering almost all aspects of material science and physics [1]. Oxides can be superconductors on one hand and insulators on the other. The bonding characteristics may be classified as covalent for one system and highly ionic for the other. Oxides find applications in many fields of technical interest, from paint pigments via nonlinear optics to sensors and catalysis. In some cases the bulk properties are important, as for example very often in nonlinear optics, in other cases the surface properties play a major role, as in catalysis.

The bulk properties of simple binary oxides are pretty well understood and there are excellent reviews and books available treating the thermodynamics [2], the structure—and its non-stoichiometric aspects [3], which are particularly important for oxides—the spectroscopy [4] as well as transport [5] and mechanical properties [3]. Bulk properties of even more complicated oxides such as ternary and quaternary oxides [5] are being intensively investigated, probably partly due to their importance in high- T_c -superconductivity.

In contrast, rather little is known about the surfaces of oxides, even the most simple ones. The present knowledge has been comprehensively reviewed recently by Henrich and Cox in their book *The Surface Science of Metal Oxides* [6]. However, due to the rapid development of the field during the last few years there are experimental as well as theoretical aspects that we feel are worth reviewing and which have not been covered in the book. In particular, we feel the observation of surface states on oxide surfaces and the whole field of thin film studies is of interest for future studies on clean and modified oxide surfaces, because it opens up areas of study on the so-called polar surfaces [7]. We want to explicitly clarify at this point, however, that the present article is self-contained and the necessary concepts are introduced independently.

For us the major objective is to contribute to the understanding not only of oxide surfaces as such but rather to provide insight into how molecules interact with clean and also with modified surfaces. In other words, we view the investigation of oxide surfaces as part of a strategy which is—somewhat naively—summarized in figure 1. Figure 1 contains two ‘coordinates’. The abscissa represents schematically ‘the pressure gap’ between the ultrahigh vacuum conditions often applied in surface science studies and the ambient conditions including high temperatures and pressure in catalysis [8]. The ordinate is an oversimplified representation of the ‘materials gap’, which opens up between the well-studied metal surfaces and the metal-modified compound surface, which may eventually even be polycrystalline.

The present review concentrates on investigations under ultrahigh vacuum conditions under which the oxide surfaces are well ordered and rather well characterized. However, we point out that certain results may have consequences with respect to catalytic processes on ‘real’ samples [9, 10]. One step towards more complex systems along the coordinate named ‘complexity’ in figure 1 is taken in this review, namely the brief discussion of the influence of modifiers, such as metals, on some properties of oxide surfaces.

2. Oxide surface preparation

‘The question of oxide preparation is central to all surface-science investigations, and herein lies what is possibly the greatest difficulty of all.’ This is a quotation from the book by Henrich and Cox [6] and it is the starting point of the present discussion. Compared with elemental solids, the preparation of any stoichiometric compound surface, in particular oxides, is extremely difficult, especially if we consider the preparation of different

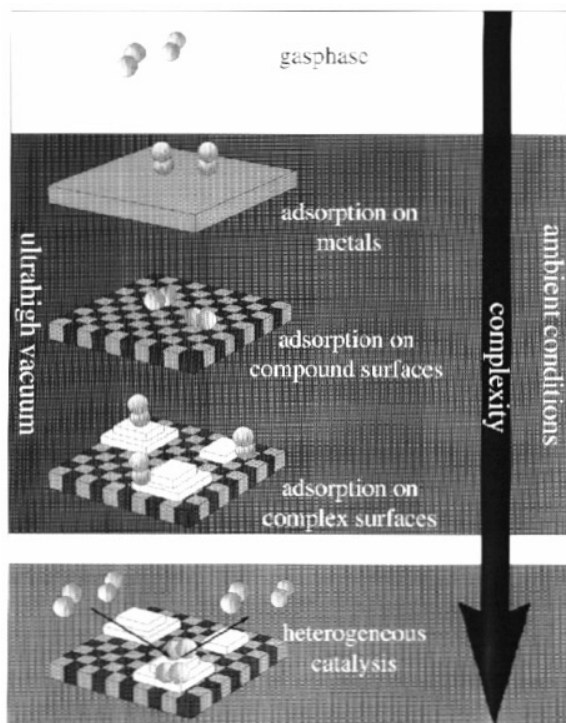


Figure 1. Schematics of adsorbate systems of different complexity illustrating the so called pressure gap.

crystallographic orientations of oxide surfaces. Figure 2 summarizes the appropriate methods of oxide surface preparation using the example of an ionic binary oxide of rock salt structure, i.e. NiO, which we shall use as the standard example throughout this review. At the top, a schematic representation of a single NiO crystal is shown. At the side of the crystal the so-called non-polar (100) surfaces are exposed, and it is cut such that it exposes the metal-ion terminated (111) surface at the front. Non-polar and polar surfaces of ionic binary oxides exhibit fundamentally different behaviour as far as cleavage, which is one of the desirable preparation methods, is concerned. The reason for this was pointed out a long time ago and is intimately connected with the surface potential [11]. Briefly, for a non-polar surface, such as the NiO(100) surface, the surface potential is finite (e.g. 1.74 J m^{-2}) [12]. Therefore, NiO may be easily cleaved along the (100) direction (see the pattern images from low-energy electron diffraction (LEED) in figure 2). In such an experiment electrons with kinetic energies of say 10–300 eV are elastically back-reflected from the sample and the diffraction pattern is recorded on a screen. However, the surface potential per unit charge diverges for a polar surface, e.g. the NiO(111) surface, according to [13]

$$V = \frac{2\pi}{S} [Nb(2\sigma - 1) + (1 - \sigma)b] \quad (1)$$

where the symbols are explained in figure 3. S corresponds to the area of the surface unit cell. N is the number of layers, separated by the distance b . The surface charge σ is measured in units of the charge on a typical bulk layer. For $N \rightarrow \infty$ the surface potential diverges so that cleavage of a rocksalt structure in this direction is not possible. Thus, if

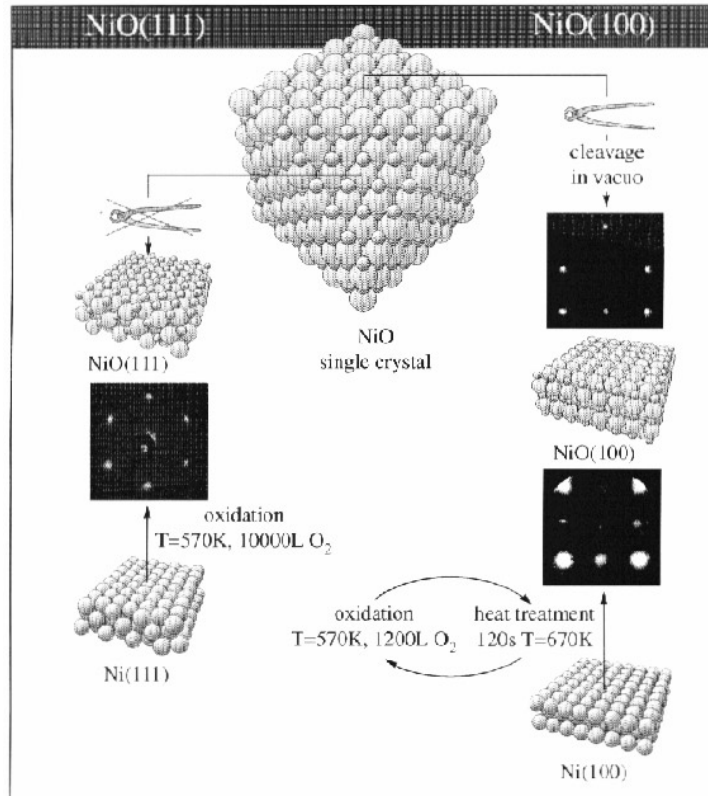


Figure 2. Methods for the preparation of NiO(100) and NiO(111) surfaces. The corresponding LEED patterns are shown.

we are interested in preparing surfaces of different surface orientation, cleavage is not the most favourable method of preparation for an ionic polar oxide surface. Table 1 [14–36] contains surfaces which have been prepared by cleavage and are well characterized.

Equation (1) shows that the surface potential for a polar surface can have a finite value for a thin film (N small) or for a single crystal provided that the surface charge is reduced; for $\sigma = \frac{1}{2}$ the first term in (1) vanishes. Such a reduction of the surface charge can be achieved in different ways: reduction of the number of ions in the topmost layer, reduction of the charge of each ion in the topmost layer (e.g. from Ni^{2+} to Ni^+), geometric reconstruction or adsorption of charged species, for instance OH^- . Consequently, there are alternative methods of preparation of stable polar surfaces. One is to cut a crystallographic plane mechanically or by spark erosion and then polish the surface [6]. This technique is similar to procedures known for the preparation of metal surfaces. Once the sample resides in the vacuum chamber, these surfaces are sputtered and consecutively annealed in oxygen in order to replace oxygen vacancies induced via sputtering. This method has been successfully applied to bulk samples. TiO_2 is an example where this method has been frequently used with apparently satisfactory results. Again, of course, preparation of polar surfaces is difficult, because these surfaces have the tendency to facet in the preparation process.

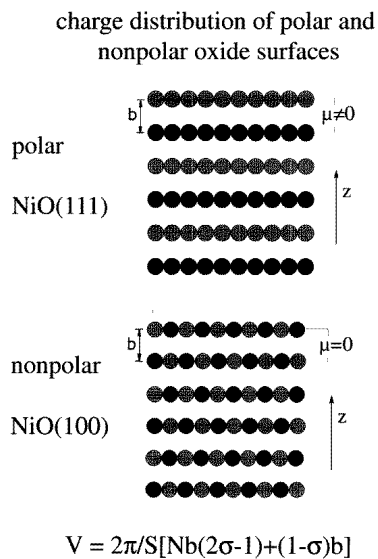


Figure 3. Charge distribution in polar oxide surfaces (cut perpendicular to the surface).

Table 1. Binary oxide surfaces prepared via cleavage.

Oxide	Orientation	Quality	References
MgO	(100)	+	[14–19]
CaO	(100)	+	[16, 20]
NiO	(100)	+	[16, 21–23]
CoO	(100)	+	[16, 24]
MnO	(100)	+	[16, 25]
EuO	(100)	+	[16, 26, 27]
TiO ₂	(100)	–	[28]
TiO ₂	(001)	–	[28]
TiO ₂	(110)	±	[28, 29, 30]
SnO ₂	(110)	±	[31]
SnO ₂	(100)	±	[31]
Ti ₂ O ₃	(10 $\bar{1}$ 2)	+	[32, 33]
V ₂ O ₃	(10 $\bar{1}$ 2)	+	[34]
V ₂ O ₅	(001)	+	[35]
ZnO	(0001)	+	[36]
ZnO	(000 $\bar{1}$)	+	[36]

Another, rather different method of preparation is also represented in figure 2. Oxide films of varying thickness may be grown on metallic substrates [37]. The geometry of the metallic substrate then determines to a large extent the structure of the oxide film. It is this technique that allows preparation of non-polar as well as polar surfaces, and we shall come back to the stabilization mechanisms for the polar surfaces later in this review [8]. We note, of course, that the structural quality of the film depends very strongly on the epitaxial relation between the lattice constants of the metallic substrate and the oxide film. In other words, we can to a certain extent control the defect structure and defect density of the layers grown by controlling the lattice mismatch. Three techniques have been mainly

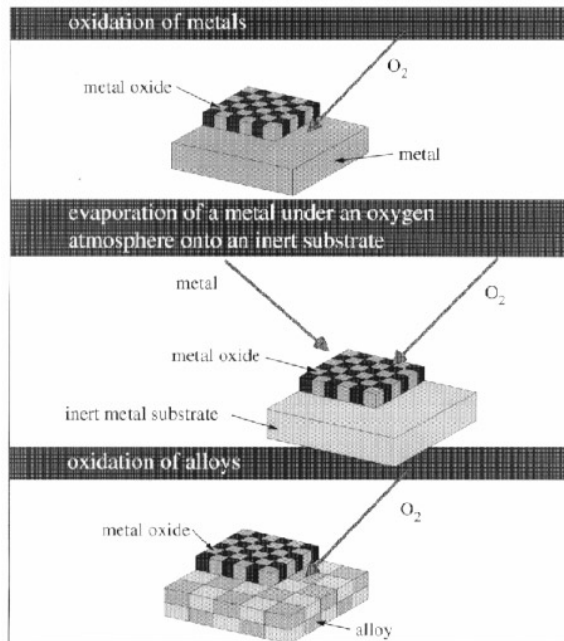


Figure 4. Different methods for the preparation of thin epitaxial oxide films.

used for this purpose [7] and are schematically summarized in figure 4. The one indicated at the top is the most simple one and makes use of the fact that a metal single crystal may be oxidized and a more or less well ordered oxide film is formed. Of course, if there is a large lattice mismatch between metal and oxide lattice constants, the film may be defect rich. An example is again shown in figure 2 for the system NiO(100)/Ni(100) in form of a LEED pattern showing rather wide spots. Less strained layers may be grown by choosing inert metal substrates, onto which the metal to be oxidized is evaporated. The oxidation may be done after or during deposition. If the lattice constants of the inert substrates are chosen properly, the grown structure may exhibit long-range order of high quality. In the preparation of the metal substrate, molecular beam epitaxy methods may be used including buffer layer techniques, etc. The third technique indicated in figure 4 is the oxidation of alloy surfaces. This technique, of course, bears the same inherent difficulties as the top one in figure 4. The advantage here is that the physical properties of the alloy may be advantageous for the preparation process. We have used this technique to grow a well ordered Al_2O_3 film on NiAl(110) [39]. The Al_2O_3 film can be heated to above $1000^\circ C$ without melting the substrate. This is of crucial importance to order the layer. On Al metal such a heat treatment would lead to a melting of the substrate before the oxide layer could order; one of the reasons why Al_2O_3 overlayers on Al are often amorphous.

3. Structural characterization

A very comprehensive collection of structural information from LEED, reflection high-energy electron diffraction (RHEED), He scattering and ion scattering spectroscopy (ISS) on bulk oxide materials can be found in [6]. Scanning tunnelling microscopy (STM) and atomic force microscopy (AFM) studies on oxide surfaces under ultrahigh vacuum (UHV) conditions,

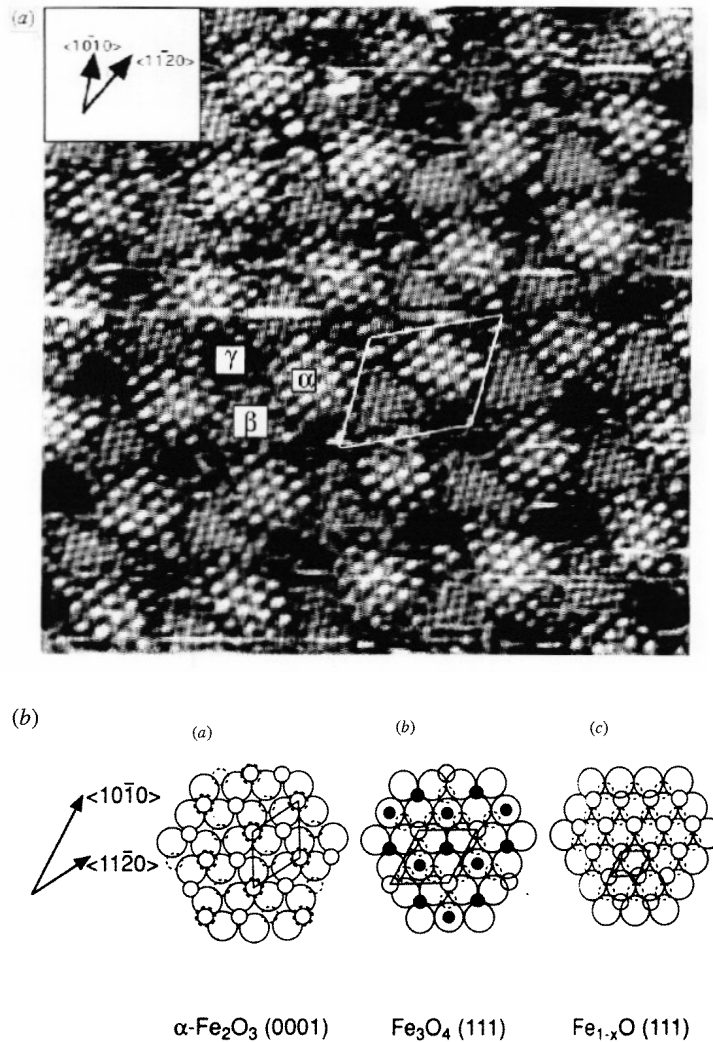


Figure 5. (a) STM topograph of an $\alpha\text{-Fe}_2\text{O}_3$ (0001) surface [59]. (b) Surface structures of different iron oxides. Iron ions are depicted as small circles and oxygen ions are shown as large circles. Reproduced from [58].

yielding atomically resolved information, are only starting to be published in the literature. For TiO_2 surfaces [40–44] in various orientations ((110), (100), (001)) STM studies under UHV conditions have been reported, and interesting novel information on reconstructions and surface steps were deduced. Most of this information is collected in [6], see also [45]. Under ambient conditions a series of oxide surfaces have been studied by STM and AFM techniques [45–58]. A particularly interesting example that demonstrates the possibilities of UHV–STM in revealing the real-space topology of an oxide surface is shown in figure 5(a). Thornton and his group have recently presented this atomically resolved STM study of an annealed $\alpha\text{-Fe}_2\text{O}_3$ (0001) surface [59]. It has been known for quite some time that a sputtered $\alpha\text{-Fe}_2\text{O}_3$ (0001) surface annealed at about 1100 K reveals a complex LEED pattern

that has been interpreted as multiple scattering across a $\text{Fe}_3\text{O}_4/\text{FeO}/\text{Fe}_2\text{O}_3$ interface [60–62]. Upon annealing at temperatures slightly below this value the surface appears to stabilize to another structure, namely $\text{Fe}_3\text{O}_4(111)$. Figure 5(a) clearly reveals the coexistence of ordered domains of $\alpha\text{-Fe}_2\text{O}_3$ and $\beta\text{-FeO}$ structures as seen by the spacings of the protrusions in comparison with the schematic drawings in figure 5(b). The areas in between exhibit an atomic arrangement compatible with a $\gamma\text{-Fe}_3\text{O}_4$ structure. In total this structure gives rise to a rather complicated LEED pattern. If the observed surface compositions are compared with the bulk phases predicted on the basis of the Fe–O phase diagram, it turns out that the surface structures are different from the predicted bulk phases [61, 62]. This has to be expected for many oxide surfaces.

In the following we shall not further discuss structures observed on bulk single crystals, but rather consider structures on thin oxide films, because this preparation technique allows us to deliberately stabilize structures not easily observable on bulk single crystals. Again we shall discuss the case of NiO as an example of a simple rocksalt structure in somewhat more detail [38, 63–75].

NiO(100) may be formed on a Ni(100) substrate via oxidation [76, 77]. Figure 6(a) shows a SPA-LEED pattern of the film [64]. Here a LEED system with special electron optics to allow spot profile analysis (SPA) has been used. The (0, 0) spot of the oxide does not coincide with the (0, 0) spot of the Ni-substrate indicating the growth of tilted terraces, which eventually cover the metal substrate completely. In figure 6(b) the situation is schematically plotted (cf figure 3), and in figure 6(c) an STM picture revealing this film morphology is shown for comparison. The tilt is compatible with the large misfit of lattice constants of 18% ($a(\text{NiO}) = 4.16 \text{ \AA}$, $a(\text{Ni}) = 3.52 \text{ \AA}$) [78]. If a NiO(100) film is grown on a Ag(100) substrate, the film quality improves as seen in the STM topographs of figure 7 [79]. A growing film shows very nice square epitaxial NiO(100) islands. Here the misfit is much smaller, namely 3% ($a(\text{NiO}) = 4.16 \text{ \AA}$ against $a(\text{Ag}) = 4.09 \text{ \AA}$) [78] and thus the film growth leads to smoother morphologies.

The growth of a polar NiO(111) surface on a Au(111) substrate is shown in figure 8 [80, 81]. Thin films with high-quality LEED patterns may be grown, which even show atomic resolution in STM. Two situations may be distinguished. In one situation three domains of a NiO(100) surface grow. For slightly different preparation conditions, on the other hand, a hexagonal structure corresponding to a $p(1 \times 1)$ NiO(111) surface can be clearly seen (figure 8). Upon heat treatment, this surface undergoes a reconstruction from the $p(1 \times 1)$ structure to a $p(2 \times 2)$ structure, as is revealed by LEED. Concomitantly, the STM shows the formation of small NiO pyramids, the tips of which form the $p(2 \times 2)$ superstructure. Figure 9 shows schematically what happens: A very thin (e.g. 4 layers) NiO(111) film has a finite but rather high surface energy (4.5 J m^{-2}) [12, 82], as deduced from (1). The surface may reconstruct according to the proposal by Lacmann [11] via the formation of an octopolar structure as plotted in figure 9. This reduces the surface energy to 4.28 J m^{-2} [12, 82]. Very similar structural changes are found for a much thicker NiO(111) film grown on top of a Ni(111) metallic substrate, but here chemical reactivity and stabilization by chemical processes play a more important role, as further discussed below in this paper [8, 70].

As a second example we would like to refer to an x-ray photoelectron diffraction (XPD) study of a thin FeO(111) film grown on Pt(111) [83]. In such an experiment the intensity variations of a core-electron ionization is recorded as a function of photon energy, thus probing internuclear scattering. In the case of FeO/Pt(111) the internuclear distances in the film have been determined by Fadley's group [83]. Table 2 summarizes the observed orientation of some thin films. Weiß and others [61, 62] also investigated the structure of a somewhat thicker iron oxide film. The LEED patterns are shown in figure 10(a).

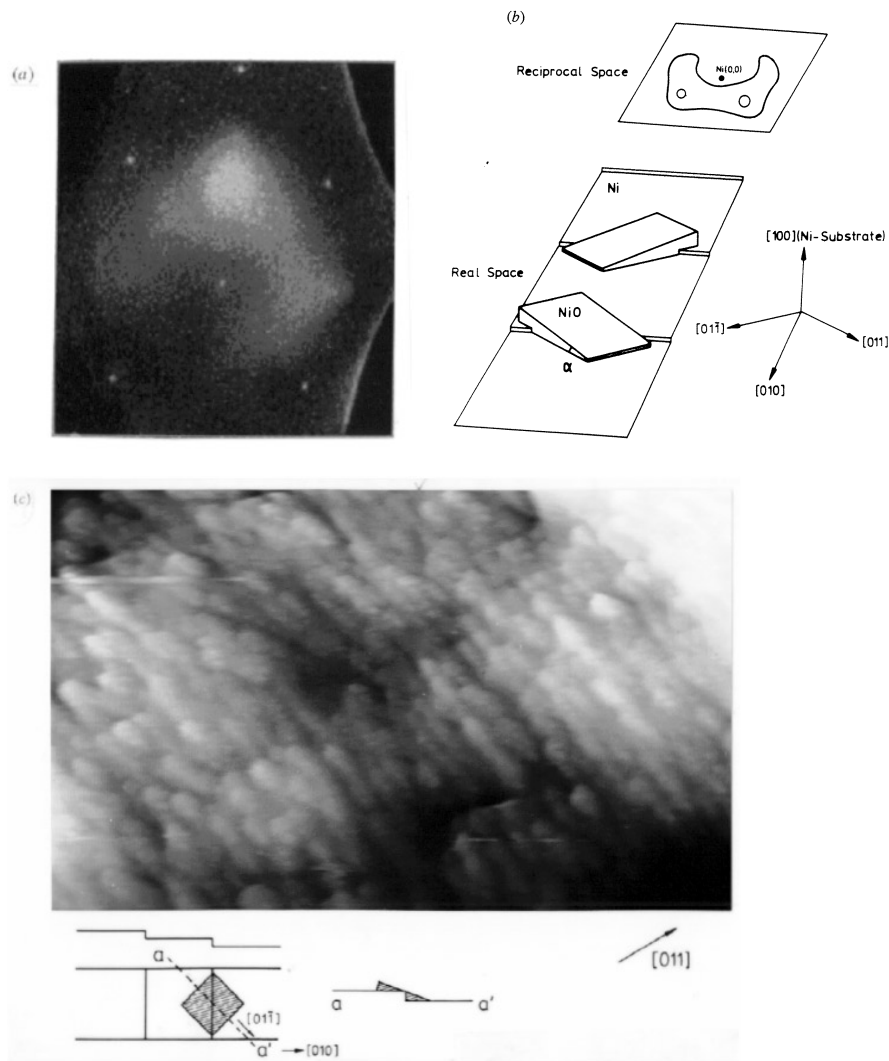


Figure 6. (a) SPA-LEED pattern of an NiO(100) film epitaxially grown on Ni(100). (b) Schematic diagram showing the experimentally found possible arrangements of the tilted NiO(100) crystallites relative to the steps on the Ni(100) substrate. (c) STM topograph of a thin NiO(100) film epitaxially grown on Ni(100). The formation of crystallites with sizes of 50–100 Å is clearly visible.

They found strong indications on the basis of a LEED analysis [61] and of XPS data [84] that oxidation of iron deposited on top of a Pt(111) single crystal surface does lead to a Fe_3O_4 surface layer rather than a reconstructed FeO surface. The $\text{Fe}_3\text{O}_4(111)$ surface and the reconstructed FeO(111) surface would lead to the same LEED pattern, since the reconstruction results in a unit mesh of twice the size of the bulk truncated FeO(111) surface [60]. One argument put forward by Weiß and others [61, 62, 84] favouring the spinell surface, i.e. $\text{Fe}_3\text{O}_4(111)$, is the instability expected for FeO under the chosen circumstances (UHV, room temperature) based on the bulk phase diagram [85]. Support for the argument is found in experiments where a Fe_2O_3 crystal surface reconstructs and leads to the same



Figure 7. STM topograph of $\frac{2}{3}$ ML of Ni on Ag(100) evaporated in an O_2 atmosphere without annealing. This procedure leads to the formation of NiO(100) on the Ag(100) substrate. $U = 1$ V, $I = 0.5$ nA, 10×17 nm².

Table 2. Parameters of some oxide films on different metallic substrates [84].

Ordered Film	Substrate	Film orientation
FeO (monolayer)		
Fe ₃ O ₄ (multilayer)	Pt(111)	(111)
FeO (monolayer)	Pt(100)	(111)
V ₂ O ₃	Au(111)	(0001)
ZrO ₂	Pt(111)	(111)

$p(2 \times 2)$ pattern which has very recently also been identified to be a Fe₃O₄ surface [60, 62] (see also figure 5(a)). Furthermore Weiß *et al* performed LEED intensity calculations for several FeO(111) reconstructed surfaces and for an unreconstructed Fe₃O₄(111) surface [61]. Best agreement with experimental data was achieved for the Fe₃O₄ surface [61, 62].

A technique which will prove very important for oxide structure determination in the near future, is x-ray scattering [86]. We would like to mention a series of such studies that have recently been published by Zabel and his group on Cr₂O₃(0001) films grown on a system of buffer layers prepared via molecular beam epitaxy (MBE) methods [87]. The same film grown on a bulk Cr(110) metal substrate exhibits similar properties [88–94]. The latter system has been studied in some detail with electron scattering methods [88–90]. Detailed STM studies on these systems have not been reported yet. The x-ray and electron scattering results agree that the orientation of the hexagonal Cr₂O₃(0001) array on the Cr(110) substrate is as indicated in figure 11 [87]. X-ray scattering can be used to show that the interface between the Cr₂O₃(0001) film and the Cr(110) substrate is sharp, it can even be used to count the number of Cr layers that are necessary to form a certain number of Cr₂O₃ layers [87]. Thus the stoichiometry of the film can be secured. In other cases,

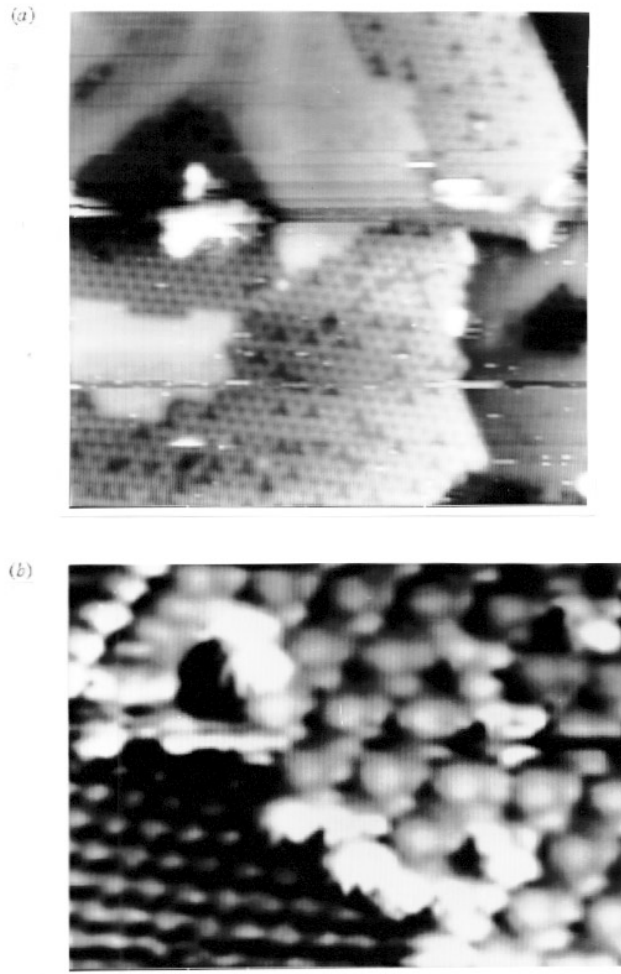


Figure 8. (a) STM image of a $p(2 \times 2)$ reconstructed surface of NiO(111) epitaxially grown on Au(111) (atomically resolved parts of the figure). $U = -5$ V, $I = 0.5$ nA, $250 \times 250 \text{ \AA}^2$. From [80]. (b) Sample as in (a). The data have been taken with a nonmetallic tip apex. $U = -0.3$ V, $I = 0.5$ nA, $35 \times 35 \text{ \AA}^2$. From [80].

and also for the Cr_2O_3 case, x-ray photoelectron spectroscopy (XPS), where electron kinetic energies are determined after the electrons have been ejected by a fixed photon energy from the core electron levels of a sample, has usually been used additionally to assure the stoichiometry within the limits of the method for quantitative analysis [88].

For the case of the $\text{Cr}_2\text{O}_3(0001)$ film grown on Cr(110) metal, the main LEED reflexes spanned a simple hexagon (figure 12(a)) at room temperature [92]. Additionally, a hexagonal diffuse patch surrounding the (0, 0) reflex is observed. Upon cooling the diffuse intensity transforms into a $(\sqrt{3} \times \sqrt{3})R30^\circ$ superstructure having its maximum intensity at ≈ 150 K (figure 12(b)). Below this temperature the superstructure vanishes again and finally a simple hexagonal LEED pattern, without any additional structure, is found (figure 12(c)). The whole temperature dependence is reversible, i.e. it can also be observed when the

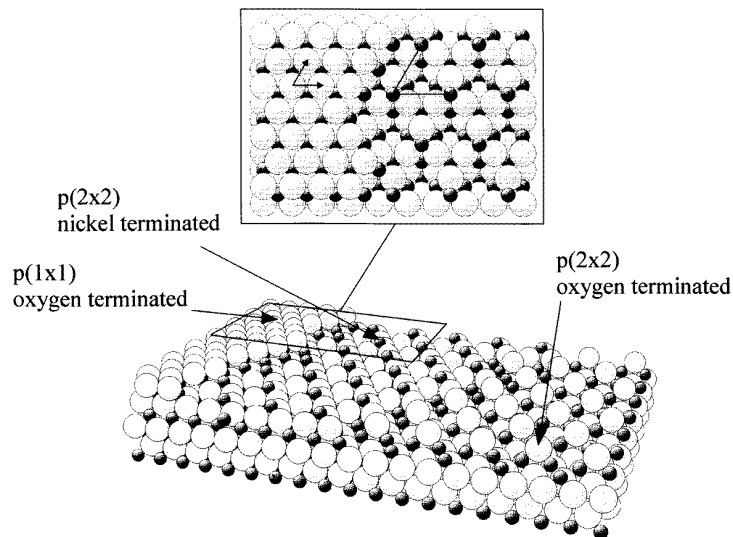


Figure 9. Schematic representation of an octopolarly reconstructed NiO(111) surface. The $p(2 \times 2)$ reconstruction involves several layers in the substrate and is shown for two possible surface terminations.

sample is warmed up starting at 90 K [92].

Figure 13 contains a plot of the intensity within an area indicated in the inset around the first-order superstructure spot as a function of temperature [92]. It is quite clear that the transition towards lower temperatures leads to a vanishing of the superstructure spot, while the transition towards higher temperatures only leads to a partial loss of intensity but an increased diffuseness of the superstructure. This is a strong indication that we are dealing with an order-to-order transition at low temperature and an order-to-disorder transition towards higher temperature.

Also, the superstructure shows a pronounced sensitivity to adsorption of various molecular species. At its maximum intensity, i.e. at ≈ 150 K, the superstructure was exposed to $5\text{--}8 \times 10^{-8}$ torr carbon dioxide, which is known to strongly chemisorb on the chromium oxide surface [90]. The superstructure was quenched immediately after the onset of exposure. It could only be recovered by flashing the sample to the temperature at which thermal desorption of the corresponding species takes place, i.e. ≈ 400 K for carbon dioxide.

From these adsorption experiments we conclude that the structural rearrangement on the clean sample takes place directly at the surface and that the interaction between the adsorbates and the substrate strongly influences the energetics of the structural rearrangement at the surface. Together with EELS experiments and the results of calculations [92], which we discuss further below, a structure model as indicated in figure 14 for the low-temperature phase has been derived. The Cr^{3+} ions occupy a site different from the one occupied in bulk Cr_2O_3 , which would correspond to site 1. At elevated temperatures the Cr^{3+} ions partially change place, which gives rise to the observed changes in the LEED pattern.

The last example of a structural investigation of an oxide film system to be mentioned in this part, refers to the preparation of Al_2O_3 on a single crystal alloy substrate [39, 95–106]. Al_2O_3 films have also been prepared on other substrates, e.g. on Ta(110) [107] and on Re(0001) [108, 109] by evaporation of aluminum in an oxygen ambient or by subsequent oxidation. Figure 15(a) shows the LEED pattern of the Al_2O_3 film on NiAl (110) [39]. In

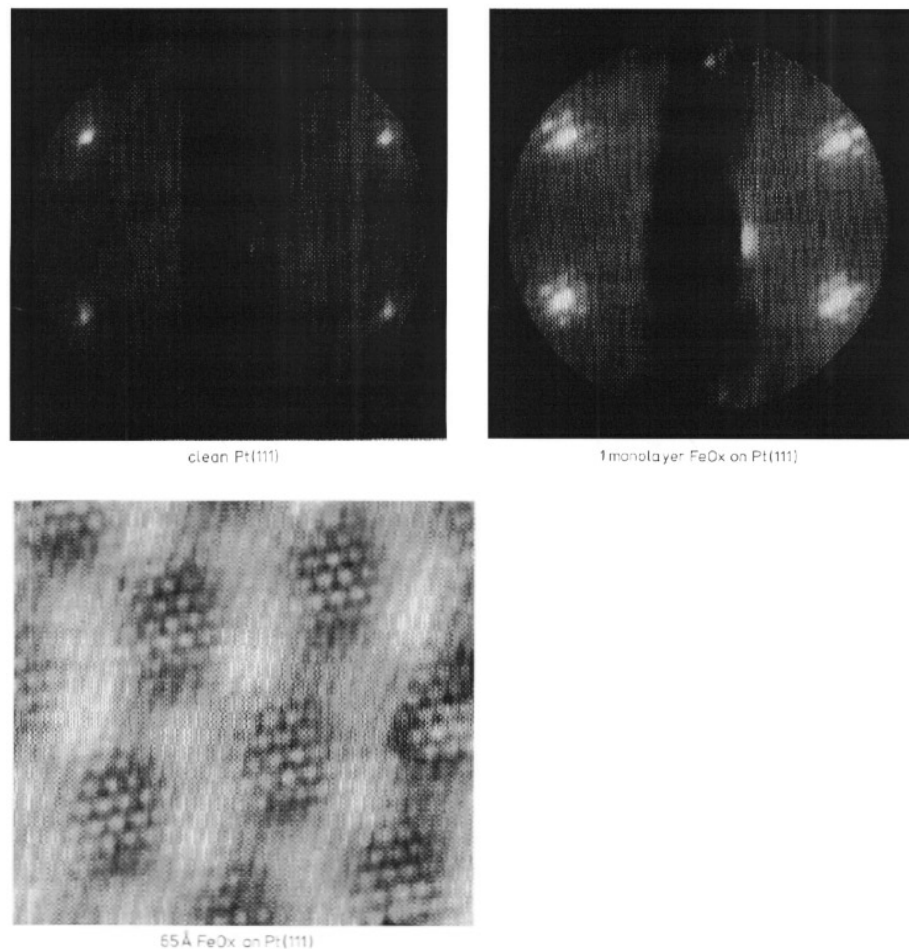


Figure 10. (a) LEED patterns for FeO_x layer on Pt(111). For comparison the pattern of clean Pt(111) is shown.

figure 15(b) an STM topograph of the growing film is plotted [99]. The thickness of the film turns out to be only 4.5 Å, as revealed through Auger spectroscopy [110] and XPS, but the film covers the whole surface. This can be checked quantitatively via CO titration within a temperature programmed desorption (TPD) measurement [100]. As has been discussed for thin alkali halide films on Ge substrates [111], we must assume that the Al_2O_3 film covers the NiAl(110) substrate, including substrate steps, like a 'carpet'. Only very few steps are found on the Al_2O_3 surface [99]. Figure 16(a) shows a large area STM picture of the film. There is a characteristic regular line pattern observed and a net of less regular white lines is overlaid. We may understand these patterns by investigating the LEED structure in more detail. Figure 15(a) assigns the spots observed to two almost rectangular unit meshes with basis vectors ($a_1 = 17.9 \text{ \AA}$, $a_2 = 10.6 \text{ \AA}$) which are rotated with respect to each other by 24° [39]. The two domains, called A and B in the following, are commensurate along the (110) direction of the NiAl(110) surface and incommensurate along the (001) direction. Figure 16(b) shows an STM close-up of a domain boundary between A and B. The unit cell of the oxide is marked by a centred rectangular, almost hexagonal, arrangement of

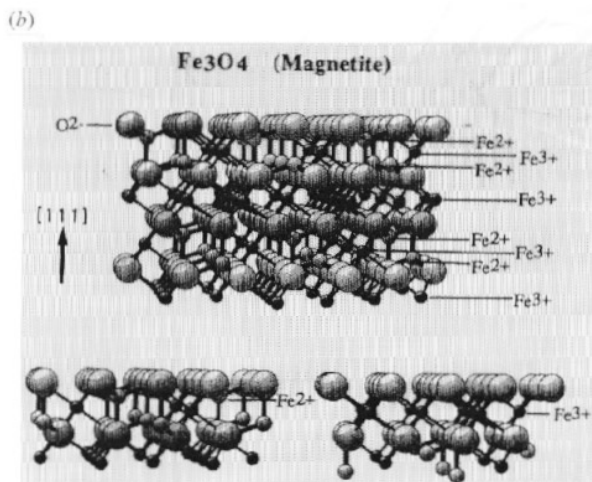


Figure 10. (b) Result of the LEED structure calculation indicates formation of Fe_3O_4 (upper panel). Two different domains are present: (right lower panel) second layer with Fe^{3+} and (left lower panel) second layer with Fe^{2+} .

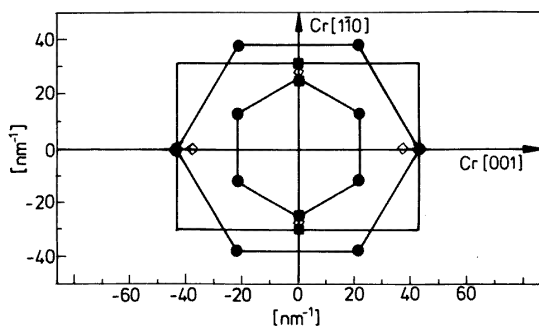


Figure 11. In-plane reflections observed with x-ray scattering from a thin Cr_2O_3 film prepared by oxidation of a $\text{Cr}(110)$ layer on a $\text{Nb}(100)/\text{Al}_2\text{O}_3(11\bar{2}0)$ buffer system. (\diamond) Nb reflection, (\blacksquare) Cr reflection, (\bullet) Cr_2O_3 reflections. Each of the six $\text{Cr}_2\text{O}_3(11\bar{2}0)$ and $(3\bar{3}00)$ reflections lie on a hexagon. The hexagons are rotated with respect to each other. From [87].

protrusions. The atomic structure cannot be resolved within the oxide layer. Therefore it is not clear what the arrangement of the atoms within the surface is. Ion scattering shows that the topmost surface is oxygen terminated [101]. High-resolution XPS indicates that there is an interface layer with Al exhibiting a chemical shift [39]. Angle resolved photoemission (ARUPS), where photoelectron spectra are recorded as a function of the direction of the electronic bandstructure and thus of the symmetry of the electronic states, is indicative of a hexagonal arrangement of the oxygen atoms within the oxygen sublattice [39]. High-resolution electron energy loss spectroscopy (HREELS), where the inelastic electron scattering by surface vibrations and electronic excitations is probed, points towards a structure similar to $\gamma\text{-Al}_2\text{O}_3$ with tetrahedral and octahedral Al sites being populated [39]. An interesting observation, however, may be made via STM if the tunnelling voltage is changed. As is learned from ARUPS spectra [39], Al_2O_3 exhibits occupied levels only at a binding energy

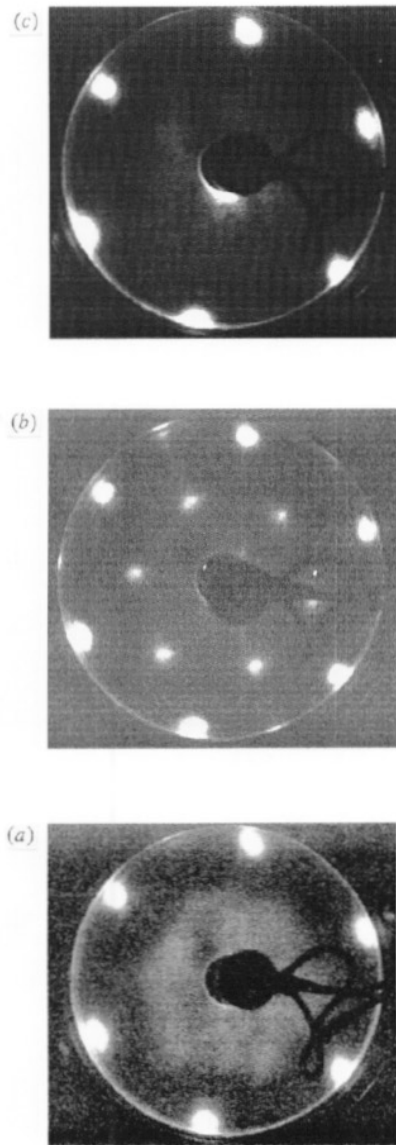


Figure 12. LEED photographs (primary energy 23.7 eV) of $\text{Cr}_2\text{O}_3(111)/\text{Cr}(110)$ after a flash to 1000 K taken at different temperatures: (a) about 300 K; (b) about 150 K; (c) about 90–100 K.

starting at 4 eV below the Fermi level. The substrate emission, which is still found at E_f due to the limited thickness of the layer [39], may be used for tunnelling as well. If the tunnelling voltage is decreased, an STM topograph as shown in figure 17(a) is found [99]. It exhibits atomic resolution and may be correlated with the structure of the bcc NiAl(110) substrate. A schematic representation of this correlation as shown in figure 17(b) suggests how the substrate has to be reconstructed within the interfacial region in order to accommodate the oxide layer. The lateral motion of a small fraction of atoms in the interface is sufficient to assure the proper local site for the repeat units. The existence of such an interfacial layer, as

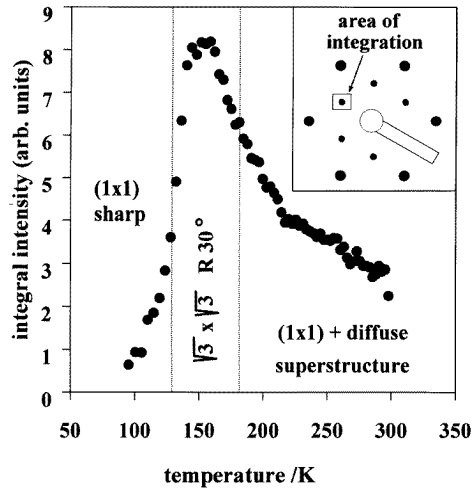


Figure 13. Temperature dependency of the first-order superstructure spot intensity of the $(\sqrt{3} \times \sqrt{3})R30^\circ$ structure on $\text{Cr}_2\text{O}_3(111)/\text{Cr}(110)$.

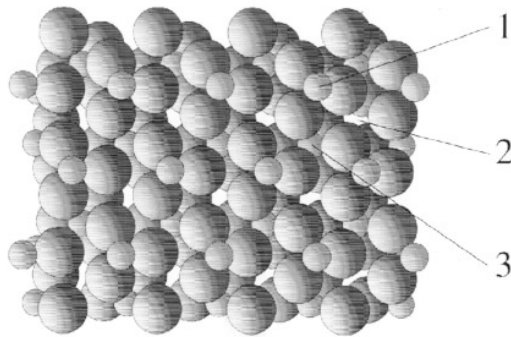


Figure 14. Arrangement of Cr ions on $\text{Cr}_2\text{O}_3(111)$ at temperatures below 150 K.

suggested by STM is also compatible with the LEED observations. In figure 15(a) there are spots not assigned to single scattering from the domains A and B. These spots are double diffraction spots occurring through scattering at the oxide metal interface. It was surprising in the beginning that the intensity of these spots is rather small, given the total thickness of only 4.5 Å of the oxide film. With the existence of an interface layer, however, which 'increases' the effective range of the scattering path for double diffraction, this becomes easily understandable. Thus the structure of the Al_2O_3 film itself, although not imaged at atomic resolution, still appears to be rather well established.

4. Theoretical treatment of oxide surfaces

Parallel to the many different experimental investigations of metal oxide surfaces and thin films, an increasing number of theoretical treatments of such systems have been published during the last five years. The main objective of these studies is to provide information on the geometric and electronic structure of the surface itself and its interaction with

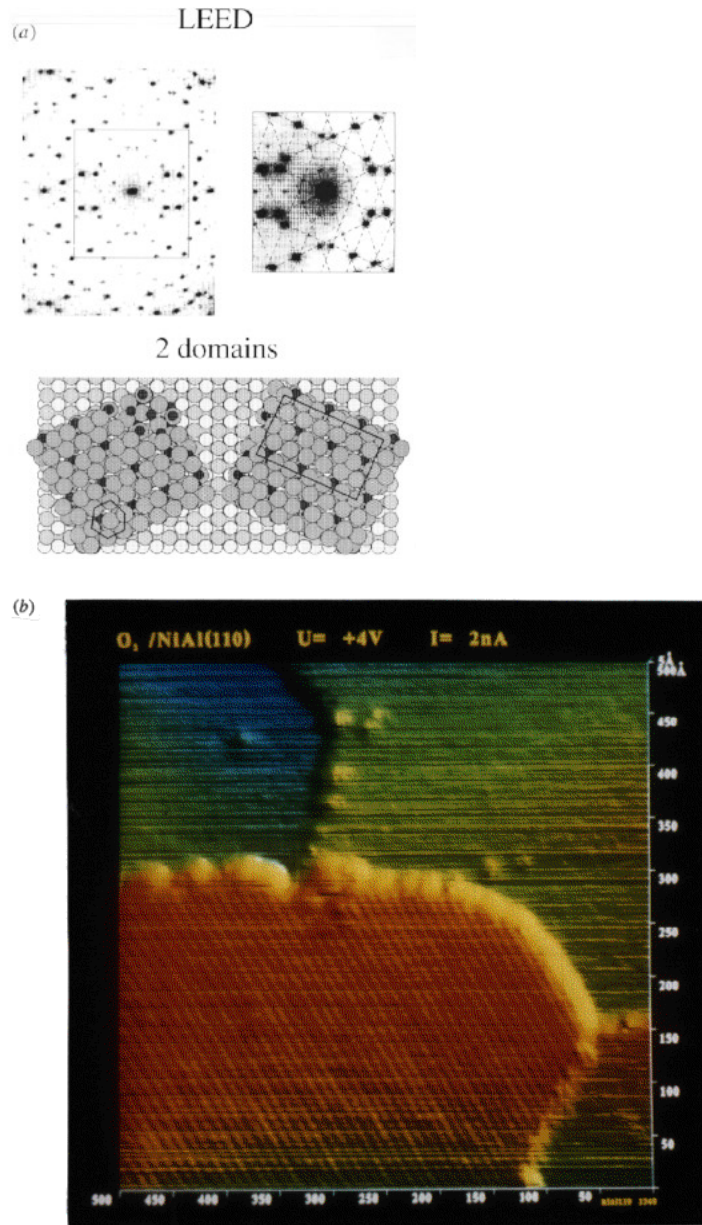


Figure 15. (a) SPA-LEED patterns of $\text{Al}_2\text{O}_3/\text{NiAl}(110)$ (top) and the unit cells in real space of two domains of $\gamma\text{-Al}_2\text{O}_3(111)$ on $\text{NiAl}(110)$ (bottom). The structure of the $\gamma\text{-Al}_2\text{O}_3(111)$ film is distorted by the interaction with the substrate, giving rise to an experimentally observed large rectangular unit cell. (b) STM topograph of the growing Al_2O_3 film (patch with diagonal lines) near NiAl step edges ($U = +4\text{ V}$, $I = 2\text{ nA}$) [68].

adsorbates, which is complementary to the information that can be obtained experimentally. For instance, the relative thermodynamic stabilities of different surface reconstructions of a polar surface can be determined much more directly by theory than by any experimental

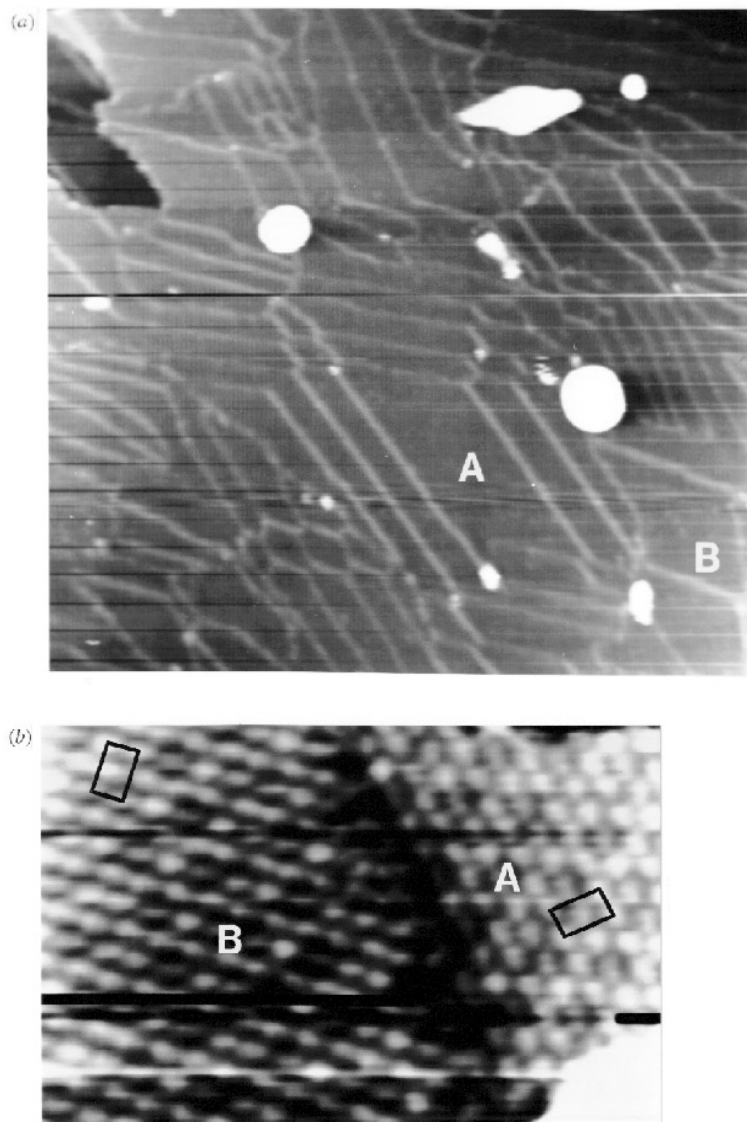


Figure 16. (a) STM topograph of $\text{Al}_2\text{O}_3/\text{NiAl}(110)$. The domain boundaries of the film are clearly visible. $U = -8\text{ V}$, $I = 0.5\text{ nA}$, $2500 \times 2500\text{ \AA}^2$. (b) STM topograph of a domain boundary on $\text{Al}_2\text{O}_3/\text{NiAl}(100)$. $U = -2\text{ V}$, $I = 0.5\text{ nA}$, $210 \times 130\text{ \AA}^2$.

technique. Or, as another example, a detailed understanding of the bonding between an oxidic substrate and an adsorbed atom, molecule or radical is only possible by means of an analysis of reliable quantum chemical wavefunctions. But in many cases theory is even more urgently needed, since many experimental observations, in particular in the field of optical and electron spectroscopy, can hardly be interpreted correctly without the help of detailed theoretical calculations. The recent advances in the methodology of electronic structure calculations and—of course—computer technology have rendered, in particular, quantum chemical *ab initio* calculations so cheap and reliable that they are indeed a helpful

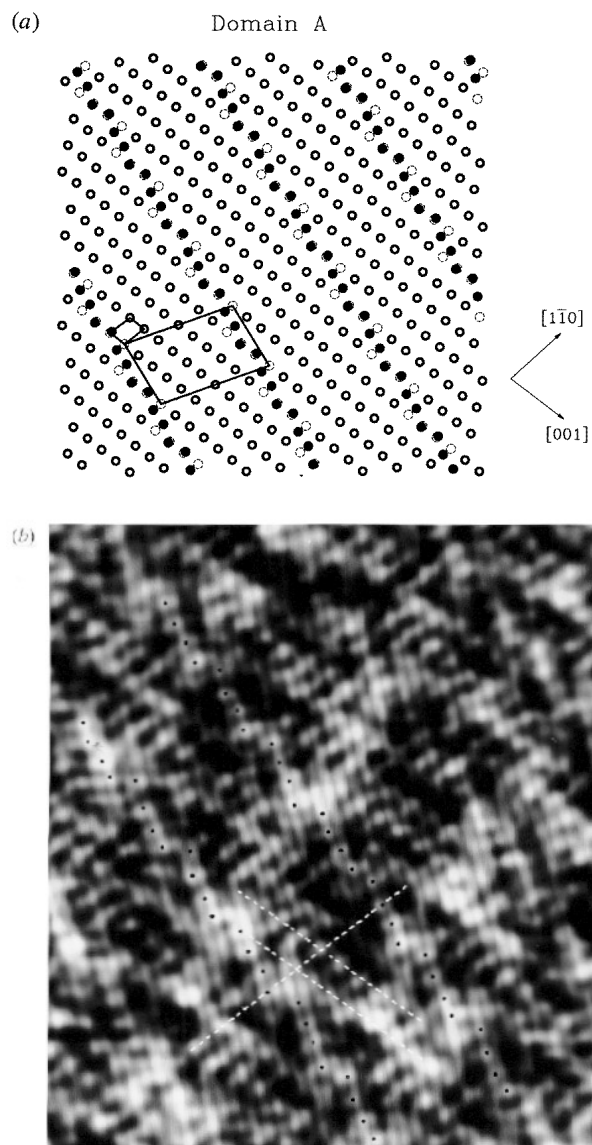


Figure 17. (a) STM topograph of $\text{Al}_2\text{O}_3/\text{NiAl}(110)$ interface. $U = -1 \text{ V}$, $I = 1.5 \text{ nA}$, $90 \times 90 \text{ \AA}^2$. (b) Schematic representation of the atomic structure of the $\text{NiAl}(110)$ surface below the Al_2O_3 film as derived from (a).

interpretative tool, even for systems as complex as oxide surfaces. This fact is reflected by an increasing number of papers that contain both experimental and theoretical results.

In the present section we briefly review the main computational methods that are currently used for studying non-local and local properties of oxide surfaces. Our main emphasis will be on those methods that have been applied to interpreting the experimental results discussed later in this review. For more thorough presentations we refer to recent textbooks on the theoretical aspects of heterogeneous catalysis [112–115] review articles

[116, 117] and conference reports [7, 118–120]. Detailed theoretical results for specific systems will be presented, together with the corresponding experimental data, in later sections of this review.

Table 3. Applicability and characteristics of different theoretical methods for oxide surfaces.

Property	Interatomic potentials	Band structure calculations	Cluster calculations
Geometrical structure			
static	+	+	+
dynamic	+	(+)	(+)
Electronic motion/ electronic structure	–	+	+
Spectroscopy			
electronic	–	+	+
vibrational	+	+	+
Local properties			
local excitations	–	–	+
defects	+	–	+
adsorption	+	(+)	+
Translational symmetry (periodicity)	+	+	–
Entries in parentheses denote properties that can be treated with the respective method, but only with larger difficulties.			
Characteristics of electronic structure calculations	Semi-empirical methods	Density functional theory	<i>Ab initio</i> calculations
Electrons treated	valence el. valence el. (PP)	all electrons valence el. (PP)	all electrons
Basis sets	minimal	flexible	flexible
Approximations involved	ZDO, NDO etc.	density functional	no
Adjustable parameters	yes	in the density functional	no
Ground states			
SCF	yes	yes	yes
dynamic correlation	no	included in the density functional	yes
Excited states	some	some	yes
Numerical effort	$\approx N^2$	$\approx N^3$	$\approx N^4$ (SCF)– N^5 (CI)
Accuracy	limited	good	good to excellent

Abbreviations: PP pseudopotentials; ZDO zero differential overlap; NDO neglect of differential overlap; SCF self-consistent field; CI configuration interaction; N number of electrons.

In accord with the vast diversity of the properties of bulk metal oxides and oxide surfaces, the theoretical methods that are applied in this field cover the whole range from purely empirical interatomic (or interionic) pair potentials via band structure methods to highly sophisticated large-scale quantum chemical *ab initio* configuration interaction (CI) calculations. Table 3 gives a schematic account of the main characteristics and fields of application of those methods that we will discuss in the following.

The simplest way to treat the energetics of ionic crystals and surfaces, including properties like equilibrium crystal structures, cohesive energies, phonon frequencies, compressibilities and so on, is the use of empirical or non-empirical *interionic pair*

potentials. Such potentials may have the simple form [121]

$$\begin{aligned}
 V_{++}(r) &= \frac{q^2}{r} \\
 V_{--}(r) &= \frac{q^2}{r} + A_{--} \exp(-r/\rho_{--}) - C_{--}r^{-6} \\
 V_{+-}(r) &= -\frac{q^2}{r} + A_{+-} \exp(-r/\rho_{+-})
 \end{aligned}
 \tag{2}$$

where it is assumed for simplicity that cations and anions have the same charge $\pm q$, that the Pauli-repulsion between the closed-shell ionic cores decays exponentially (Buckingham-type potential) and that the Pauli-repulsion between the small cations as well as the van der Waals interaction between the cations and between cations and anions can be neglected. Of course, potentials with other functional forms (e.g. of Lennard–Jones type), with many more parameters and with the inclusion of three-body terms can be used as well and have been proposed in the literature [122–127], but even the above form, which satisfies only the minimum requirements for describing the underlying physics (Coulomb interaction, Pauli-repulsion, and van der Waals attraction), contains six adjustable parameters: q , A_{--} , A_{+-} , ρ_{--} , ρ_{+-} and C_{--} . These parameters can be determined completely empirically, e.g. by fitting to experimental data, or non-empirically by *ab initio* calculations. In both cases, the reliability of specific results obtained by means of pair potentials depends to a large extent on the quality of the interaction potentials.

Interatomic pair potentials are currently used in the whole field of metal oxides for many purposes—from the investigation of structural properties of pure metal oxides (e.g. for MgO [123], α -Al₂O₃ [124], α -Fe₂O₃ [125]) or clean and modified surfaces [126, 127] to the dynamics of adsorbed molecules [128] and the simulation of catalytic processes. Computer programs employing interatomic potentials are now included in several of the commercial program packages which are widely used for the simulation of adsorption processes and catalytic reactions. Here we will briefly present two examples, which are related to the later discussion of polar surfaces and adsorption.

The first example concerns the stability of polar surfaces. Wolf [12] and Freitag [82] estimated the surface energies of the unreconstructed NiO(111) surface—which because of equation (1) is unstable—and various possible reconstructions by using interionic potentials of the form given in (2) and parameters as proposed by Catlow *et al* [129]. They found that the octopolar $p(2 \times 2)$ reconstruction (cf figure 9) is the most stable form of the pure NiO(111) surface with a surface energy of 5.16 J m^{-2} as long as the geometrical parameters of unrelaxed bulk NiO are used. Other possible reconstructions follow at considerably higher surface energies: hexagonal, missing row and rhombic reconstructions at 7.73, 8.18 and 11.11 J m^{-2} , respectively [82]. If relaxations of the geometries are allowed, all surface energies are lowered, but the octopolar reconstruction remains the most stable form with a surface energy of 4.28 J m^{-2} [12]. (In this example, the relative stabilities of the different reconstructions are not dependent on the set of interionic potentials used to estimate the surface energies.) This result confirms the proposal of Lacmann [11] and is in agreement with the LEED and STM experiments on the geometrical structure of the NiO(111) surface as discussed above.

The interaction between metal oxides or other ionic crystals and adsorbed molecules is also frequently modelled through pair potentials, in particular if one is interested in the structures of adsorbed monolayers, phase transitions between them, and the dynamics of adsorbed particles, which can be investigated by the application of Monte Carlo or

molecular dynamics techniques as soon as interaction potentials are available. Again, the main problem is the determination of reliable potentials, which in such cases have to describe three types of interaction: among the ions in the oxide, among the gas phase molecules, and between the surface and the adsorbates. The latter part causes particular difficulties because it is rather complicated, containing electrostatic, inductive, repulsive and van der Waals (dispersion) terms, and because generally not enough experimental data are available for the determination of all necessary parameters. Furthermore, the interaction energies between oxide surfaces and neutral molecules are rather small and are based on a delicate balance between attractive and repulsive parts in the potential. Therefore, calculated properties of a substrate/adsorbate system may depend very sensitively on the potential employed.

A very illustrative example for this problem is the system CO/NaCl(100) which is— together with CO/MgO(100)—the best studied example for the adsorption of CO on an ionic crystal. Lakhlifi [130] and Picaud *et al* [131] used semi-empirical pair potentials containing an electrostatic contribution V_E (with distributed multipoles instead of simple point charges), an inductive part V_I (which turned out to be very small and could be discarded as well) and a dispersion–repulsion contribution V_{DR} , which was represented either by a Lennard–Jones 12/6 or a Buckingham exp–6 potential. Picaud *et al* [131] were able to reproduce the isosteric heat of adsorption quite accurately (154 and 187 meV for the (1×1) monolayer of adsorbed CO, calculated with the LJ and exp–6 potentials, respectively, as compared to the experimental value of 176 ± 20 meV at 55 K [132]) and to confirm the existence of two energetically equivalent commensurate (1×1) and (2×1) phases of the adsorbed CO monolayer. However, the adsorption geometry for a single CO molecule turned out to be different for the two potentials. If the Buckingham exp–6 potential is used CO adsorbes on top of Na^+ in an upright orientation, with the LJ potential it is shifted along the Na^+ row by about 1.2 Å and is tilted by 30° . The authors close the paper by stressing the necessity of reliable *ab initio* calculations. Similarly, Lakhlifi [130] finds CO shifted and tilted on NaCl(100) (a Lennard–Jones ansatz for the dispersion–repulsion term was also used), and Lakhlifi and Girardet [133] find CO shifted and tilted on MgO(100) also in contrast to all electronic structure calculations on this system, which have been reviewed recently by Sauer *et al* [117].

The situation is even worse for the adsorption on more complicated surfaces such as $\text{TiO}_2(110)$ (rutile). It is not only the complex geometrical structure of the surface (missing row), but the difficulty of representing the charge distribution in bulk TiO_2 or at the (110) surface by a suitable model of point charges or distributed multipoles (the formal oxidation numbers +4 and –2 represent much too high ionicities) that render the determination of empirical potentials as well as of realistic embedding models extremely difficult [134–136].

The main advantage of interatomic potentials is that they provide a very fast method for simulating the static geometrical structures and the dynamical properties of systems with a rather large number of particles, as for instance a substrate/adsorbate system consisting of bulk and surface ions and adsorbed molecules. However, they do not describe the electronic structure of the constituent particles. As (2) indicates, it is only the global properties of the atoms or ions that enter into the parametrization (charge, ionic radius, polarizability, etc). This has two consequences. First, pair potentials can only be used if these properties are not changed by interaction among the particles in the system, i.e. if the ions keep their identity in the ensemble (like, e.g. individual molecules in a fluid system). This holds to a large extent for the ions in a metal oxide, provided that the bonding is predominantly ionic as in the late transition metal oxides, but certainly not for metal atoms in a bulk metal crystal or at a metal surface. Secondly, changes in the electronic structure, for instance d–d excitations within the 3d shell of a Ni^{2+} ion in NiO, cannot be accounted for by interatomic

potentials. This is generally no limitation for alkali or alkaline earth metal oxides because these cations do not possess low-lying excited electronic states and their interactions can be very well described using the charges, ionic radii, etc. of the respective electronic ground states. For transition metal oxides, on the other hand, many interesting properties, e.g. EEL spectra (see below) or magnetic couplings, cannot be described at all by means of pair potentials; for other properties, for instance adsorption energies or geometries, one has to check carefully whether or not details of the electronic structure of the partly filled shell play a role or can be neglected. The main difference between the bonding of CO and NO to the NiO(100) surface, for instance, is caused by the singly occupied 3d orbitals in Ni²⁺. The CO molecule, which does not contain unpaired electrons, is only bound by electrostatic forces to the (100) surface (physisorption) [137] while the unpaired electron of NO can form a weak chemical bond with the singly occupied 3d_{z²} orbital in Ni²⁺. This is the origin of the weak chemisorption and of the tilt angle of NO with respect to the surface normal in NO/NiO(100) [63, 138–140].

The methods that describe the electronic structure explicitly and are used in the investigation of oxide surfaces can be divided into two groups. One group contains band structure calculations, i.e. methods which take care of the infinite periodic structure of a single crystal or a single crystal surface from the very beginning and calculate one-electron wave functions (= orbitals) $\phi_i(k)$ and one-electron energies $\epsilon_i(k)$ as functions of the wave vector k in the reciprocal space. Due to the explicit incorporation of the periodicity of the crystal lattice, the actual dimension of such a calculation depends only on the size of the unit cell [141]. The alternative possibility is cluster calculations [118, 120], in which a finite cluster of atoms or ions is treated explicitly, like a small molecule, and can be further embedded in an external field in order to simulate the rest of the crystal or film. Such a description is particularly suitable if one is interested in local effects like adsorption, local excitations, defects and so on. Of course, the quality of the results of a cluster description depends on the size and form of the cluster, on the localizability of the effect to be studied and to a large extent on the nature of the chemical bond in the crystal. The numerical effort involved in cluster calculations increases rather quickly with the size of the cluster. An advantage of cluster calculations is that one can use the whole spectrum of quantum chemical methods, as developed for small molecules, almost without modifications. For transition metal oxides, where configuration interaction among the many-electron configurations of the incompletely filled 3d shell and the O(2p) shells is necessary, this is really a decisive advantage.

Both band structure and cluster calculations can be performed at different levels of sophistication. Semi-empirical methods, density functional theory, and *ab initio* calculations are all used for the treatment of oxide surfaces. Some of the characteristics of these approaches are summarized in the second part of table 3. For practical applications, the main differences lie in the necessary computer time which due to the inherent approximations, scales only with N^2 for semi-empirical methods, with N^4 (SCF) to N^5 (CI) or even higher for *ab initio* methods, while density functional approaches are in between. Roughly speaking, the accuracy that can be achieved behaves in the opposite manner, but recent advances in density functional theory (general gradient corrections) [142–144] make this method a fast and very reliable tool, in particular for determining equilibrium geometries. In the following we will concentrate on *ab initio* methods since most of the experiments to be discussed in this review are concerned with spectroscopic properties and weak interactions between the oxidic substrates and adsorbates, and for these properties *ab initio* methods yield more reliable results than the other approaches.

The most natural method for studying the electronic structure of a pure, clean, well-

ordered single-crystal surface or film is *band structure theory* in either its semi-empirical, density functional or *ab initio* SCF form. However, its results are only of rather limited value for oxide surfaces. Of course, the geometrical structures of crystals, surfaces, films and adsorbed monolayers can be generally determined to a rather high degree of accuracy, but these properties are in most cases known experimentally. Reliable information about electronic charge distributions and ionicities can be obtained as well. On the other hand, the calculated band structures themselves are often not very reliable unless final state effects are included [145], since screening effects are large in oxides and may differ considerably from one band to the other, e.g. from localized Ni(3d) to delocalized O(2p) orbitals. Furthermore, the systematic band structure description of the electronic structure of 3d transition metal oxides, in particular for the antiferromagnetic insulators such as CoO and NiO is still controversially discussed [146]. A local description can offer several advantages. The same holds true for adsorption processes, which—at least for oxide surfaces—are predominantly local in nature. They can be treated by band structure methods using the ‘supercell’ technique [147, 148], which consists in repeating the local adsorption site periodically and applying periodic boundary conditions. This technique has been applied, e.g. to H₂O/TiO₂ [149] or CO/MgO [150], but the more direct access to local processes is the cluster approach.

The majority of the theoretical treatments of oxide surfaces, in particular if local properties like core ionization, d–d excitations, adsorption processes, or defects are considered, are currently performed by means of *cluster calculations*, some of them with semi-empirical methods, but many more with density functional or *ab initio* techniques. In the following we will not give a systematic and complete survey of the existing literature (for this purpose we refer to the recent review by Sauer *et al* [117] and the workshop reports edited by Pacchioni *et al* [118, 120], but we will discuss the possibilities and limitations of the cluster approach for the example of the neutral NiO(100) surface [63, 69, 137–140, 151]. Other cubic oxides (MgO, CaO, CoO) and neutral surfaces of oxides with more complicated crystal structures (TiO₂(110)) can be treated similarly. This is also possible for unstable polar surfaces (NiO(111), Cr₂O₃(111), these two examples are discussed below, ZnO(0001) [152] and Cu₂O(100) [153]) provided that a reasonable cluster model and embedding scheme can be designed.

The local adsorption site for the adsorption of CO, NO, CH₃ and similar small molecules or the local environment for d–d excitations within a Ni²⁺ cation at the NiO(100) surface is represented by a NiO₅⁸⁻ cluster as indicated in figure 18. Such a cluster satisfies the minimum requirements for a reasonable description of crystal field effects, the Ni–O (ionic and covalent) bonding in the bulk and at the surface and the interactions between Ni²⁺ or O₂⁻ ions and the approaching molecule. However, this cluster is highly negatively charged and therefore not stable against loss of electrons; furthermore, the electrostatic field around it is quite different from the electrostatic field above the real NiO(100) surface. Both defects can be improved by embedding the cluster in an environment that simulates the remainder of the half-infinite single crystal or the film. Two techniques are employed for this purpose. One possibility is to saturate the charges by protons which yields a neutral Ni(OH)₂(H₂O)₃ cluster [137] as shown in figure 18(a), the other one is to embed the NiO₅⁸⁻ cluster in an extended point charge field (Madelung field) where the positions of the point charges are determined by the bulk crystal structure of NiO and the charges themselves have to be chosen reasonably (figure 18(b)). A few hundred point charges are generally sufficient for a good representation of the Madelung field. For highly ionic systems such as NiO and MgO the formal oxidation numbers +2 and –2 are rather close to the true charges of the ions and can be used without further modification. The analysis of the electronic wavefunctions of periodic *ab initio* SCF calculations for MgO [154, 155] has shown that the partial charges

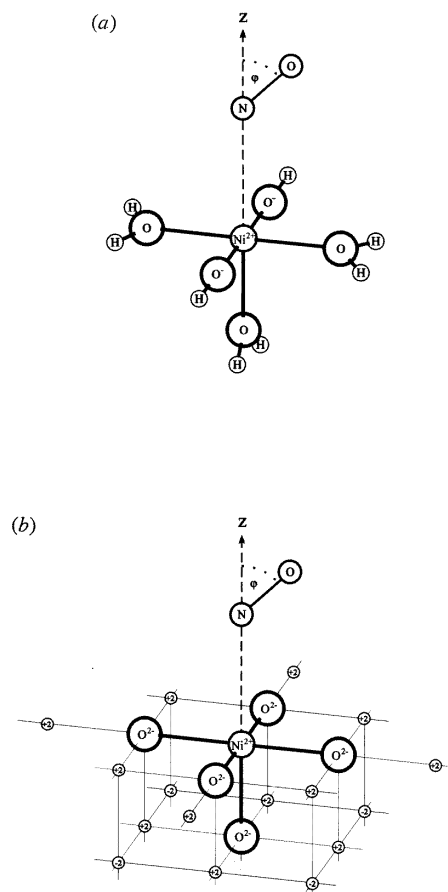


Figure 18. Cluster model for the adsorption of NO at the NiO(100) surface. The NiO_5^{8-} cluster is saturated by protons (a) or embedded in a semi-infinite Madelung field (b) (only a few point charges are indicated).

at the ions are very close to $+2.0$ (1.98 ± 0.03 , slightly different values were obtained with different basis sets), density functional calculations [150, 156] gave slightly lower ionicities of about 1.8. It should be noted that partial charges are not physical observables, and different schemes for analysing the electronic wavefunctions (population analysis, Bader's topological analysis, or effective Madelung field [156]) will in general yield different results, so do different computation schemes (SCF, CI or density functional approaches, periodic or cluster calculations). It is generally assumed that SCF calculations overestimate ionicities. For MgO and NiO, all estimated ionicities lie in the rather narrow range between 1.8 and 2.0 both for ions in the bulk and at the (100) surface. Semiempirical calculations, however, yield consistently much lower ionicities, for MgO only of the order of 1.0 [157].

For more covalently bound systems such as TiO_2 and for ions at polar surfaces the true ionicities might deviate appreciably from the formal oxidation numbers. In TiO_2 , point charges of about $+2.6$ and -1.3 represent the charge distribution much better than $+4$ and -2 [134, 158], but so far all attempts to embed a small TiO_5^{6-} cluster, representing the local adsorption site of the $TiO_2(110)$ surface of rutile, in a reasonable field of point charges or distributed multipole moments have been only partly successful [134–136]. For

this system probably larger clusters are necessary [159]. In the case of ZnO, 'experimental' estimates of the ionic charges range between 0.4 and 1.1, cluster calculations between 1.3 and 1.8 depending on the method of calculation and the size of the cluster [82, 152], while MINDO/3 calculations yield about 0.7 [82, 152]. Since a polar surface (e.g. ZnO(0001)) can be stabilized by charge transfer from bulk ions towards the surface large differences are to be expected between the ionicities of ions in the bulk and at polar surfaces.

The NiO_5^{8-} cluster embedded in a point charge field is small enough as to allow the application of sophisticated *ab initio* methods together with flexible basis sets. This is in particular necessary for transition metal oxides in which many experimentally observed spectroscopic properties (d-d and charge transfer excitations, s-d exchange splitting, UPS and core level spectra, etc.) depend explicitly on the angular momentum and spin coupling of the partly occupied 3d-orbitals. Configuration interaction (CI) calculations that take care of differences in the 3d occupation as well as of $\text{O}(2p) \rightarrow \text{Ni}(3d)$ charge transfer and possibly also substrate \leftrightarrow adsorbate charge exchange are necessary for describing these effects and can indeed be used. On the other hand, the NiO_5^{8-} cluster (for the NiO(100) surface) and similarly the NiO_6^{10-} cluster (for bulk NiO), both embedded in the appropriate point charge fields, are large enough to contain nearly all physical effects which are important for local processes: $\text{Ni}^{2+}-\text{O}_2^-$ bonding, crystal field effects, electrostatic potential above the NiO(100) surface and so on.

CI calculations on such embedded clusters yield results which are both qualitatively correct and quantitatively accurate enough (e.g. errors of about 0.1–0.2 eV in the lowest excitation energies) to enable a convincing interpretation of the EEL spectra of NiO(100), CoO(100), NiO(111) and $\text{Cr}_2\text{O}_3(111)$, which are discussed later in this review. The energetic order of the low-lying electronic states, crystal field splittings, the removal of degeneracies if the symmetry is reduced from O_h in bulk NiO to C_{4v} at the NiO(100) surface, the differences in the excitation energies of Cr^{3+} ions at different surface positions, and the shift of the excitation energies upon adsorption of NO or CO at the surface agree fairly well with the corresponding experimental findings.

However, it should be noted that there are limitations as to the applicability and reliability of cluster calculations as long as comparatively small embedded clusters are used. As mentioned above, one necessary prerequisite seems to be that the oxide is highly ionic and that one can describe the embedding electrostatic field by a reasonably chosen point charge model. But even if this is possible, there are properties that are non-local in nature and cannot be accurately described by using small clusters. One example is a defect that carries a charge different from that of the normal ions, e.g. a Cr^{3+} ion in MgO [160]. Local charge and geometry relaxation can be accounted for by a small cluster, but the additional charge polarizes the whole crystal and since this is a long-range effect it cannot be accounted for by a small cluster. Similar effects are encountered in the calculation of optical band gaps [161, 162] because of the creation of a large dipole moment upon charge transfer excitations. In their pioneering paper on the optical band gap in NiO [161] Janssen and Nieuwpoort have decomposed the bulk polarization of the whole crystal due to an additional charge at a regular lattice position in NiO into an intracuster and an extracuster contribution. The first contribution is calculated by SCF and CI for the embedded NiO_6^{10-} cluster at about 2.1 eV, the latter one is estimated by means of a classical continuum model at about 3.5 eV. These polarization energies lower the calculated band gap from 10.0 to about 4.4 eV, their inclusion is absolutely necessary for obtaining reasonable agreement with experiment. The same problem exists for the calculation of core ionization spectra because of the local charge created upon ionization out of a localized orbital [161, 163] or the adsorption of charged species and charge transfer excitations from the surface to the adsorbate, which are

important, for instance, in the laser desorption of NO from NiO(100) [164]. The calculation of photoemission spectra is even more complicated, since such polarization or relaxation effects (which are sometimes called screening effects) are generally different for ionization from different orbitals [165–167].

It is rather surprising that small clusters suffice to treat the adsorption of small molecules on oxide surfaces. This has been systematically investigated by Pacchioni *et al* [150] for the adsorption of CO on MgO(100) by varying the cluster size from MgO₅ to Mg₉O₉, Mg₁₃O₁₃ to a three-layer periodic model of the MgO(100) surface with one CO adsorbed on every fourth Mg²⁺ ion (supercell treatment). Most of the calculated properties (distance between Mg²⁺ and CO, C–O distance, adsorption energy, CO stretching frequency) varied only insignificantly with the size of the cluster and the results for even the smallest (embedded) MgO₅⁸⁻ cluster were very close to those of the periodic calculation. This is a justification for all those calculations which are designed for calculating adsorption geometries and energies for similar systems and employ clusters of the type of NiO₅⁸⁻ or not much larger. In other studies it has also been found that the increase of the cluster size or different embedding schemes have only small effects on the calculated equilibrium geometries or adsorption energies. The reason for this surprising observation is that the bonding between CO or similar closed-shell molecules and neutral oxide surfaces is predominantly electrostatic and a fairly reasonable description of the electric field above the surface is already obtained with a small cluster embedded in the correct Madelung field. The details of the bonding mechanism have been elucidated by Pacchioni and Bagus [168–170] for CO/MgO(100) using the CSOV (constrained space orbital variation) analysis and by Pöhlchen and Staemmler [137] for CO/NiO(100). Contrary to the Blyholder model [171], which is the appropriate model for explaining the much stronger bond between CO and transition metals, there is no σ -bonding and π -backbonding for CO adsorbed on metal oxides. The attractive part of this bond is the electrostatic interaction between the multipole moments of the approaching molecule (mainly the quadrupole moment in the case of CO) and the electric field above the ionic crystal. This attraction is balanced by the Pauli-repulsion between CO and—predominantly—the O₂⁻ anions. If the approaching molecule possesses unpaired electrons, as for instance in NO [63, 140] or CH₃ [151], there can also be a small chemical contribution to the bond. The large difference in the bonding between CO on metals and on oxides is caused by the fact that the 4s and 4p atomic orbitals (AOs) on the metal, which are needed to construct empty spd-hybrids, which point toward CO and can accept electrons from the doubly occupied 5 σ orbital of CO, are not available in metal oxides because there is no space for them among the bulky electronic charge distributions of the O₂⁻ anions with fully occupied 2p shells.

Though the bonding mechanism between oxide surfaces and adsorbed molecules is well understood in principle, it has not been possible so far to obtain quantitatively correct values for adsorption energies, neither from cluster nor from supercell *ab initio* calculations. The calculated binding energies are in all cases substantially lower than those obtained experimentally from TPD (temperature programmed desorption) experiments or IRAS (infrared reflection absorption spectroscopy) measurements. Again, CO/MgO(100) is the best studied example: Pacchioni *et al* [150] obtain a binding energy of 0.08 eV in their best cluster calculation (largest cluster, best basis) while the most reliable experimental value is 0.43 eV [172]. Similar problems arise in all systems studied so far, e.g. CO/NiO(100) [137], NO/NiO(100) [140], CO/ZnO(0001) [152]. Density functional and semi-empirical calculations do not suffer from this defect due to the ‘overbinding’ problem of the local density approximation and the empirical parametrizations in the various semi-empirical schemes. The origin of this discrepancy is not yet completely understood. The main reason

is that the rather small adsorption energies between CO and the oxide surface depend on the precise balance between attractive and repulsive contributions. To achieve this it is necessary to describe the multipole moments of the molecule and the spatial extent of the O_2^- anions rather accurately. This is possible on the SCF level, provided that flexible basis sets are used. For the inclusion of van der Waals interactions, which contribute of the order of 0.05–0.10 eV to the adsorption energy, the inclusion of dynamic correlation effect on the MP2 or CI level is necessary. The second source of uncertainty might be the use of too small clusters, but as outlined above neither larger clusters nor supercell calculations can yet give better agreement.

Of course, it is in principle easily possible to enlarge the size of the cluster. For alkali or alkaline earth oxides, for which the ionic cores can be safely represented by pseudopotentials and one is left with only a small number of valence electrons N , this is possible. For semi-empirical or density functional methods, which scale only with N^2 or N^3 , the use of larger clusters is no problem at all, e.g. in the treatments of MgO [157], CaO [173], or TiO_2 [174], where the cluster size can be easily extended to several hundred ions. However, *ab initio* calculations on transition metal oxides for which all d-electrons have to be treated explicitly do run quickly into problems with computer times if the cluster size is increased: The next coordination shell of positive ions around the NiO_5^{8-} cluster at the NiO(100) surface contains 13 Ni^{2+} ions; with the N^4 scaling of the necessary computer time and space requirements their inclusion blows up the *ab initio* calculation quite dramatically. An alternative way is to improve the embedding by representing the next coordination shell or shells by ‘pseudopotentials’ or *ab initio* model potentials [175–179], which are not fixed from the very beginning like the point charge model, but adjust themselves in a self-consistent manner to the changes in the electronic structure of the small cluster which is considered explicitly.

Concluding this rather general and short section we can state that there exists a variety of theoretical methods that are currently applied to the properties of oxide surfaces and that are capable of yielding useful information for understanding the properties of oxide surfaces and interpreting experimental observations.

5. Electronic structure of oxide surfaces

In order to gain deeper insight into the behaviour of oxide surfaces as far as reconstruction and adsorption are concerned it is important to have a handle on the electronic structure of oxides. The obvious method of studying electronic structure is photoelectron spectroscopy. During the last few years, for example, the band structure of several oxides has been investigated with a major emphasis on comparison with calculations of the bulk band structure [63, 180–182]. Very early contributions in this field came from Allen *et al* [180], from Thornton and his collaborators [181] as well as from Neumann and his group [182].

In figure 19 we show the result of the work of Kuhlbeck *et al* on NiO(100) [63] because this allows a direct comparison with results on NiO(100) films. The data on a NiO(100) cleaved single crystal were taken in normal emission along the so-called $\Gamma - X$ direction. Photon energies were chosen such as to access the first and the second Brillouin zones. Choosing a proper inner potential of 3.5 eV allows us to fold back the data from the second into the first Brillouin zone. In the figure we have included the latest band structure calculation of NiO [145]. A straightforward interpretation of the NiO band structure in terms of initial state effects is not possible, because it has been known for a long time that the creation of holes in the photoemission process induces final state effects especially in NiO that lead to strong distortions of the simple band structure picture [183]. The effect

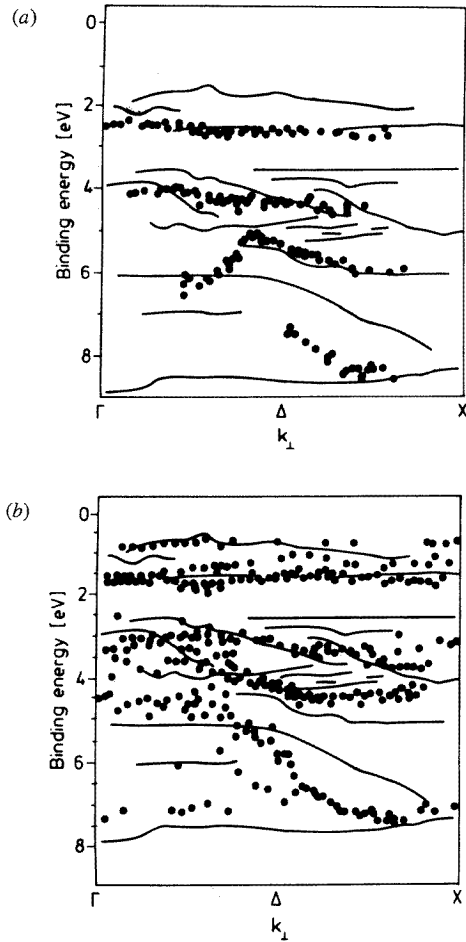


Figure 19. (a) Experimentally determined band structure of NiO(100) epitaxially grown on Ni(100) [63] in comparison with a calculated band structure [145]. (b) Experimentally determined band structure of NiO(100) cleaved in vacuo [63] in comparison with a calculated band structure [145].

is a strong mixing of oxygen and metal character in the bands. Along the $\bar{\Gamma} - \bar{X}$ direction we observe five bands. At $\bar{\Gamma}$ they degenerate to three bands. The dispersion of the topmost four bands is small and of the order of 0.2 eV at most. Only the band at the highest binding energy exhibits considerable band dispersion. The naive interpretation would be to correlate the topmost bands with Ni ionization because the Ni–Ni interaction in NiO is small compared with the O–O interaction. The three bands would be correlated with the five d levels which are split in t_{2g} and e_g sublevels at $\bar{\Gamma}$ due to the cubic symmetry. Along $\bar{\Gamma} - \bar{X}$ the degeneracy of the t_{2g} is partly lifted so that three bands result. The oxygen levels are degenerate at $\bar{\Gamma}$ according to t_{1u} symmetry. Again the threefold degeneracy is lifted and one band is split off. This band shows the largest dispersion of all, compatible with the strong oxygen–oxygen interactions. The dispersion moves the band to higher binding energy towards the Brillouin zone boundary because the phase relation for p-orbitals forming σ -bonds puts the anti-bonding combinations at $\bar{\Gamma}$ and the bonding combinations at \bar{X} .

Even though there are no obvious contradictions as far as the above interpretation is concerned, this naive interpretation needs considerable improvement. The main point is: as soon as an electron is emitted from a Ni level, screening of the hole on the Ni may occur through charge transfer from neighbouring oxygen ions. The resulting state is then a strong mixture of Ni and oxygen levels, and a detailed assignment may only be made on the basis of detailed calculations including the effects of ionization. These calculations have to properly treat many particle effects because in photoemission rather intense satellite structure may cause dramatic changes in the spectral function $A(\omega, \mathbf{k})$ including redistribution of intensities over several states with comparable weight such that the 'band structure' may no longer be recognized. The band structure $\epsilon(k)$ which is connected with the orbital energies ϵ may be recovered via [184]:

$$\epsilon(\mathbf{k}) = \int_0^{\infty} A(\omega, \mathbf{k}) \omega d\omega. \quad (3)$$

Such an analysis has not been performed frequently so far, because a detailed assignment has to be the basis for this. In the case of an adsorbate system, where satellites are known to be important, an analysis of the spectral function using the recipe in equation (3) has been performed [185]. For NiO several calculations of the spectral function of the valence and core electrons have been reported. For the valence electrons, Fujimori *et al* [166] performed a semi-empirical calculation which indicated that, as alluded to above, the topmost bands contain both oxygen and Ni character. Experimentally, the Ni or oxygen character of a spectral feature may be checked via its photon energy dependence. Figure 20 shows valence band spectra of NiO in the range of 19 eV to 120 eV [63]. While in this energy range the oxygen 2p cross section decreases with increasing photon energy, the Ni 3d cross section goes through a maximum. It is quite obvious that the levels near the Fermi energy show the expected resonant behaviour typical for Ni 3d derived levels. A quantitative determination of the oxygen against Ni content of the wavefunctions has not yet been performed experimentally. *Ab initio* calculations are needed to solve this question. Coming back to the measured band structure, one should realize that the involvement of many particle effects always leads to hole induced localization effects which then in turn may let an interpretation in terms of dispersions at least appear questionable.

As the above discussion has indicated, the bulk electronic structure cannot be fully understood if only photoemission is studied. In addition, we have so far not considered specifically the electronic structure of the surface. It is well known, however, from the investigation of metals, that within gaps of the bulk band structure surface states may exist which can be detected via photoemission [186]. They show no dispersion in k -space perpendicular to the surface and they may be quenched or shifted by interaction with adsorbates. The reason for the appearance of surface states of course is the change of the electronic structure at the surface with respect to the bulk. The atoms in the surface feel a different potential because their coordination number is reduced and consequently the energy levels change. For oxide surfaces, photoemission has, so far, not been successfully used to detect intrinsic surface states. Neither in valence electron photoelectron spectroscopy nor in core-electron spectroscopy has a clear detection of surface state effects been possible so far. This is somewhat surprising and it may be due to the presence of strong satellites, which make a clear differentiation difficult.

We will show in the following that electron energy loss spectroscopy (EELS) can be used to clearly identify surface states on several transition metal oxide surfaces that show the expected behaviour against adsorption from the gas phase. The examples are grouped in two parts. In the first part we shall discuss transition metal oxides with rock salt

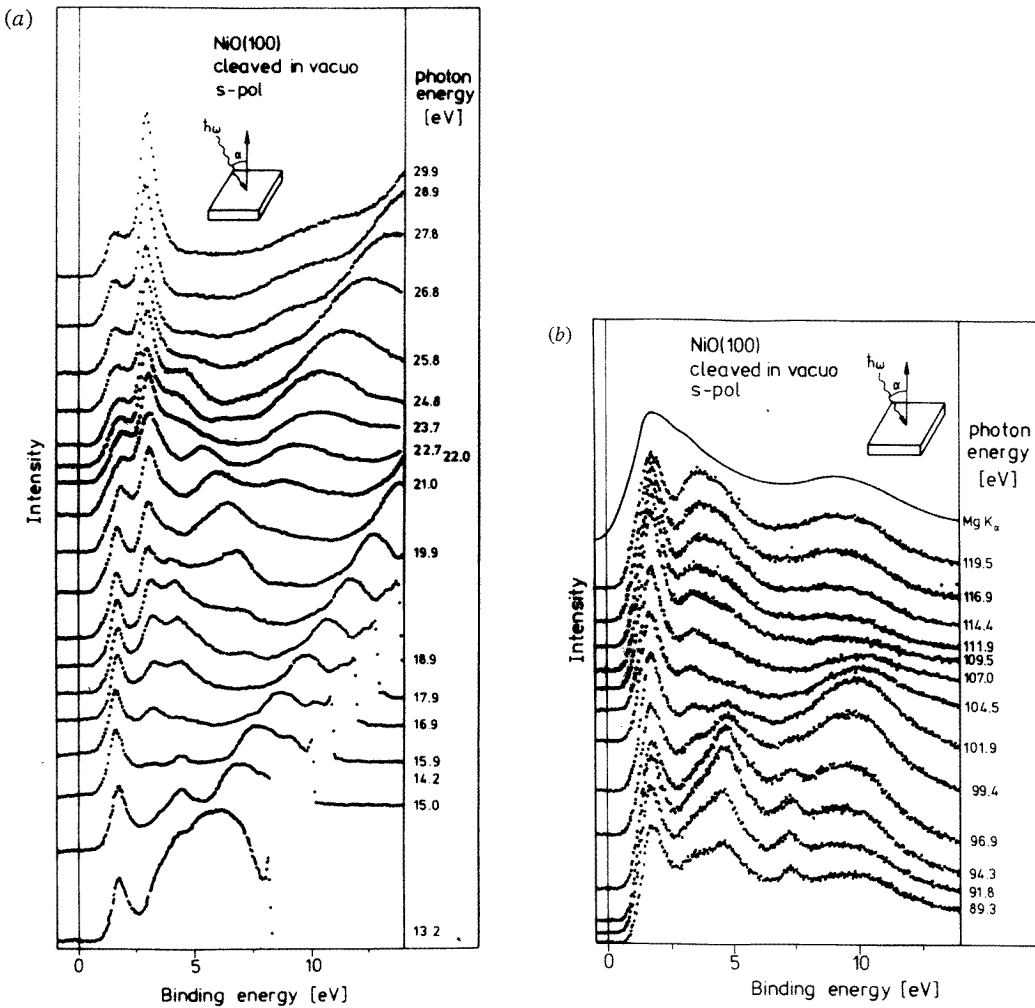


Figure 20. (a) Photoelectron spectra of NiO(100) cleaved in vacuo as a function of photon energy taken in normal emission with mainly s-polarized light ($E_{\text{ph}} = 13.2\text{--}29.9$ eV). (b) Photoelectron spectra of NiO(100) cleaved in vacuo as a function of photon energy taken in normal emission with mainly s-polarized light ($E_{\text{ph}} = 89.3\text{--}119.5$ eV). For comparison a valence band spectrum taken with Mg K α radiation is also shown, see the second reference in [111].

structure, namely NiO and related materials. In the second part we shift our attention towards corundum type structures, i.e. more complicated systems, such as Cr₂O₃ where the surface provides enhanced structural flexibility. For rock salt type materials we divide the section into non-polar, i.e. stable surfaces and polar, i.e. non-stable surfaces.

5.1. Rock salt type structures

5.1.1. Stable surfaces The idea is to investigate electronic transitions of the transition metal ions which are optically forbidden for the free ions. These transitions are characterized by relatively small band widths and usually they are energetically located within the optical

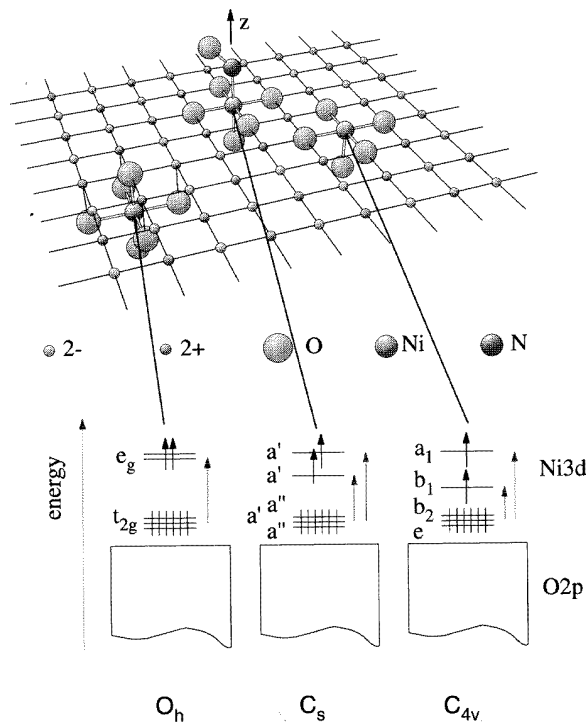


Figure 21. *Top.* Different coordinations of Ni^{2+} and O^{2-} ions on $\text{NiO}(100)$. *Left* bulk; *centre* NO adsorption site; *right* surface; *bottom* schematic representations of the energy levels of the Ni^{2+} ions for the situations depicted in the top of this figure.

band gap of the material. Several groups have used EELS to identify such transitions for various materials [69, 187–193]. A comprehensive collection of spectra accompanied by the appropriate interpretation can be found in the book by Cox [1]. These are all based on the situation depicted in figure 21 which schematically shows the coordination of metal and oxygen in a rock salt type structure bulk and at the (100) surface. The energies of the 3d levels of the transition metal ion in different surroundings are given in figure 21, and this diagram is representative for all transition metal ions. This is true to a reasonable degree of accuracy, because the d levels, especially of the late transition metal ions, are highly localized in space and the direct metal–metal coupling is negligible [63, 180].

Figure 22(a) shows an ELS spectrum of NiO as an example [69]. The wide scan allows the identification of the optical band gap as indicated by the arrow. It is also obvious from the optical absorption spectrum of bulk NiO which is shown for comparison [194]. The d–d excitations have been assigned on the basis of calculations and comparison with literature data (see [69]). It is clear that in an EEL spectrum, in addition to the optically allowed transitions, spin-forbidden transitions can also be observed. This is particularly true for the region above 2–3 eV excitation energy. The assignments given are based on the available literature [187, 191, 194, 195] and we do not want to discuss their limitations at this point. The important point for the present discussion is the statement that there are transitions, marked in the spectrum, which cannot be assigned to d–d excitations of a Ni ion coordinated in the octahedral ligand field of the bulk ion. There are two possibilities for assigning such states: (i) states localized at the Ni ions in the surface; or (ii) states localized at Ni ions

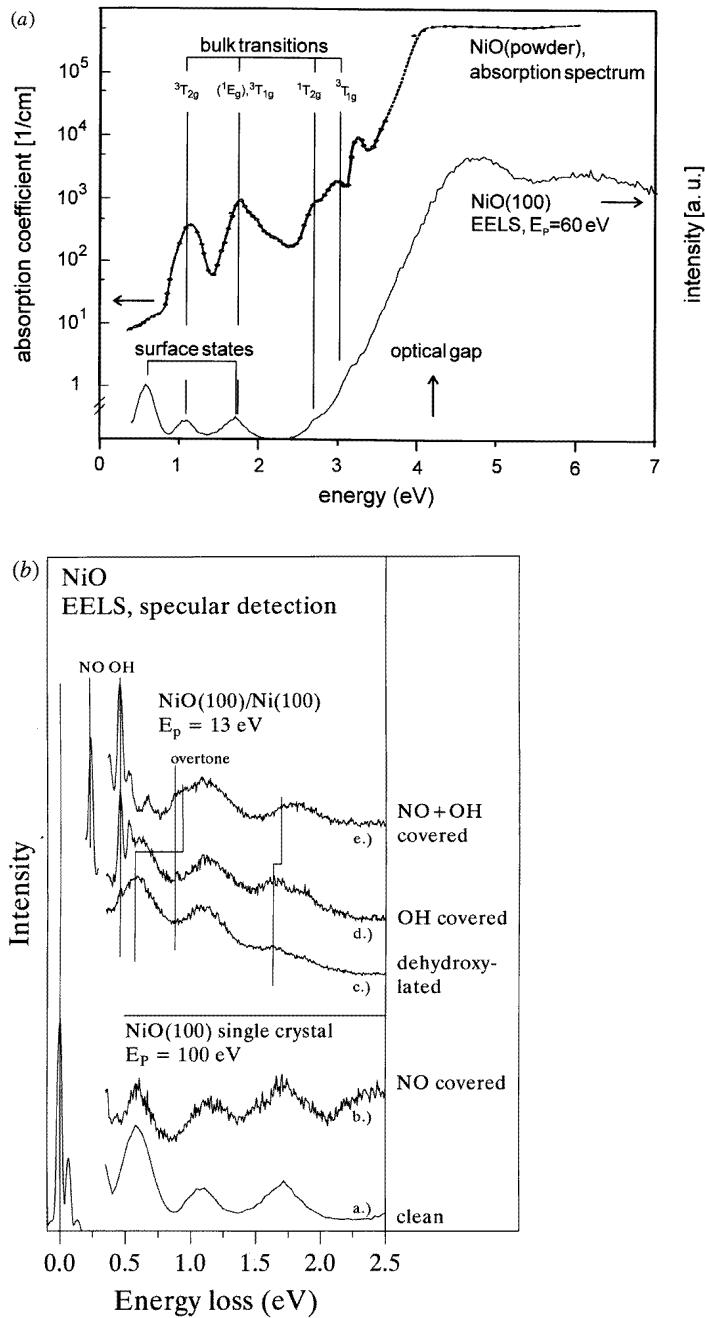


Figure 22. (a) Wide scan ELS spectrum of a NiO(100) single crystal cleaved in vacuo in comparison with an optical absorption spectrum [194]. (b) ELS spectra of NiO(100)/Ni(100) and NiO(100) cleaved in vacuo. In both cases spectra of surfaces with and without adsorbates are shown.

next to an oxygen vacancy in the bulk. *Ab initio* calculations described in detail elsewhere

[69, 137] indicate that both situations would lead to d–d excitation spectra compatible with the above experimental findings. Simple reasoning can explain the basic physics. Consider the five-fold coordination of a Ni ion in the NiO(100) surface as shown in figure 21. In comparison with the bulk, the missing ligand in the (100) direction strongly reduces the ligand field and stabilizes the d-levels with lobes pointing in this direction. This has two main consequences. One is the general reduction in symmetry, which leads to a lifting of degeneracies. The other is the pronounced stabilization of one of the orbitals from the initially degenerate e_g subset. Schematically, in the level diagram of figure 21 these effects can be identified. A very similar, i.e. almost identical situation, could arise if we considered a Ni ion in a direct neighbourhood of an oxygen vacancy in the bulk. Therefore, the EEL spectrum that we expect in both cases will be rather similar. Note, of course, that the electronic excitations within the degenerate 3d levels cannot be calculated and assigned within the framework of single particle excitations, but rather detailed CI calculations taking into account electron correlation as well as spin coupling effects, have to be performed [69, 137, 167].

Let us now consider the lowest excited state of a fivefold coordinated Ni ion. The comparison between theory and experiment reveals that the peak at 0.6 eV excitation energy in figure 22(a) may be a good candidate for this excitation. Several appropriate ways to differentiate between an excitation at a bulk vacancy or an excitation of a surface state may be taken. Energy and angle dependencies of the intensities in the EEL spectra could be recorded to study the surface sensitivity of the excitations [191]. However, the easiest way is to use the sensitivity of the surface potential with respect to the presence of adsorbates. We will discuss the interesting aspects of adsorbates in detail further below in this review. Here, we only need to be sure that the adsorbate resides at the Ni ions so that its presence influences the surface potential at this site. That this is by no means trivial is shown by the case of dissociative H_2O adsorption taking place only at surface defects of NiO(100) [70]. NO, however, does adsorb in the desired way [63, 70]. Figure 22 shows the EEL spectra of a NiO(100) single crystal surface cleaved in vacuo and compares it with the spectra of a NiO(100) film grown on Ni(100). This film has the pronounced advantage that it is easy to cool to liquid nitrogen temperature so that NO can be adsorbed and EEL spectra can be taken without charging problems at low temperature. The film contains defects which we have blocked through dissociative H_2O adsorption before NO was admitted. While H_2O itself does not affect the 0.6 eV excitation it is now clear that NO shifts the surface excitation towards higher excitation energies as is indicated in figure 22. Note that dissociative H_2O adsorption gives rise to the vibrational progression on top of the surface excitation (see below).

The effect of NO documented in figure 22(b) can be understood by going back to figure 21. Its middle part shows the situation for a Ni ion on the surface with an additional NO molecule from the gas phase coordinated to it. The d level diagram indicates the consequences for the excitation energies in this case. The presence of the NO, which is probably coordinated via the nitrogen atom in a tilted orientation (see below), increases the ligand field at the Ni ion position almost to the same value as a sixth oxygen ion. Concomitantly, the lowest surface excitation is shifted close to the bulk excitation. Also other surface excitations are affected by the presence of NO, but a detailed analysis is difficult in those cases due to the limited resolution of the experiment. Summarizing the adsorption experiments at this point, it may be concluded that those excitations of a NiO(100) sample, which are not assignable to bulk excitations originate from excitations of Ni ions on the surface of the samples, thus proving them to be surface states.

There are several important implications of these findings. One is the possibility

of experimentally determining the metal ion site on the surface. In other words, if the coordination site of the ion changes on the surface, the EEL spectrum will also change. We will show further applications below. Another implication is connected with the possibility of determining the site of adsorption of molecules. Due to the localized nature of the d-d excitations only in the case where the adsorbate is directly coordinated to the excited metal ion, can a shift of the surface state be expected. In turn, if a shift is observed, the adsorbate molecule must reside on the excited site. Therefore, spectroscopy of the ligand field effects at oxide surfaces may be used as a structural tool for the determination of the adsorbate site. At the same time this method does not suffer the drawbacks of infrared spectroscopy by having to rely on a site dependent frequency shift. This latter correlation has been recently proven wrong in many cases of adsorbates on metal surfaces through comparison with x-ray photoelectron diffraction data [196]. Before we apply ligand field spectroscopy to structurally more complex systems, we discuss what happens when we change the metal ion, e.g. from Ni to Co, but keep the structural environment the same.

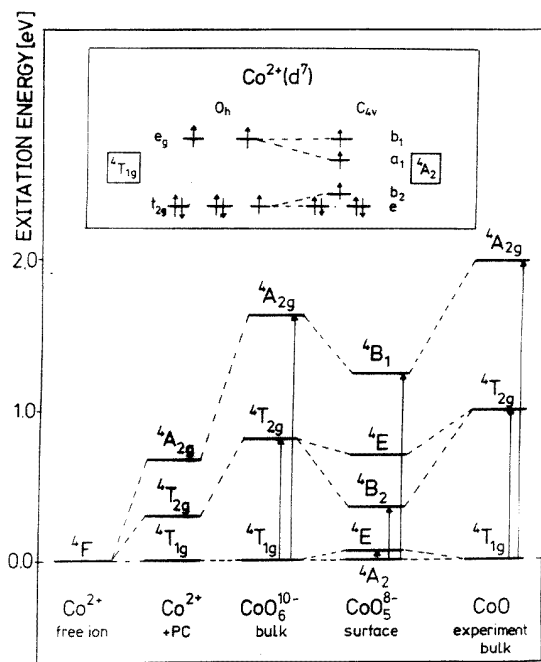


Figure 23. Correlation diagram for the excitation energies of Co^{2+} in different environments as calculated with *ab initio* methods [197]. PC denotes the situation where all surrounding ions of CoO are substituted by point charges.

Figure 23 shows the corresponding energy level diagram for Co^{2+} in different bulk sites of CoO [197]. In many respects the situation for CoO is very similar to NiO. The spatial parts of the one-electron orbitals are identical for CoO(100) and NiO(100). Therefore, we should find very similar differences between EEL spectra for the bulk and the surface states. However, the electronic occupation of the orbitals is somewhat different. Co^{2+} is a d^7 system, Ni^{2+} is a d^8 system. While the ground state of a d^8 system in O_h symmetry is a spatially nondegenerate $^3A_{2g}$ state, the ground state of a d^7 system in O_h symmetry is a spatially degenerate $^4T_{1g}$ state. The important point for the following discussion and the interpretation of the experimental observations is to recognize that this spatial degeneracy

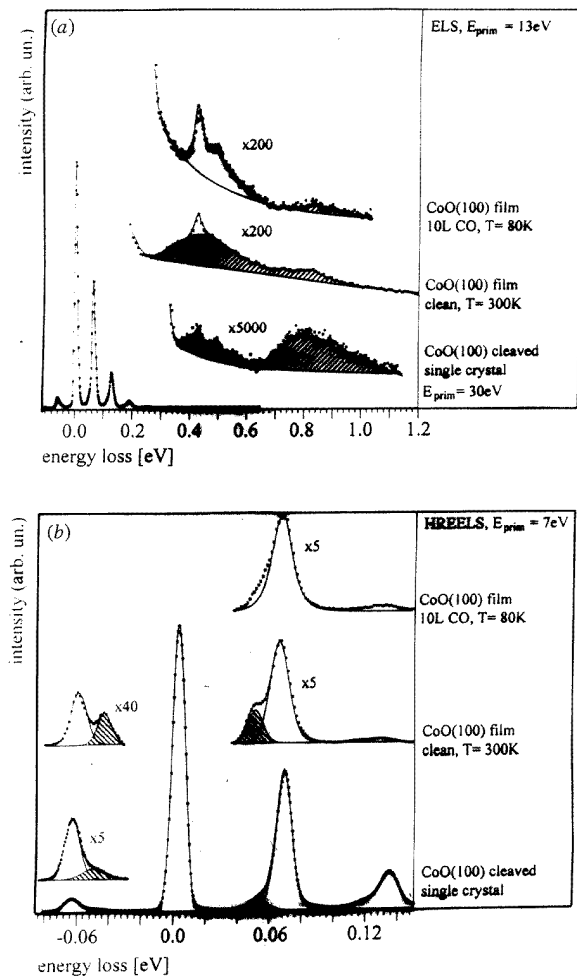


Figure 24. ELS spectra of CoO(100)/Co(11 $\bar{2}$ 0) and CoO(100) cleaved in vacuo for the clean and the CO covered surfaces.

of the ground state is lifted upon lowering the O_h symmetry of the bulk coordination. This is the case for a Co^{2+} ion within the ligand field of C_{4v} symmetry in the CoO(100) surface. The splitting resulting from this effect is very small [197]. The E state lies only 55 meV above the now non-degenerate A ground state. The other excited states on a CoO(100) surface occur at excitation energies similar to those in NiO(100), for example, the second excited state at 0.45 eV as compared to 0.6 eV in NiO(100). The reason for this similarity is that the manifold of states in the d^7 and d^8 configuration are identical, but their energetic order is inverted [191]. Figure 24 shows the experimental EEL spectra in the energy range 0–1.2 eV for a CoO(100) film. The broad bump at 0.45 eV in figure 24(a) which is due to the surface excitation can be clearly identified. The bulk peak at ≈ 0.9 eV is also shown and may be assigned on the basis of literature data [188, 191, 198]. Again, the peak at 0.45 eV is shifted upon adsorption of molecules (e.g. CO in this case) which proves its surface nature, similar to the case of NiO.

However, the interesting energy range in the case of CoO(100) is the range below

200 meV. At 55 meV we expect the surface state resulting from the split off from the ground state. In figure 24(b) the typical set of Fuchs–Kliwer excitations due to substrate phonons can be identified for the CoO(100) cleaved single crystal. Their intensity follows a Poisson distribution as has been demonstrated for many systems. Goodman and his group showed for the case of MgO(100) films grown on top of a Ru(0001) single crystal surface that by choosing higher excitation energies than typically used for recording vibrational spectra (i.e. 5 eV) the higher-order Fuchs–Kliwer excitations may be attenuated considerably, such as to allow easier identification of adsorbate induced vibrational excitations [199]. Due to the very high intensity of the primary phonon excitation this reduction of intensity is not of great help in the present case. If we investigate the range of the phonon excitations, we notice a very tiny asymmetry at the foot of the line. Comparison with corresponding data from NiO(100) shows clearly that this feature is not present for NiO(100). For the gain peak we observe a similar feature. As will be discussed in the following, this feature is connected with an electronic transition. The very small relative intensity of this transition is of course due to the large probing depth of the Fuchs–Kliwer phonons giving rise to intense phonon losses. If we limit the thickness of the CoO(100) film, we do have the chance to attenuate the phonon intensity, and thus increase the relative intensity of the surface excitation because its contribution stays constant. Indeed, if we look at the EEL spectra of a CoO(100) film (figure 24(b)), we see a considerable increase in the relative intensity of the feature at around 50 meV. This is true for the loss as well as for the gain region. In the loss region we can now also see the additional feature for the second phonon loss. The separation from the second phonon loss is the same as from the first phonon loss, indicating that this is not a double loss of the primary features. However, the feature may be easily explained as a combination mode between a double Fuchs–Kliwer excitation and the electronic surface excitation. Its surface nature can again be seen by studying the sensitivity towards adsorption. It is very obvious from figure 24(b) that the peak is basically quenched upon adsorption. We note that the intensity attenuation is completely reversible.

At this point a general comment on the question ‘How do we know that this feature is not due to a vibrational phenomenon but rather to an electronic phenomenon?’ seems to be appropriate. The best way to prove this would be to grow an oxide film with a different oxygen isotope. Then the vibrational features shift while the electronic feature remains energetically constant. This has not been done so far but there are several arguments that support the interpretation as an electronic excitation. First of all, the comparison with NiO is clear evidence that it is a CoO specific phenomenon because the vibrational properties of the two systems are very similar. Secondly, it is not an adsorbate induced phenomenon. When films are grown, it is very hard to avoid hydroxyl formation on the surface. Since this is true for both NiO and CoO, we would expect the occurrence of such peaks also for NiO, if the peaks were associated with hydroxyl adsorption. However, this has not been observed. Thirdly, the intensity of the feature split off from the second-order Fuchs–Kliwer phonon does not follow a Poisson distribution, which it should if it were a pure phonon effect. However, its intensity can be very well described by assuming it to be a combination mode. The observation, which is still not well understood, is the line width of the peak as well as its relative intensity. Generally, the peak widths of electronic excitations are large (≈ 100 meV) with respect to vibrational excitations (~ 5 meV, resolution determined). In addition, the maximum intensities of electronic excitations for forbidden d–d excitation are smaller by a factor of 50 than Fuchs–Kliwer excitations. It seems that in the present case neither line width nor intensity follows the general trend. Note, however, that in the present case the excitation energy is very low so that the lifetime of the excited state may be unusually high. Also, we cannot exclude the fact that we have to deal with electron–phonon

coupling phenomena, which enhance the intensity of the electronic state due to intensity borrowing [200]. Together with isotopic labelling experiments these questions have to be addressed in the future.

With these comments we conclude the discussion of surface states on stable surfaces of rock salt materials and move on to structurally more complex polar surfaces.

5.1.2. Polar surfaces Stabilization of a polar surface is possible, as discussed above, by reduction of the surface charge which may occur via various routes. For example, if the top layer of an oxygen terminated NiO(111) surface consists of OH⁻ instead of O₂⁻, this would reduce the surface charge per atom from -2 to -1, thus stabilizing the surface [70, 201]. Alternatively, geometric reconstruction of the surface layer can lead to surface stabilization [11, 12, 70]. The most stable reconstruction of a polar surface of an ionic crystal is, according to Lacmann [11] and to Wolf [12], the so called octopolar reconstruction as mentioned above and shown in figure 9. The octopolar reconstruction leads as discussed above to a p(2 × 2) unit cell on the surface and is characterized by the removal of three out of four oxygen ions in the first layer (in the case of an oxygen terminated surface) and one out of four nickel ions within the second layer. The third layer again contains a complete hexagonally close packed oxygen layer. A p(2 × 2) reconstruction has been observed for iron oxide [61, 62, 84, 202] and nickel oxide [70], but only in the latter case are there indications that an octopolar reconstruction has actually taken place. In the following we shall be concerned with the electronic structure of various polar surfaces.

NiO(111)/Ni(111) and NiO(111)/Au(111) Figure 2 shows the LEED pattern of a NiO(111) film grown epitaxially on a Ni(111) single crystal surface. The oxide spots are still considerably broader than the metal reflexes because of the imperfections induced by the large lattice mismatch between metal and metal oxide (18%) [64] but the substrate spots are no longer observed.

The EEL spectra in figure 25(a) indicate the adsorption of considerable amounts of hydroxyl groups on the NiO(111) surface by the observation of strong losses at 460 meV. The OH groups may be partially exchanged through exposure of the surface to D₂O which leads to an isotope shift as seen in figure 25(a). These losses are located on top of a background of electronic excitations within the NiO band gap as has been discussed above for the NiO(100) surface. In figure 24(a) the EEL spectrum of the NiO(100) surface is also shown. The comparison shows similar, but not identical, features of the electronic excitations for both surfaces. The reasons for this are twofold. Firstly, if the hexagonal (111) surface is OH terminated the Ni ions are all in octahedral environments, thus only contributing to the bulk signals present at both (100) and (111) surfaces. Secondly, if the (111) surface is not OH terminated, but rather reconstructed, a small part of the Ni ions are in a threefold ligand field thus leading to a corresponding surface spectrum different from (100) (fourfold symmetry). All other Ni ions in the reconstructed layer are in environments typical for a NiO(100) surface. From a weighted superposition of the spectra we do not expect enormous differences between the surface excitations on NiO(100) and NiO(111). In figure 25(b), fits to the ELS spectra are shown which basically corroborate the above assignments. The fits are based upon a mixture of experimental [69, 201] and theoretical [82, 201] information. Freitag and Staemmler [82] have calculated excitation energies for Ni²⁺ ions in various crystal fields and we have used this as input for our fits.

It was shown earlier that the adsorbed hydroxyl groups lead to a pronounced shoulder in the O 1s XP spectra at approximately 1.5 eV higher binding energy [201] as compared

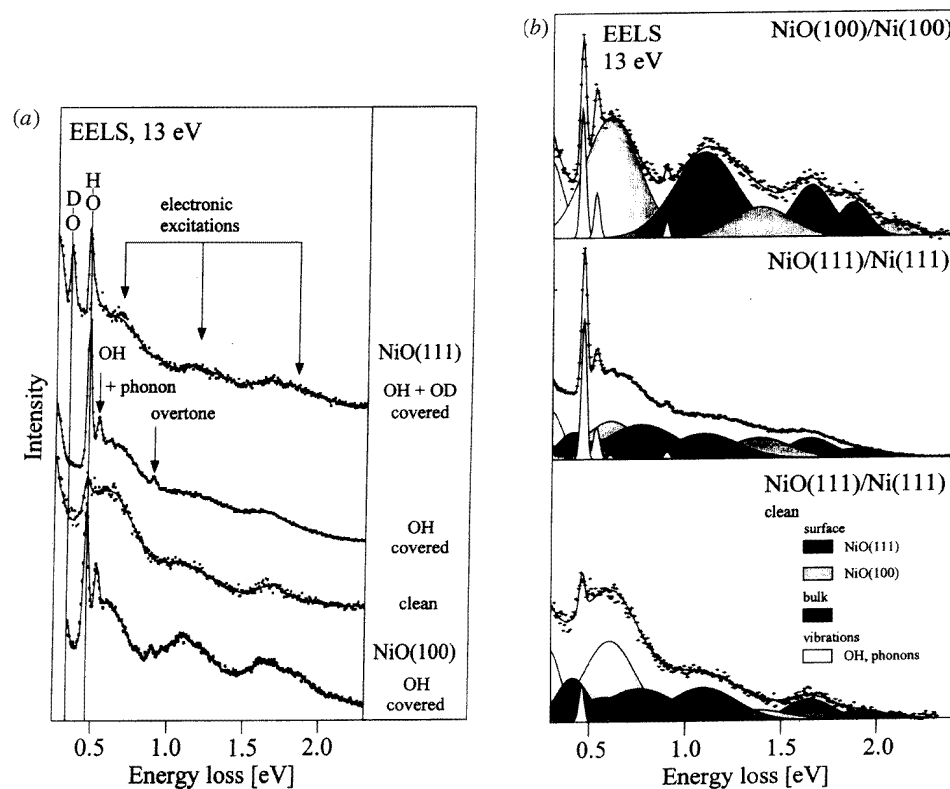


Figure 25. (a) EELS spectra of NiO(100)/Ni(100) and NiO(111)/Ni(111) with and without adsorbed hydroxyl groups. (b) Fits of some of the spectra shown in figure 24(a). Result of *ab initio* calculations by Freitag and Staemmler [82] for Ni²⁺ ions in NiO have been used as starting inputs for the calculations.

with the lattice oxygen feature.

As monitored via EELS and XPS, the hydroxyl groups can be removed to a large extent by a simple heat treatment. Figure 25(a) also shows the EEL spectra after removal of the majority of the hydroxyl groups. Due to the larger number of Ni ions in (100) coordination in the reconstructed surface, the spectrum is more similar to the one of the (100) surface. In conjunction with this change in composition, changes in the LEED patterns are observed. Figure 26(a) shows a two-dimensional SPA-LEED pattern of the oxide film taken at an electron energy of 80 eV. This pattern corresponds to the $p(1 \times 1)$ NiO pattern in figure 2. The distortion of the symmetry of the pattern is due to the experimental arrangement in the SPA-LEED setup. If the sample is heated to slightly above 600 K we see changes in the intensity distribution of the LEED pattern. Figures 26(b) and (c) show SPA-LEED patterns taken at two different electron energies because there is considerable variation of spot intensity with electron energy. At 65 eV electron energy the fractional-order $p(2 \times 2)$ spots in the second Brillouin zone are intense, while the fractional-order (2×2) spots in the first Brillouin zone and the integral-order spots have very low intensity. At 78 eV electron energy, on the other hand, intense integral-order and first-order $p(2 \times 2)$ spots are found. Even though the SPA-LEED patterns are distorted, it is clear that the $p(2 \times 2)$ NiO spots are not located near the positions of the sharper $p(2 \times 2)$ O/Ni(111) spots reported in [70].

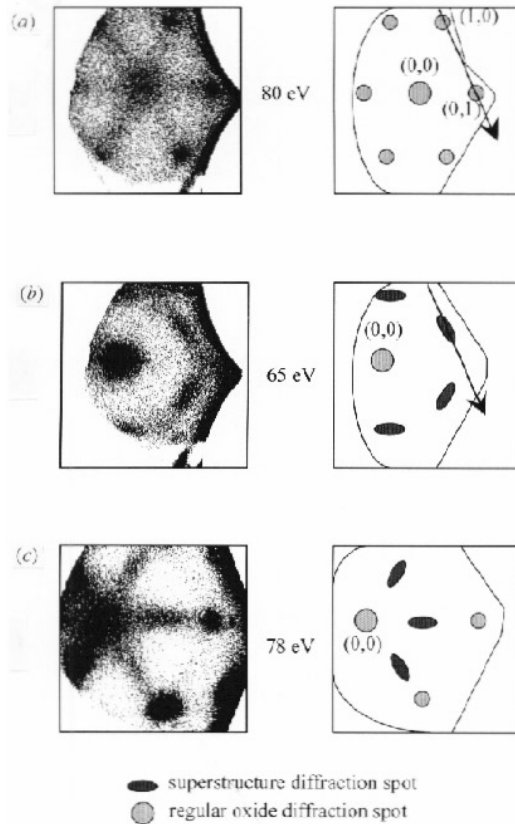


Figure 26. SPA-LEED patterns of NiO(111)/Ni(111). (a) Unreconstructed surface; (b), (c) $p(2 \times 2)$ reconstructed surface.

Therefore, the $p(2 \times 2)$ reconstruction is clearly connected with the NiO lattice. A detailed structure determination, however, has not been undertaken yet. One reason is the sensitivity of the substrate towards the impinging electron beam in commercial standard LEED systems. Channel-plate LEED systems [204] have to be set-up which operate with electron currents in the nano ampere regime, with which one shall be able to tackle this problem in the near future. It is very likely that the present $p(2 \times 2)$ reconstruction is of the octopolar type predicted earlier and schematically shown in figure 9.

The patterns are rather diffuse but various attempts to find optimal preparation conditions to form a well ordered structure failed. The $p(2 \times 2)$ fractional spot intensity is sensitive to the background pressure, while the integral-order structure is rather insensitive. In fact, after several hours the fractional $p(2 \times 2)$ spots are strongly attenuated. The same result can be obtained if we expose the $p(2 \times 2)$ structure to 0.3 L (Langmuir = 10^{-6} Torr s) H_2O . The process is completely reversible and may be cycled. Therefore, it is experimental fact that the NiO(111) surface reconstructs after the OH covered surface has been heated to 600 K. This reconstruction does not lead to a well ordered surface as indicated by the large spot widths. Nevertheless, the process is perfectly reproducible in every preparation cycle. The reconstruction can be lifted upon exposure to water, and this process is also reversible.

It is quite probable that the sensitivity of surface structure to the presence of water on

the surface has general consequences for the reactivity of the oxide surfaces. It has been demonstrated [201] that the number of adsorbed NO molecules—as monitored via thermal desorption—increases by about a factor of three after desorption of the hydroxyl groups. In addition, high-temperature desorption of NO (above 400 K) is observed indicating the reaction of adsorbed NO, tentatively to NO₂ for example. In this sense, water steers the reactivity of the oxide surface and in particular the polar surface patches as a function of surface temperature where the temperature for OH desorption sets the threshold to activate the sample. Whether this observation is relevant to catalytic processes, is not clear at present but there are indications that the catalytic activity of NiO catalysts prepared through topotactic dehydration of Ni(OH)₂, i.e. by forming crystallites with (111) orientation [205], is strongly influenced by water in the gas phase and on the sample. If the NiO(111) surface is prepared on a substrate with smaller lattice mismatch, e.g. a Au(111) surface, the LEED patterns observed are considerably sharper [80, 81]. The p(2 × 2) structure, as discussed above, is found and the surface is stable with respect to water adsorption. This may be due to the finite thickness of the film (approximately four layers) so that electrostatic arguments are less important.

CoO(111)/Co(0001) The LEED patterns of the clean Co(0001) surface exhibit sharp spots in contrast to the oxidized surface, which shows the more diffuse LEED spots typical for a CoO(111) surface formed via oxidation [71, 206–208]. The situation is thus very similar to the one encountered for NiO(111). HREEL spectra in the vibrational regime again indicate the presence of hydroxyl groups as the only observable adsorbed chemical species [71, 208]. As in the case of the NiO(111) surface it is possible to exchange the hydroxyl groups partly via D₂O exposure at higher temperature. The conclusion from the EELS investigation is very similar to the one drawn for NiO(111): CoO(111) is covered with hydroxyl groups which stabilize the unstable clean (111) rock salt type surface. The next obvious step is to try and remove the hydroxyl groups by a heat treatment as in the case of the NiO(111) surface. However, so far it has not been possible to desorb the hydroxyl groups without partly destroying the oxide film. This is the main reason for not having been able to observe the p(2 × 2) reconstruction of the CoO(111) surface.

FeO(111)/Fe(110) The iron oxide system has been studied in detail in the past [61, 62, 71, 84, 202, 209–217]. Out of the many results we would like to mention the observation that a FeO(111) film, prepared epitaxially on a Pt(111) surface, exhibits a reconstruction to form a p(2 × 2) LEED pattern [61, 62, 71, 84, 202]. This is connected, as mentioned above, with the formation of Fe₃O₄ on the surface [203, 71]. The driving force for this surface reconstruction may be found in the phase diagram of the Fe–O system [218]. The thermodynamically stable phase under the given oxygen pressure and the limited Fe supply is the Fe₃O₄ phase. However, if the films, as discussed above, are not grown on top of a Pt(111) surface but rather on a Fe surface, e.g. on a Fe(110) surface, the situation is different. In this case the high iron concentration in the system [212, 219] will shift the equilibrium towards the FeO system according to



The LEED pattern of an oxidized Fe(110) crystal clearly shows a p(2 × 2) structure suggesting the formation of a Fe₃O₄ overlayer as in the case of the iron oxide film on the Pt(111) surface. The EEL spectrum indicates very little OH on the surface, only of the magnitude seen for the reconstructed NiO(111) surface [201]. However, while H₂O would remove the reconstruction in the NiO case, in the case of iron oxide we may actually grow a thick H₂O

film on the surface and remove it again without the formation of additional hydroxyl on the surface. This is revealed by XPS measurements [71, 209]. An answer to the question whether the surface is a Fe_3O_4 or a FeO overlayer may be found if we investigate the Fe 2p photoemission spectra. There are clear differences to be expected on the basis of the literature data. The Fe 2p spectra of Fe^{2+} , which is the only oxidation state in FeO, exhibit strong satellite features, while the mixed valence compound Fe_3O_4 does not exhibit intense satellites. Also, a slight shift of the main ionization line is observed [71]. On the basis of this fingerprint FeO and Fe_3O_4 may be differentiated. It is clear that the film grown on the Fe(110) surface contains Fe^{2+} as in FeO while the system grown on the Pt(111) surface is, indeed, a Fe_3O_4 layer.

5.2. Corundum type structures

As discussed above, the structural rearrangement in NiO(111) involves three layers of the oxide. The mass transport involved leads to a relatively disordered surface indicated by diffuse LEED superstructure spots. There are other polar oxide surfaces, however, where the creation of the most stable surface does not involve more than the top layer [6, 88, 90, 220, 221].

The (0001) surface of Cr_2O_3 , crystallizing within the corundum type has been recently studied in our laboratories in some detail [89–93]. If a Cr_2O_3 (0001) film is prepared on top of a Cr(110) substrate, LEED and x-ray diffraction have shown that high-quality oxide structures can be prepared [90, 222–224]. LEED diffraction data of a surface held at 100 K exhibit the typical hexagonal pattern as discussed in the section on structures. As the temperature is changed, the surface exhibits changes in the LEED pattern [92]. This is different from the rock-salt type (100) surfaces as discussed before, and we shall come back to this temperature dependence after we have investigated the surface states at lowest temperature.

Figure 27 shows EEL spectra taken from the clean, flashed oxide surface at different temperatures [92]. At 90 K the spectrum exhibits two signals at loss energies of ~ 1.2 eV and ~ 1.4 eV, denoted by A and B, respectively. They are accompanied by a broad feature C at about 1.8 eV. As the temperature rises, signals A and B loose intensity whereas the intensity of feature C increases. All three signals A, B and C lie in the regime of d–d transitions of chromium ions [88, 225] and we shall present a detailed assignment further below.

The EEL spectrum in the considered energy region changes dramatically when various adsorbates are present, i.e. peaks A and B vanish and peak C is attenuated [68, 89, 90, 92]. Thus we assign signals A through C to d–d transitions of surface chromium ions which are sensitive to the presence of adsorbates. Feature C may also contain some contribution from d–d excitations of bulk chromium ions in a distorted octahedral crystal field. This assignment is supported by optical spectra of bulk chromium oxide samples [226] as well as of ruby crystals [227] and is also in line with the observation that in the range of feature C some intensity remains after adsorbate formation. After the surface states have been identified the temperature dependence of the EELS data may be analysed by assuming that a Boltzmann ansatz is appropriate to describe the processes (which could be debated). Then it is possible to plot the logarithm of the quotient of intensities of feature A and feature C against $1/T$. From the slope an energy difference of 8 meV between the state of the surface characterized by feature A and the state of the surface characterized by feature C has been deduced [228]. This energy is of the order of magnetically dominated interactions.

On the basis of such observations, a model has been proposed which explains the

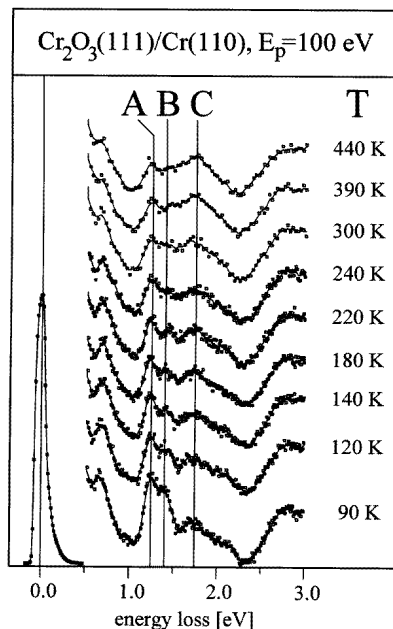


Figure 27. EELS spectra of $\text{Cr}_2\text{O}_3(111)$ as a function of temperature.

structural changes on the clean chromium oxide surface. We consider the low temperature (90 K) phase to be the ideal $\text{Cr}_2\text{O}_3(0001)$ surface with half a layer of Cr^{3+} ions present at the surface as shown in figure 14. This leads to the (1×1) LEED pattern in figure 12. Upon raising the temperature above 100 K, a $(\sqrt{3} \times \sqrt{3})R30^\circ$ structure appears, indicating a larger unit cell (figure 12(b)). The low transition temperature of 150 K already provides evidence that the process is connected with a relatively low activation energy. As a rule of thumb one would estimate activation energies in the range of 0.3 eV, which would be consistent with surface diffusion processes. The kind of structure resulting from such diffusion processes is indicated in figure 28. There are several reasons why such a structural rearrangement may take place, which are connected with the question about the most stable surface site.

We start with the situation at lowest temperature where the Cr^{3+} ions are all at equivalent sites. These sites could be those also occupied in the bulk (site 1, figure 14). There are two more threefold sites (sites 2 and 3, figure 14) which are available for occupation. One of course, is the other site occupied in the bulk (site 2). It is characteristic for this site that there is never a Cr^{3+} ion in the second layer below the top oxygen layer. The second alternative is the site characterized by an open oxygen triangle (site 3). There are Cr^{3+} ions in the second layer below this site. The question is, which is the most stable site populated at lowest temperature. EELS data in comparison with the theoretical calculations indicate that the outer Cr^{3+} sites (site 1) are occupied at lowest temperature. Each surface Cr^{3+} ion has a direct counterpart in the next layer down. If a magnetic coupling in the first layers similar to the bulk situation is assumed, then there is antiferromagnetic coupling to the second Cr layer of the order of 12 meV [229], but within the topmost layer the Cr ions are ferromagnetically or very weakly antiferromagnetically coupled. The magnetic coupling that is important in this case, is between the topmost Cr^{3+} layer and the one below the quasi-hexagonally packed O_2 layer. Locally, this means that two Cr^{3+} ions are exchange

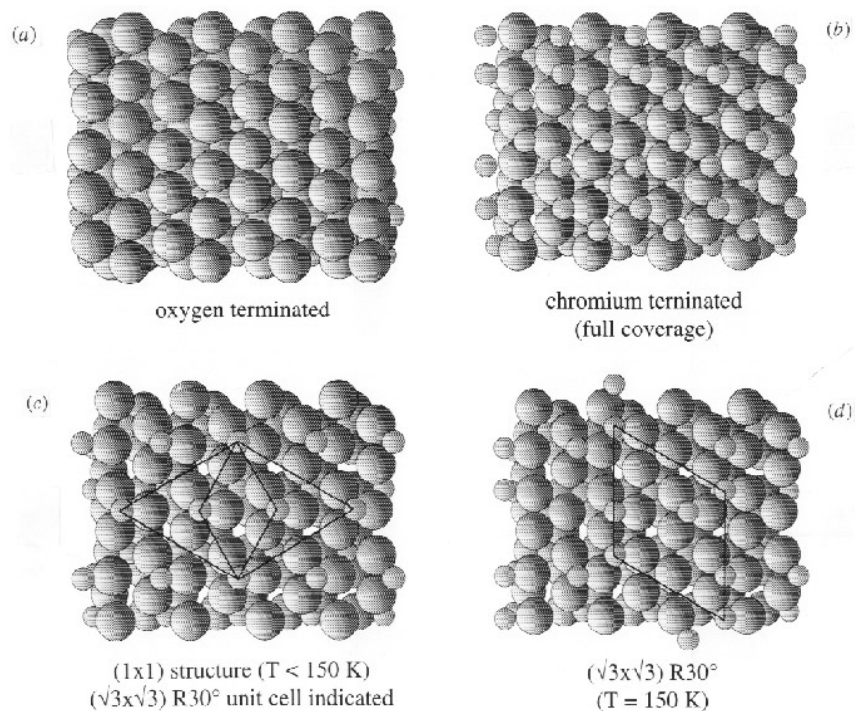


Figure 28. Four different terminations of the chromium oxide surface. (a) By a close oxygen layer. (b) By a full chromium layer. (c) By half a chromium layer with the (1×1) and $(\sqrt{3} \times \sqrt{3})R30^\circ$ unit cells shown. (d) As (c), but with half of the chromium ion hopped to a different site (site 3 in figure 14), which gives rise to the indicated $(\sqrt{3} \times \sqrt{3})R30^\circ$ unit cell.

coupled via three oxygen ions forming a $\text{Cr}^{3+}\text{-O-Cr}^{3+}$ angle of approximately 85° . This situation is similar to a binuclear Cr^{3+} complex where the transition metal ions are bridged by three hydroxyl groups. In this latter case the exchange splitting has been measured to be 8 meV [230]. This energy has to be surmounted to magnetically decouple the ions. If the temperature is raised, half or less of the Cr^{3+} ions at the surface may be decoupled from the second layer and may change site. Consequently, a larger unit cell with a $(\sqrt{3} \times \sqrt{3})R30^\circ$ unit mesh is observed. A schematic representation is shown in figure 28(d). As is revealed by the schematic drawing, the Cr^{3+} ions reside only at sites that have a second Cr^{3+} ion underneath in the second layer, i.e. site 1 or 3. There are basically two reasons for this. Primarily, the thermal dependence of the EEL spectra is consistent with this occupation. The intensity of the surface peaks A and B goes down indicating that the occupation of site 1 is reduced. Since site 2 is not stable with respect to the motion of the Cr^{3+} through the oxygen plane into the second layer, the Cr^{3+} ions can only move to the stable site 3. Secondly, there is an antiferromagnetic coupling among the Cr^{3+} ions in each Cr layer, which is about half as large as through the $\text{Cr-O}_3\text{-Cr}$ bridge [230]. Therefore, each ion is antiferromagnetically coupled within the top layer and also with respect to the second Cr^{3+} ion layer down. Such effects may represent the driving force for the process to occur. The energy differences between differently magnetically coupled states are of the order of 6 meV [163] compatible with our temperature dependent EEL spectra. At room temperature the two different stable Cr^{3+} sites at the surface are statistically occupied, giving rise to a unit mesh typical for a lattice gas. This again leads to a $p(1 \times 1)$ structure with very diffuse

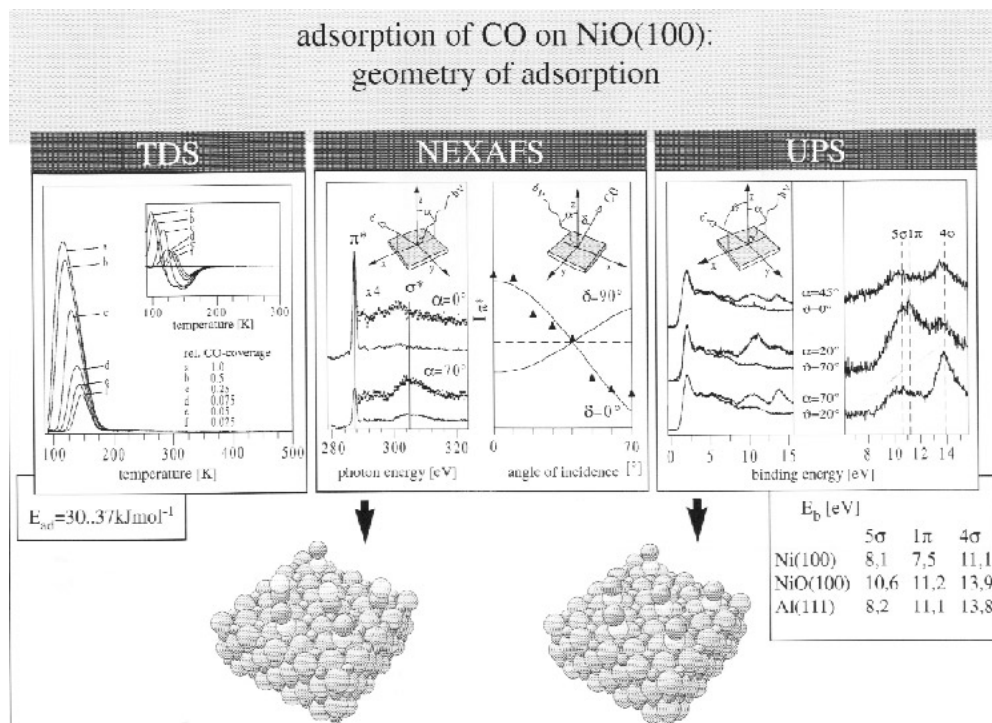


Figure 30. (a) Thermal desorption spectra of CO/NiO(100)/Ni(100) as a function of CO coverage. The inset shows the derivatives of the spectra. (b) Carbon *K*-edge NEXAFS spectra of CO/NiO(100)/Ni(100) as a function of the light incidence angle as indicated in the inset. (c) Angle-resolved photoelectron spectra of CO/NiO(100) in comparison with spectra of the clean surfaces for different experimental geometries.

6. Adsorbates on oxides

In the previous paragraphs we have made use of the change of certain properties induced by the interaction of molecules with oxide surfaces. However, we have not answered questions as to how these molecules bind towards the surface. For metal surfaces the most studied adsorbate is carbon monoxide. In order to make contact with the studies on metal surfaces, it is useful to consider the interaction of CO and NO with the non-polar (100) surfaces of simple rock-salt type materials. Notably, the discussion [7] on the electronic and geometric structure of adsorbates on such surfaces has profited considerably from an intense exchange between theoreticians [137–140, 231–235] and experimentalists [63, 64, 236–251] not only including single crystal surfaces but also on well characterized powder samples [252–254]. As discussed above, from the theoretical studies a clear picture for the bonding of, for example, carbon monoxide towards NiO(100) or MgO(100) has emerged, even though there still seem to be unresolved problems with respect to the theoretical reproduction of the experimentally observed enthalpy of adsorption [137–140, 231–237]. Contrary to metal surfaces, where bonding is strong ($\Delta E_a \approx 1\text{--}2 \text{ eV}$) due to σ/π -charge exchange between the molecule and the surface [171, 252], bonding to a (100) oxide surface of rock-salt type is dominated by multipolar electrostatic forces, which leads to rather weak bonding ($\Delta E_a \approx 0.1\text{--}0.5 \text{ eV}$). As a consequence of the rather weak bonding, energy differences between various orientations of molecules, i.e. bonding of CO with its C-end against its

O-end towards the surface or parallel to the surface, are rather small and of the order of 0.05–0.1 eV [138, 150, 235]. Since these energy values are well within the error range of the theoretical predictions, experimental studies are needed. Figure 30(a) shows the TPS spectra of CO/NiO(100) as a function of coverage. The spectra indicate indeed rather weak bonding between the CO molecule and the NiO surface, contrary to typical CO adsorbates on metal surfaces. The chemical bonding between CO and the oxide surfaces is dominated by long-range electrostatic effects and short-range Pauli repulsion. There are several reasons responsible for this bonding mechanism as has been discussed by Pöhlchen and Staemmler [137] and summarized in the theoretical part of this review.

Since there is no argument favouring a particular orientation, the orientation has to be determined experimentally and separately for each oxide system. Figure 30(b) shows an example of how such an experimental study would be carried out. X-ray adsorption spectra taken near the C–K edge using polarized light from a storage ring allow us to use symmetry selection rules and determine the orientation of the CO axis from an angle dependent experiment [73, 253]. The question whether the molecule is oriented C-end or O-end towards the surface, can be answered via photoelectron spectroscopy. The idea is to determine the shift of the valence ionizations of CO with respect to the gas or condensed CO phase. From figure 30(c) we conclude that the 5σ ionization, located mainly on the carbon atom of the molecule, is shifted with respect to the 1π and 4σ ionizations, indicating that the interaction with the surface takes place through the carbon end of the CO molecule. It is surprising that this shift is so large (~ 2.0 eV) though the adsorption energy ΔE_a itself is quite small (0.3–0.5 eV [73] and first reference in [241]). Again, it is the electrostatic interaction between the oxide surface and CO that stabilizes the 5σ orbital [73, 254]. This effect is nearly as strong as for CO chemisorbed on metals, but the origin of the shift is different, because for CO on metals the 5σ orbital is stabilized by σ -donation, i.e. by a moderately strong chemical bond [171].

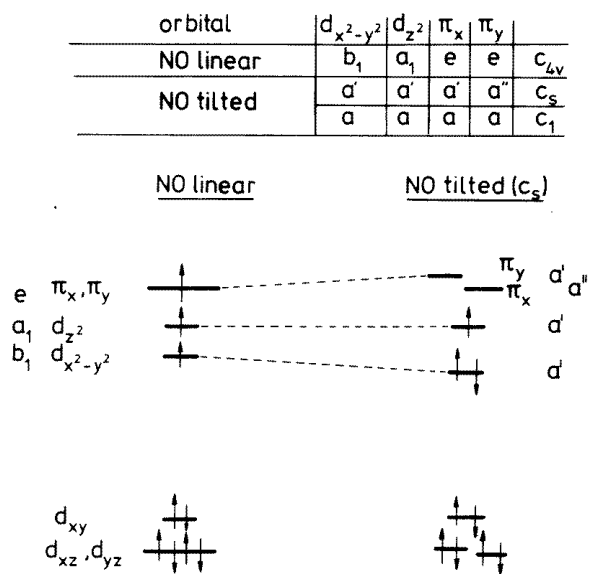


Figure 31. One-electron scheme of the Ni 3d and NO 2π levels for NO adsorbed on NiO(100) in a linear and a bent configuration.

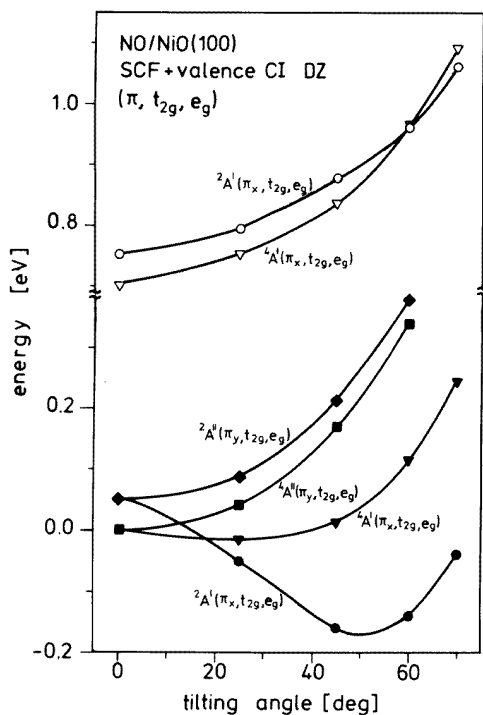


Figure 32. Calculated energies of a NO–NiO₅ cluster for some electronic states as a function of the tilting angle of the NO molecule. Energies are referenced relative to the ground state of NO adsorbed in a linear configuration.

The adsorption properties of CO/NiO(100) may be compared with those of NO/NiO(100). The latter system is slightly more strongly bound, i.e. by 12.2 kcal mol⁻¹ as determined from similar TD data [63]. The higher adsorption energy for NO reflects the different bonding characteristics with respect to CO. This has been predicted by several theoretical calculations and for this comparison in detail by Staemmler and his group [137, 138]. While CO is held almost exclusively by multipolar electrostatic interactions, NO bonding to NiO(100) does exhibit some covalent chemical bonding contributions. *Ab initio* cluster calculations on a NiO₅⁸⁻ cluster embedded in a semi-infinite array of point charges and interacting with a single NO molecule being bound via the N atom to the Ni site, see figure 18(b), may be used to illustrate the reasons [63, 127, 164]. In figure 31 the results are presented in a simplifying one-electron picture. For a perpendicularly oriented NO molecule the relevant part of the MO scheme is shown in the left part: the Ni 3d levels are split into a set of three closely spaced fully occupied orbitals, the remnant of the t_{2g} orbitals in octahedral NiO₆, and an only slightly split subset of two singly occupied Ni 3d orbitals remnant of the e_g orbitals in octahedral NiO₆. Above the Ni levels the singly occupied NO 2π orbital is situated. The three unpaired electrons may be coupled to form quartet and doublet states. The ground state turns out to be the quartet state. NO 2π and Ni orbitals transform according to different irreducible representations of the C_{4v} point group as indicated in figure 31. Consequently, the bonding interaction is very weak if there is any at all. However, if the NO molecular axis is tilted the symmetry is reduced, and the irreducible representations change. Now, one component of the NO 2π

transforms according to the same irreducible representation as the Ni 3d levels and there will be mixing, i.e. formation of bonding and antibonding orbitals. This leads to a stabilization of the lowest Ni 3d level. If this level is doubly occupied the system gains energy and is stabilized. Thus, in this simple one-electron scheme a bent configuration is the stable arrangement. Detailed calculations show that the true wavefunction is a superposition of electronic configurations of which the one in figure 31 is only one component. Figure 32 shows the results of a configuration interaction calculation on the above system where the binding energies for some low lying electronic states are plotted as a function of the angle between the molecular axis and the surface normal. While for a vertical geometry the 4E state is the ground state of the system, the ${}^2A'$ component of the excited 2E state in a vertical geometry is stabilized in a tilted geometry as predicted on the basis of the simple one-electron picture. At about 45° tilting the energy has a minimum. Near-edge x-ray absorption fine structure (NEXAFS) measurements using a tunable synchrotron light source may be used for molecular structure determination. Our NEXAFS studies for NO/NiO(100) [63] indicate indeed a strong inclination of the molecular axis of about 40° with respect to the surface normal, thus corroborating the theoretical predictions very convincingly. We think that this predicted and observed bending of the NO–Ni bond axis represents strong evidence for a chemical bonding component in this system with a clear preference for the N end oriented towards the Ni ion.

The covalent component of the bonding is also reflected in the vibrational properties of CO compared to NO. In figure 33 the NO and CO stretching vibration frequencies on the various surfaces investigated are compared. Firstly, it can be seen that all NO frequencies are shifted towards smaller values compared to the gas phase, whereas all CO frequencies lie at or close to the gas phase value. As mentioned above, this reflects the bonding. CO is weakly, electrostatically bound and the frequency of the CO stretching vibration is close to gas phase value. Interestingly, this is truly independent of surface orientation and whether the surface is hydroxyl covered or reconstructed. NO exhibits a covalent contribution leading to a change in 2π population, which in turn changes the stretching vibration frequencies. On the clean oxide surfaces, whether regularly structured or reconstructed we do find similar stretching frequencies. However, for NO, the coadsorbed hydroxyl species lead to noticeable differences. For the case of CoO(111) we were able to find indications for the existence of interactions between adsorbed species (eg. NO and CO) which may be the reason for the observed systematics [237].

In all cases discussed so far we have strong indications that the molecular axis is oriented perpendicularly to the surface plane or only moderately tilted. However, there are also cases where we have experimental evidence for a strongly inclined bonding geometry. CO/Cr₂O₃(0001) is such a case. Figure 34 shows photoelectron spectra of the $(\sqrt{3} \times \sqrt{3})R30^\circ$ CO structure, recorded for various collection geometries as indicated in the figure, in comparison with a normal emission spectrum of a physisorbed monolayer CO on Ag(111) [255]. There are two CO induced features visible in the spectra of the CO adsorbate on Cr₂O₃(0001); one at 17.5 eV and a slightly asymmetric one at 20.2 eV. The CO σ valence emission should be intense at the photon energy the spectra have been taken with, i.e. 36 eV, whereas the 1π emission should be rather weak. Thus we identify the two CO induced features as the σ -ion states of molecularly adsorbed CO.

The electronic binding energies of CO on Cr₂O₃(0001) are larger by several eV compared to those of the CO physisorbate on Ag(111). This holds also for CO adsorbates on other metals (see for instance [185, 255, 256]), indicating that the substrate–CO interaction on Cr₂O₃(0001) is appreciably different from that on metals and on the (100) surfaces of cubic oxides.

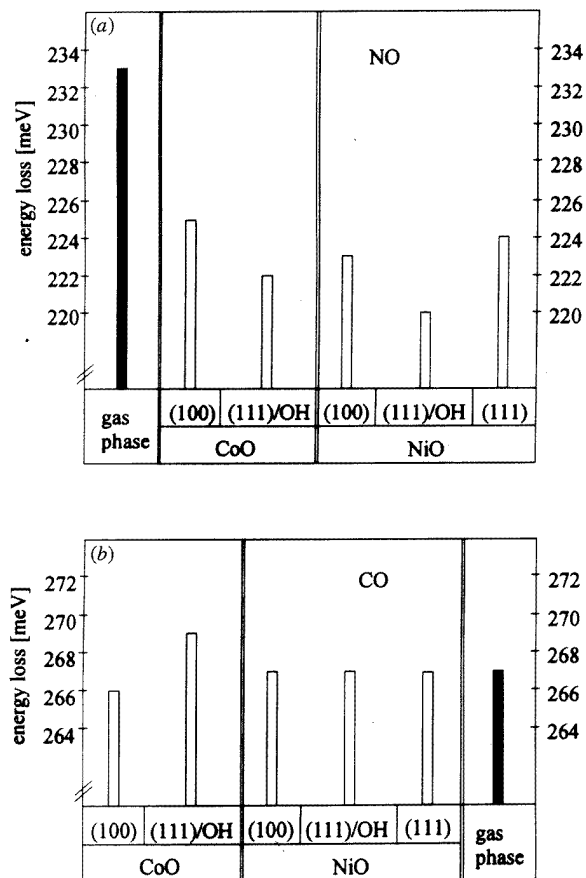


Figure 33. Energies of the NO (a) and CO (b) stretching vibrations on different CoO and NiO surfaces in comparison with gas phase data [75].

From the data in figure 34 information on the orientation of the molecular axis can be deduced. This figure displays a set of photoelectron spectra taken with a constant angle, i.e. 90° , between the directions of light incidence and electron detection.

From figure 34 it is obvious that the σ -ion states exhibit the highest intensities for near normal light incidence and near grazing electron emission $\alpha = 0, \vartheta = 90^\circ$ whereas at grazing light incidence these features are strongly attenuated, in strong contrast to CO adsorbed standing up on most metal surfaces. Since at a photon energy of 36 eV the σ states emit with highest intensity if the polarization direction and the direction of electron detection both coincide with the CO molecular axis, this behaviour is only compatible with an orientation of the molecular axis approximately parallel to the surface.

In the inset of figure 34 we compare the emission intensities of the CO σ valence states as a function of photon energy for two different experimental geometries. The data shown in the upper panel were taken at a light incidence angle of 20° with respect to the surface normal, collecting the electrons 70° off normal whereas the data in the lower panel were taken at normal electron emission and near grazing light incidence ($\alpha = 80^\circ$). Obviously a strong σ shape resonance is observed only for grazing electron detection, again clearly indicating that the CO molecules must be strongly tilted.

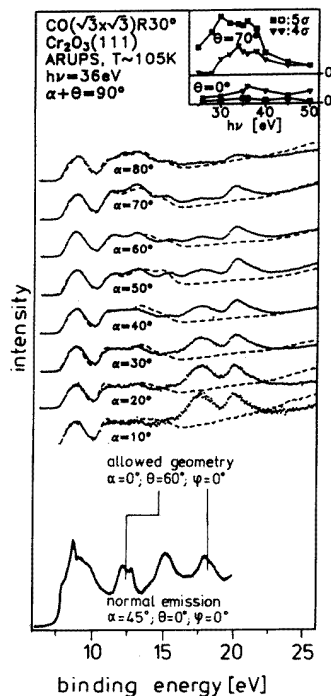


Figure 34. Series of angle resolved ultraviolet photoemission spectra for CO adsorbed on $\text{Cr}_2\text{O}_3(111)/\text{Cr}(110)$. The angle between the light incidence direction and the electron detection direction has been kept at a fixed value, i.e. 90° (α is the angle of light incidence with respect to the surface normal). For comparison a spectrum of CO on $\text{Ag}(111)$ is shown at the bottom. Binding energies are given relative to the vacuum level. *Inset.* The emission intensities of the CO valence bands as a function of the photon energy for grazing incidence and near perpendicular electron detection (bottom) and near perpendicular light incidence, detecting the electrons at a grazing angle (top).

The same conclusion about the molecular geometry must be drawn from the analysis of our NEXAFS data [90]. These data show that the intensity of the π resonance varies only slightly as a function of the light incidence angle as expected for CO molecules lying flat on the surface since one 2π component is oriented parallel to the surface whereas the other one sticks out of the surface. A quantitative estimation of the tilting angle was not possible from our NEXAFS data since the σ resonance was so weak that its intensity could only be evaluated with very large error bars. Tentatively we estimate this angle to be larger than about 70° .

An open question is: where are the 1π orbitals? For flat lying CO molecules the 1π levels are expected to split into two components, $1\pi_{xy}$ and $1\pi_z$, the first one oriented parallel to the surface and the other oriented perpendicular to the surface. Whereas the $1\pi_{xy}$ emission might be hidden below the σ emissions because this level should be intense at grazing emission angles like the σ orbitals, the $1\pi_z$ should be intense at normal emission where the σ emission is weak. As can be seen from figure 34 the 5σ emission is nearly totally suppressed at near normal electron emission so that the $1\pi_z$ level is most likely not situated near to the 5σ level as is the case for the 1π levels of CO adsorbed on most metals. One might suppose that the $1\pi_z$ orbital would interact strongly with these bands it is most likely to have been shifted to higher binding energy because the substrate levels are energetically located above the 1π levels. Considering this it seems to be rather unlikely that the 1π levels are located somewhere in the region of the oxide emission.

Whereas the 5σ emission is nearly totally suppressed at near normal emission, a broad feature remains in the region of the 4σ between 19 and 22 eV (figure 34). Since the 4σ and the 5σ emission intensity should behave similarly, it is tempting to attribute the remaining emission between 19 eV and 22 eV to the $1\pi_z$ level. Another possible assignment would

be that this feature is due to a σ shake up state. However, we consider this to be unlikely because such shake up states should be intense at emission angles where the σ main lines are also intense, which is not the case. All binding energies are larger than the corresponding values known from metal surfaces [90]. They are even larger than the gas phase values. This holds also for the C 1s ionization which is found 0.7 eV below its gas phase value [90]. The most interesting finding, however, is the energetic position of the $1\pi_z$ level, which is in the present case most probably situated near to the 4σ level, indicating a fundamentally different interaction of the molecule with the surface as compared with all cases observed so far. We propose that the CO lone pairs (4σ and 5σ) are bound towards two different Cr ions in the sense of two electrostatic interactions which shift the σ binding energies to higher values. If this is true then it is very reasonable to assume that the 1π levels interact predominantly with the oxygen layer underneath the terminating Cr layer. This latter interaction between the closed shell O_2^- ions and CO must be basically repulsive. Since the oxygen levels are situated at lower binding energies than the CO 1π levels, the $1\pi_z$, which is the one that strongly interacts with the O_2^- ions, is shifted towards higher binding energy and the interacting O_2^- levels are rearranged as well. The shift of the $1\pi_z$ level is recognized in the data, while it is more difficult to identify the effect on the oxygen levels. If we compare the observed shifts of CO on $Cr_2O_3(0001)$ with those of gaseous CO we find a shift of all CO levels to higher binding energies. The shift of the 5σ level is larger than the one of the 4π level. This is very reasonable because it follows the individual polarizabilities of the levels involved. The interaction may be separated into the two bonding Cr–CO(5σ) and Cr–OC(4σ) interactions, and into a repulsive O_2^- –CO(1π) interaction, leading to a weakly chemisorptive CO– Cr_2O_3 bond. The bonding of CO towards $Cr_2O_3(0001)$ is completely different from the bonding of CO to a metallic Cr surface. It is a pure accident that CO binds to metallic Cr in a flat bonding geometry as well.

While on the transition metal oxide surfaces, CO molecules exhibit desorption temperatures above 100 K indicating an interaction with the substrate more substantial than physisorption, which would be dominated by van der Waals interactions, the interaction of CO with an Al_2O_3 surface turns out to be considerably weaker, of the order of 0.14–0.17 eV [96,97].

In figure 35 we show the EEL spectrum ($E_p = 18$ eV) of a CO multilayer on the $Al_2O_3(111)/NiAl(110)$ substrate [96,97]. In the lowest trace we see on the left the elastic peak, and, due to the relatively low resolution, only a slight indication of the Al_2O_3 phonons (see [39] for a well resolved phonon spectrum) followed by the CO vibrational stretch loss in its electronic ground state. At 6 eV (note the change in energy scale) losses due to excited states start. The assignment of the spectrum is rather straightforward for the adsorbate because it compares favourably with the gas phase spectrum, shown for comparison [257]. A detailed assignment of the progressions is shown in the inset. In the following we shall consider in more detail the optically forbidden (but allowed in electron scattering) progression of the $a^3\Pi$ state. The population of the $a^3\Pi$ state involves primarily the excitation of a 5σ electron into the 2π orbital.

Figure 36 shows a set of EEL spectra of this excitation as a function of coverage. Clearly, as has been discussed in detail elsewhere [96], there is a pronounced intensity of this excitation visible in the monolayer regime. The line width at 0.2 L exposure is rather large, but the remaining structure allows us to fit (least square) a single Franck–Condon distribution to the peaks. The TPD spectra at this dose suggest the presence of a single species. Increase to 0.3 L leads to the appearance of a peak at 58 K desorption temperature in the TPD spectra. This new state should have its own characteristic Franck–Condon distribution. The fit therefore shows two distributions: one due to the one determined

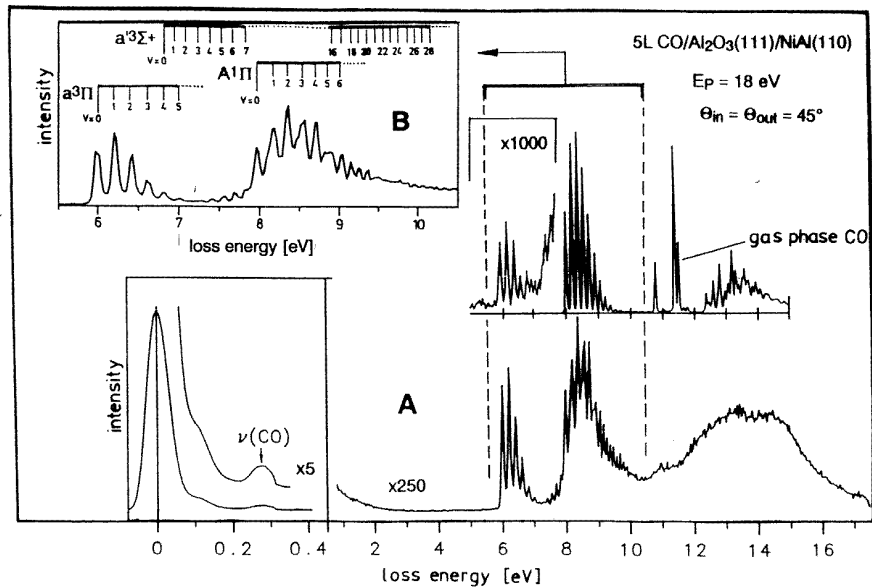


Figure 35. Electron energy loss spectra at $T = 35$ K of a CO multilayer on $\text{Al}_2\text{O}_3/\text{NiAl}(110)$ in comparison with a gas phase spectrum [97]. An enlarged view of the vibrational progressions is shown in the top inset. Note, that the vibrational loss part is plotted on an expanded energy scale.

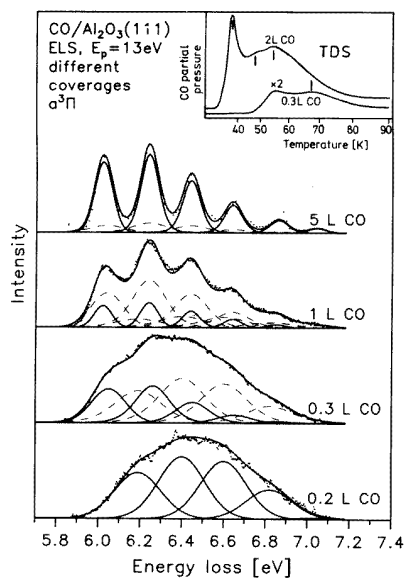


Figure 36. Electron energy loss spectra at $T = 35$ K of $\text{CO}/\text{Al}_2\text{O}_3/\text{NiAl}(110)$ in the range of the $\text{Co } a^3 \Pi$ excitation as a function of coverage. Relevant TD spectra are shown in the inset.

from the 0.2L exposure, which was then fixed and a second one which was optimized to fit the total progression at 0.3L exposure. This second progression is clearly shifted with

respect to the first one by 170 meV as indicated by the line. At 1 L exposure the multilayer progression starts to contribute. It is only shifted by 25 meV with respect to the second progression. In total, the multilayer signal is shifted with respect to the most strongly bound excitation by 195 meV.

This leads to the following immediate conclusions. The electronic ground state of CO molecules most strongly bound to the surface is stabilized through interaction with the substrate by 0.19 eV, i.e. with respect to the multilayer by 0.11 eV. Since the excitation energy for the monolayer species is larger by 0.195 eV compared with the multilayer, the excited state must be destabilized by 0.085 eV. One reason for this destabilization may be the expected stronger repulsion between molecule and substrate because population of the 2π orbital increases the average size of CO and leads to a more pronounced Pauli repulsion between CO and the top oxygen layer of the substrate which behaves electronically like a layer of rare gas atoms ($\text{Ne} \leftrightarrow \text{O}_2^-$). Since the CO molecule is physisorbed on Al_2O_3 we have assumed in this case that the potential curve of the adsorption CO in the $a^3\Pi$ state is very similar to the gas phase. We can provide evidence for this by performing a Birge-Sponer analysis for the multilayer progression. From this analysis we can determine the dissociation energy and the anharmonicity in comparison to the gas phase. The well depths are the same within the experimental error while the anharmonicity seems to be slightly increased with respect to the gas phase [258].

Table 4. Experimentally determined molecular parameters of three different CO species on $\text{Al}_2\text{O}_3/\text{NiAl}(110)$.

Species	Adsorption enthalpy [meV]	FWHM [meV]	$E(v' = 0)$ [eV]	$E(v' = 1) - E(v' = 0)$ [meV]	Lifetime [10^{-15} s]
$T_{\text{des}} = 67$ K	-170	260	6.19	210	2.5
$T_{\text{des}} = 55$ K	-140	190	6.04	200	3.5
multilayer	-88	70	6.02	200	9.5
gas phase [257]			6.02	202	some ms
1 ml CO/Ag(110)	≈ -150	large	?	?	small

Next, we consider the line widths of the observed spectra. Table 4 collects the important information. We have discussed this in detail in [96] and will not repeat the rather involved discussion. We want to comment that the observed lifetimes are rather large compared to the time electronic excitations need to occur. The reason may be that the energy of the $a^3\Pi$ state is not sufficient to excite electron hole pairs in the substrate considering the large gap size of 9.5 eV. The situation is very different on a metal surface. In figure 37 we compare the set of spectra on the Al_2O_3 substrate with a set of spectra of CO on Ag(110) [259]. While in the multilayer on the metal surface we observe spectra comparable with those on the oxide surface, it is clear that in the monolayer regime below 1.2 L exposure there is no excitation discernible from the background in the case of the metal substrate. The reason appears to be rather obvious: there is no band gap in a metal, energy dissipation through electron hole pair creation is not hindered and the line widths are very large.

In addition to CO adsorbates, O_2 adsorbates on Al_2O_3 at low temperatures have also been studied [97]. The interaction with the surface in this case is again very weak and the EELS data reveal that the spin coupling within the O_2 molecule prevails as it is adsorbed on the surface.

In addition to the investigation of molecular adsorbates, it is also interesting to study

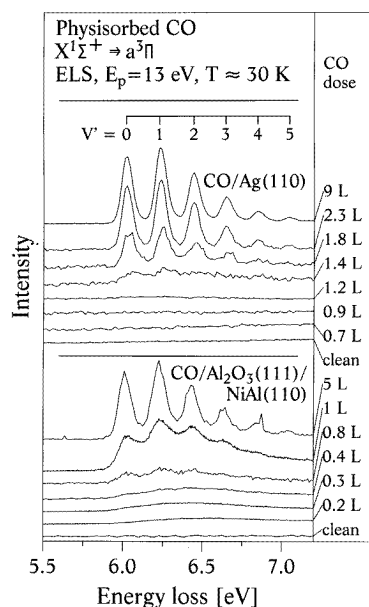


Figure 37. Comparison of EELS spectra ($a^3\Pi$) of CO on $\text{Al}_2\text{O}_3/\text{NiAl}(110)$ with spectra of CO on $\text{Ag}(110)$ at $T = 35\text{ K}$ as a function of exposure.

the adsorption of metals onto oxide surfaces. Several systems have been studied.

Detailed structural investigations on a variety of systems have been performed by Møller and his group [260–266]. $\text{Cu}/\text{TiO}_2(110)$ [260], $\text{Ni}/\text{TiO}_2(110)$ [261], including CO adsorption [262] $\text{Cu}/\text{Al}_2\text{O}_3(0001)$ [263], $\text{Cu}/\text{Zn}(1010)$ [5], $\text{Cu}/\text{Zn}(1010)$ [265], and $\text{Cu}/\alpha\text{-Fe}_2\text{O}_3(0001)$ [266], were studied just to name a few of the recent results published. Also other groups have made important contributions to field: Campbell and his group for the system $\text{Cu}/\text{ZnO}(0001)$ [267, 268], Gorte and collaborators for Rh [269], Pd [270], and Pt [271] on $\text{Al}_2\text{O}_3(0001)$. Madey and workers have dealt with different metals (Cu, Fe, Cr, Hf, Pt [272–275] on $\text{TiO}_2/110$). Henry *et al* [276–278] report studies for Pd on MgO. Various groups [279–284] have published data for Pd and Cu on $\text{Al}_2\text{O}_3(0001)$.

We have investigated Na deposition on $\text{Cr}_2\text{O}_3(0001)$ and on $\text{NiO}(111)$ and its consequences on the electronic structure of adsorbate and substrate. On the basis of bulk thermodynamic data one would expect that Na reduces both surfaces to the metallic state [285, 286]. While this is true for Na on $\text{NiO}(111)$ [285], it does not occur under any of the tested circumstances when we tried to reduce $\text{Cr}_2\text{O}_3(111)$ with metallic Na towards the metallic state [68, 91]. For Mg on the other hand, the free reaction energy towards reduction is large enough to induce the formation of metallic Cr on the Cr_2O_3 surface [286]. A detailed study of Na adsorption shows, however, that even though reduction of the metal is prohibited, the surface Cr ions are reduced in the oxidation state [286]. This is interesting because alkali as well as alkali earths are used as electronic promoters in catalytic reactions involving oxides.

Figure 37 shows the result of an EELS experiment [286], where a spectrum of clean $\text{Cr}_2\text{O}_3(0001)$ is shown as the bottom trace. The assignment of the various peaks have been discussed previously [88–92]. If a thick (several) layer of Na is deposited onto the $\text{Cr}_2\text{O}_3(0001)$ surface at 90 K, the substrate excitations disappear and two new bands are observed. As will be discussed in detail elsewhere [286], the band at 4.0 eV is due to

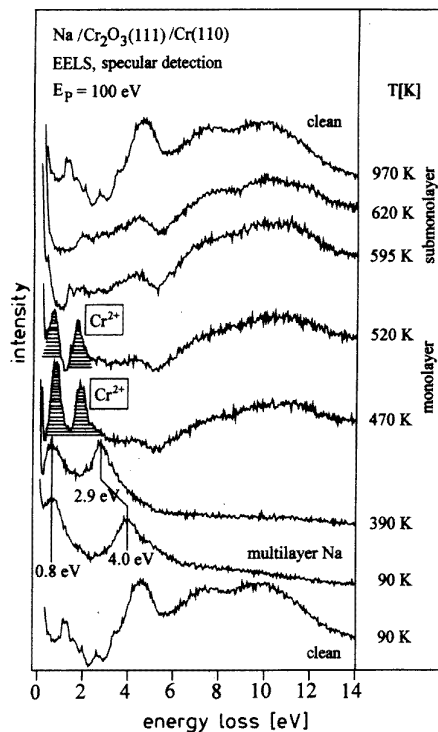


Figure 38. EELS spectra of clean and Na covered $\text{Cr}_2\text{O}_3(111)/\text{Cr}(110)$ as a function of the sodium coverage.

the Na surface plasmon [287] and the peak at 0.8 eV is assigned to an Na/oxide interface excitation [286]. Upon raising the surface temperature, some Na evaporates and the layer thickness is reduced, but it is still considerably larger than a monolayer. As is expected for thin metal films in contact with a dielectric on one side and vacuum on the other, the two interface excitations are coupled and they change energy as the thickness varies [288]. The Na surface plasmon changes energy considerably from 4.0 eV to 2.9 eV while the interface ($\text{Cr}_2\text{O}_3(0001)/\text{Na}$) only varies slightly from 0.8 eV to 0.7 eV. If the temperature is raised above 420 K the Na multilayer has completely been desorbed and we reach the monolayer regime. The spectrum taken at 470 K is characteristic for this situation. Substrate excitations between 6 and 14 eV are visible. However, in the d–d–excitation regime below 3.5 eV we find new sharp features. *Ab initio* calculations by Staemmler [92] have shown that a Cr^{2+} ion at a threefold site on a $\text{Cr}_2\text{O}_3(0001)$ surface has d–d excitations at exactly these energies. This allows us to propose that in the range of Na monolayer coverage the $\text{Cr}_2\text{O}_3(0001)$ surface is covered with a Cr^{2+} layer. With decreasing Na coverage parallel to increasing surface temperature, the Cr^{2+} d–d excitations reappear, and finally close to 1000 K the surface is Na free and the spectrum of the clean surface is revealed.

The results are summarized in figure 38, where the surface species are correlated with the temperature range where they exist. Above 600 K EELS does not directly indicate the presence of Na. Therefore results based on XPS measurements must be included in the discussion [285]. Due to the larger probing depth of the latter methods, the presence of a second non-metallic Na species is indicated. One of the two species appears to be localized at the surface, while the second one resides in the near surface region or in the bulk.

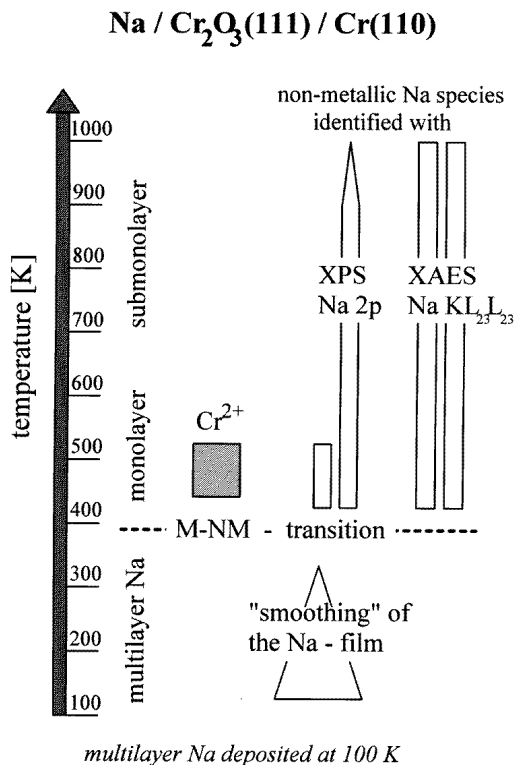


Figure 39. Existence range of different Na species on Cr₂O₃(111) as determined with different spectroscopies.

Similarly, AES shows the presence of two species, but both seem to be present in the bulk. It is therefore possible that three different non-metallic Na species exist in the system. Whether these species are connected with the formation of sodium chromate is not clear at present.

So far structural information on such systems is rather rare but this will be an active field in the future. It is important, however, to correlate the geometric information with investigations on the electronic structure. In this area a combination of electron spectroscopy with scanning tunnelling microscopy will lead to major new insights.

7. Synopsis and perspectives

We have reviewed the geometric and electronic properties of oxide surfaces and have concentrated mainly on the oxide films. Clean surface properties as well as adsorbate covered surfaces have been studied. The adsorbates covered molecular adsorbates and metal films. It will be important in the future to combine these studies and investigate molecular adsorption onto ultrathin metallic films. Some early steps in this direction have been taken, but much more has to come. With such studies we may be able to close the materials gap as indicated in figure 1 to a certain extent, and if we then could also work at higher pressures, we might be in a position to really contribute to an understanding of catalysis.

Acknowledgments

We are grateful to a large number of coworkers who have contributed over the years and who are mentioned in the references. We have profited from grants of the following agencies: Deutsche Forschungsgemeinschaft, Bundesministerium für Bildung und Forschung, Ministerium für Wissenschaft und Forschung des Landes NRW, European Communities (BRITE-EURAM, COST), the German–Israeli Foundation, as well as the Fonds der Chemischen Industrie.

References

- [1] Cox P A 1992 *Transition Metal Oxides. An Introduction to their Electronic Structure and Properties* (Oxford: Clarendon)
- [2] Johnson D A 1982 *Some Thermodynamic Aspects of Inorganic Chemistry* (Cambridge: Cambridge University Press)
- [3] Sorensen O T (ed) 1981 *Non-stoichiometric Oxides* (New York: Academic)
- [4] Hamnett A and Goodenough J B 1984 Binary transition metal oxides *Physics of Non-tetrahedrally Bonded Compounds* ed O Madelung, Landolt-Börnstein, New Series III, vol 17 (Berlin: Springer)
- [5] Owen J F, Teegarden K J and Shanks H R 1978 *Phys. Rev. B* **18** 3827
- [6] Henrich V E and Cox P A 1994 *The Surface Science of Metal Oxides* (Cambridge: Cambridge University Press)
- [7] Freund H-J and Umbach E (ed) 1993 *Adsorption on Ordered Surfaces of Ionic Solids and Thin Films (Springer Series in Surface Sciences, vol 33)* (Heidelberg: Springer)
- [8] Freund H-J 1995 *Ber. Bunsenges. Phys. Chem.* submitted
- [9] Kung H H 1989 *Transition Metal Oxides: Surface Chemistry and Catalysis* (Amsterdam: Elsevier)
- [10] Davidov A A 1990 *Infrared Spectroscopy of Adsorbed Species on the Surface of Transition Metal Oxides* (New York: Wiley Interscience)
- [11] Lacmann R 1965 *Colloq. Int. CNRS* **152** 195
- [12] Wolf D 1992 *Phys. Rev. Lett.* **68** 3315
- [13] Tasker J W 1979 *J. Phys. C: Solid State Phys.* **12** 4977
Tasker J W 1979 *Phil. Mag. A* **39** 119
- [14] Legg K O, Prutton M and Kinniburgh C 1974 *J. Phys. C: Solid State Phys.* **7** 4236
- [15] Kinniburgh C G 1975 *J. Phys. C: Solid State Phys.* **8** 2382
- [16] Prutton M, Walker J A, Welton-Cook M R, Felton R C and Ramsey J A 1979 *Surf. Sci.* **89** 95
- [17] Welton-Cook M R and Berndt W 1982 *J. Phys. C: Solid State Phys.* **15** 5691
- [18] Urano T, Kanaji T and Kaburagi M 1983 *Surf. Sci.* **134** 109
- [19] Blanchard D L, Lessor D L, LaFemina J P, Baer D R, Ford W K and Guo T 1991 *J. Vac. Sci. Technol. A* **9** 1814
- [20] Prutton M, Ramsey J A, Walker J A and Welton-Cook M R 1979 *J. Phys. C: Solid State Phys.* **12** 5271
- [21] Netzer F P and Prutton M 1975 *J. Phys. C: Solid State Phys.* **8** 2401
- [22] Kinniburgh C G and Walker J A 1977 *Surf. Sci.* **63** 274
- [23] Welton-Cook and Prutton M 1980 *J. Phys. C: Solid State Phys.* **13** 3993
- [24] Felton R C, Prutton M, Tear S P and Welton-Cook M R 1979 *Surf. Sci.* **88** 474
- [25] Lad R J and Henrich V E 1988 *Phys. Rev. B* **38** 10860
- [26] Bas E B, Bäninger U and Mülethaler H 1974 *Japan. J. Appl. Phys., Suppl.* **2** (part 2) (*Proc. 2nd Int. Conf. on Solid Surfaces* pp 671–3)
- [27] Felton R C, Prutton M and Matthew J A D 1979 *Surf. Sci.* **79** 117
- [28] Henrich V E and Kurtz R L 1981 *Phys. Rev. B* **23** 6280
- [29] Chung Y W, Lo W J and Somorjai G A 1977 *Surf. Sci.* **64** 588
- [30] Onishi H, Aruga T, Egawa C and Iwasawa Y 1988 *Surf. Sci.* **193** 33
- [31] Cox D F, Fryberger T B and Semancik S 1988 *Phys. Rev. B* **38** 2072
- [32] Kurtz R L and Henrich V E 1982 *Phys. Rev. B* **25** 3563
- [33] McKay J M and Henrich V E 1984 *Surf. Sci.* **137** 463
- [34] Kurtz R L and Henrich V E 1987 *Phys. Rev. B* **36** 3413
- [35] Poelman H, Vennik J and Dalmai G 1987 *J. Electron Spectros.* **44** 251
Fiermans L, Clauws P, Lambrecht W, Vandenbroucke L and Vennik J 1980 *Phys. Stat. Sol. A* **59** 485

- [36] van Hove H and Leysen R 1972 *Phys. Stat. Sol. A* **9** 361
- [37] Wandelt K 1982 *Surf. Sci. Rep.* **2** 1
- [38] Winkelmann F, Wohlrab S, Libuda J, Bäumer M, Cappus D, Menges M, Al-Shamery K, Kuhlbeck H and Freund H-J 1994 *Surf. Sci.* **307-9** 1148
- [39] Jaeger R M, Kuhlbeck H, Freund H-J, Wuttig M, Hoffmann W, Franchy R and Ibach H 1991 *Surf. Sci.* **259** 235
- [40] Murray P W, Leible F M, Fischer H J, Flipse C F J, Muryn C A and Thornton G 1992 *Phys. Rev. B* **46** 12877
- [41] Fan F R F and Bard A J 1990 *J. Phys. Chem.* **94** 3761
- [42] Rohrer G S, Henrich V E and Bonnell D A 1990 *Science* **250** 1239
- [43] Rohrer G S and Bonnell D A 1990 *Chemistry of Electronic Ceramic Materials (NIST Special Publication, 804)* (Washington, DC: NIST) p 447
- [44] Rohrer G S, Henrich V E and Bonnell D A 1991 *Mater. Res. Soc. Symp. Proc.* **209** 611
- [45] Beitel G, Markert K, Wiechers J, Hrbek J and Behm R J 1993 *Adsorption on Ordered Surfaces of Ionic Solids and Thin Films (Springer Series in Surface Sciences, vol 33)* ed H-J Freund and E Umbach (Heidelberg: Springer)
- [46] Hochella M F Jr, Eggleston C M, Elings V B, Parks G A, Brown G E Jr, Wu C M and Kjoller K 1989 *Am. Mineralogist* **74** 1233
- [47] Hochella M F Jr 1990 *Rev. Mineral.* **23** 87
- [48] Johnsson P A, Eggleston C M and Hochella M F Jr 1991 *Am. Mineralogist* **76** 1442
- [49] Eggleston C M and Hochella M F Jr 1992 *Am. Mineralogist* **77** 911
- [50] Antonik M D, Edwards L C and Lad R J 1992 *Proc. Mater. Res. Soc.* **237** 459
- [51] Lad R J and Antonik M D 1991 *Ceramic Trans.* **24** 359
- [52] Bonnell D A and Clarke D R 1988 *J. Am. Ceramic Soc.* **71** 629
- [53] Rohrer G S and Bonnell D A 1991 *Surf. Sci.* **247** L195
- [54] Itaya K and Tomita E 1989 *Surf. Sci.* **219** L515
- [55] Wiesendanger R, Shets I V, Bürgler D, Tarrach G, Güntherodt H-J, Coey J M D and Gräser S 1992 *Science* **255** 583
- [56] Tarrach G, Bürgler D, Schaub T, Wiesendanger R and Güntherodt H-J 1993 *Surf. Sci.* **285** 1
- [57] Nelissen B 1993 *PhD Thesis* Catholic University of Nijmegen
- [58] Condon N G, Murray P W, Leible F M, Thornton G, Lemic A R and Vaghan D J 1994 *Surf. Sci.* **310** L609
- [59] Thornton G, private communication
- [60] Lad R J and Henrich V E 1988 *Surf. Sci.* **193** 81
- [61] Weiss W, Barbieri A, van Hove M A and Somorjai G A 1993 *Phys. Rev. Lett.* **71** 1848
- [62] Barbieri A, Weiss W, van Hove M A and Somorjai G A 1994 *Surf. Sci.* **302** 259
- [63] Kuhlbeck H, Odörfer G, Jaeger R, Illing G, Menges M, Mull Th, Freund H-J, Pöhlchen M, Staemmler V, Witzel S, Scharfschwerdt C, Wennemann K, Liedtke T and Neumann M 1991 *Phys. Rev. B* **43** 1969
- [64] Bäumer M, Cappus D, Kuhlbeck H, Freund H-J, Wilhelmi G, Brodde A and Neddermeyer H 1991 *Surf. Sci.* **253** 116
- [65] Bäumer M, Cappus D, Illing G, Kuhlbeck H and Freund H-J 1992 *J. Vac. Sci. Technol. A* **10** 2407
- [66] Kuhlbeck H and Freund H-J 1993 Adsorption and reaction of small molecules on oxide surfaces *Springer Proceedings in Physics* **73** 227
- [67] Uhlenbrock St, Scharfschwerdt Chr, Neumann M, Illing G and Freund H-J 1992 *J. Phys: Condens. Matter* **4** 7973
- [68] Freund H-J, Dillmann B, Ehrlich D, Haßel M, Jaeger R M, Kuhlbeck H, Ventrice C A, Winkelmann F, Wohlrab S, Xu C, Bertrams Th, Brodde A and Neddermeyer H 1993 *J. Mol. Catal.* **82** 143
- [69] Freitag A, Staemmler V, Cappus D, Ventrice C A, Al-Shamery K, Kuhlbeck H and Freund H-J 1993 *Chem. Phys. Lett.* **210** 10
- [70] Rohr F, Wirth K, Libuda J, Cappus D, Bäumer M and Freund H-J 1994 *Surf. Sci. Lett.* **315** 2977
- [71] Cappus D, Haßel M, Neuhaus E, Rohr F and Freund H-J 1995 *Surf. Sci.* **337** 268
- [72] Klinkmann J, Cappus D and Freund H-J 1995 *J. Electr. Spectr. Rel. Phen.* **72** 37
- [73] Cappus D, Klinkmann J, Kuhlbeck H and Freund H-J 1995 *Surf. Sci. Lett.* **325** L421
- [74] Freund H-J *Phys. Stat. Sol.* in press
- [75] Schönnenbeck M, Cappus D, Klinkmann J, Freund H-J, Pettersson L G M and Bagus P S *Surf. Sci.* submitted
- [76] Dalmai-Imelik G, Bertolini J C and Rousseau J 1977 *Surf. Sci.* **63** 67
- [77] Conrad H, Ertl G, Küpper J and Latta E E 1975 *Sol. Stat. Commun.* **17** 497
- [78] Wyckoff R W G 1965 *Crystal Structures* 2nd edn (New York: Wiley Interscience)

- [79] Bertrams Th, Marre K and Neddermeyer H 1995 *Proc. 3rd Surface Science Symp.* ed P Varga (Austria: Kitzsteinhorn)
- [80] Ventrice C A Jr, Hannemann H, Brodde A and Neddermeyer H 1994 *Phys. Rev. B* **49** 5773
- [81] Hannemann H, Ventrice C A, Bertrams Th, Brodde A and Neddermeyer H 1994 *Phys. Stat. Sol. A* **146** 289
- [82] Freitag A and Staemmler V, to be published
Freitag A 1995 *PhD Thesis* University of Bochum
- [83] Fadley C S, private communication
- [84] Weiß W, Boffa A B, Dunphy J C, Galloway H C, Salmeron M B and Somorjai G A 1993 *Adsorption on Ordered Surfaces of Ionic Solids and Thin Films* (Springer Series in Surface Sciences **33**) ed H-J Freund and E Umbach (Heidelberg: Springer)
- [85] Ulnau A 1958 *Am. J. Sci.* **256** 171
- [86] Zabel H 1994 *Appl. Phys. A* **58** 109
Feidenhans'l R 1989 *Surf. Sci. Rep.* **10** 105
- [87] Stierle A, Bödeker P and Zabel H 1995 *Surf. Sci.* **327** 9
- [88] Xu C, Haßel M, Kuhlbeck H and Freund H-J 1991 *Surf. Sci.* **258** 23
- [89] Xu C, Dillmann B, Kuhlbeck H and Freund H-J 1991 *Phys. Rev. Lett.* **67** 3551
- [90] Kuhlbeck H, Xu C, Dillmann B, Haßel M, Adam B, Ehrlich D, Wohlrab S, Freund H-J, Ditzinger U A, Neddermeyer H, Neuber M, Neumann M and Bunsenges Ber 1992 *Phys. Chem.* **96** 15
- [91] Ventrice C A, Ehrlich D, Garfunkel E L, Dillmann B, Heskett D and Freund H-J 1992 *Phys. Rev. B* **46** 12892
- [92] Bender M, Ehrlich D, Yakovkin I N, Rohr F, Bäumer M, Kuhlbeck H, Freund H-J and Staemmler V 1995 *J. Phys: Condens. Matter* **7** 5289
- [93] Haßel M, Hemmerich I, Kuhlbeck H and Freund H-J *Surface Sci. Spectra* submitted
- [94] Rohr F, Bäumer M and Freund H-J, to be published
- [95] Wuttig M, Hoffmann W, Jaeger R, Kuhlbeck H and Freund H-J 1991 *Mat. Res. Soc. Symp. Proc.* **221** 143
- [96] Jaeger R M, Kuhlbeck H and Freund H-J 1993 *Chem. Phys. Lett.* **203** 41
- [97] Jaeger R M, Libuda J, Bäumer M, Homann K, Kuhlbeck H and Freund H-J 1993 *J. Electron Spectrosc. Relat. Phenom.* **64-5** 217
- [98] Libuda J, Bäumer M and Freund H-J 1994 *J. Vac. Sci. Technol. A* **12** 2259
- [99] Libuda J, Winkelmann F, Bäumer M, Freund H-J, Bertrams Th, Neddermeyer H and Müller K 1994 *Surf. Sci.* **318** 61
- [100] Wohlrab S, Winkelmann F, Kuhlbeck H and Freund H-J Adsorption on epitaxial oxide films as model systems for heterogeneous catalysis *Springer Proceedings in Physics* accepted
- [101] Bertrams Th, Winkelmann F, Uttich Th, Freund H-J and Neddermeyer H 1995 *Surf. Sci.* **331-3** 1515
- [102] Libuda J, Sandell A, Bäumer M and Freund H-J 1995 *Chem. Phys. Lett.* **240** 429
- [103] Bäumer M, Libuda J, Sandell A, Winkelmann F, Freund H-J, Graf G, Bertrams Th, Neddermeyer H and Bunsenges Ber *Phys. Chem.* in press
- [104] Sandell A, Libuda J, Brühwiler P, Andersson S, Bäumer M, Maxwell A, Mårtensson N and Freund H-J *J. Vac. Sci. Technol.* accepted
- [105] Sandell A, Libuda J, Brühwiler P, Andersson S, Bäumer M, Maxwell A, Martensson N and Freund H-J *J. Electr. Spectr. Rel. Phen.* accepted
- [106] Sandell A, Libuda J, Bäumer M and Freund H-J *Surf. Sci.* accepted
- [107] Chen P J and Goodman D W 1994 *Surf. Sci. Lett.* **312** L767
- [108] Wu Y, Tao H S, Garfunkel E, Madey T E and Shinn N D 1995 *Surf. Sci.* **336** 123
- [109] Wu Y, Garfunkel E and T E Madey, in preparation
- [110] Isern H and Castro G R 1989 *Surf. Sci.* **211** 865
- [111] Pfnür H, Schwennicke C and Schimmelpfennig J 1993 *Adsorption on Ordered Surfaces of Ionic Solids and Thin Films* (Springer Series in Surface Sciences **33**) ed H-J Freund and E Umbach (Heidelberg: Springer)
- [112] Moffat J B (ed) 1990 *Theoretical Aspects of Heterogeneous Catalysis* (New York: Van Nostrand Reinhold)
- [113] van Santen R A 1991 *Theoretical Heterogeneous Catalysis* (Singapore: World Scientific)
- [114] Desjonquères M C and Spanjaard D 1993 *Concepts in Surface Physics* (Springer Series in Surface Sciences **30**) (Berlin: Springer)
- [115] Yoshida S, Sakaki S and Kobayashi H 1994 *Electronic Processes in Catalysis* (Weinheim: VCH)
- [116] Sauer J 1989 *Chem. Rev.* **89** 199
- [117] Sauer J, Ugliengo P, Garrone E and Saunders V R 1994 *Chem. Rev.* **94** 2095
- [118] Pacchioni G, Bagus P S and Parmigiani F (ed) 1992 *Cluster Models for Surface and Bulk Phenomena (NATO ASI Series, Series B: Physics, vol 283)* (New York: Plenum)

- [119] Menzel D and Rösch N (ed) 1993 Special issue: Molecules at surfaces: Electronic structure and dynamics *Chem. Phys.* **177** (2)
- [120] Bagus P S and Pacchioni G (ed) 1994 Special issue: Cluster approach to the chemistry and physics of surfaces and interfaces *J. Electron Spectrosc. Relat. Phenom.* **69** (1)
- [121] Catlow C R A, Faux I D and Norgett M J 1976 *J. Phys. C: Solid State Phys.* **9** 419
- [122] Catlow C R A and Mackrodt W C 1982 *Computer Simulation of Solids* (Berlin: Springer)
- [123] Allan N L and Mackrodt W C 1987 *Adv. Ceram.* **23** 257
- [124] Catlow C R A, James R, Mackrodt W C and Stewart R F 1982 *Phys. Rev. B* **25** 1006
- [125] Mackrodt W C, Davey R J, Black S N and Docherty R 1987 *J. Cryst. Growth* **80** 441
- [126] Mackrodt W C 1989 *J. Chem. Soc. Faraday Trans.* **85** 541
- [127] Gay D H and Rohl A L 1995 *J. Chem. Soc. Faraday Trans.* **91** 925
- [128] Alavi A and McDonald I R 1990 *Molec. Phys.* **69** 703
- [129] Catlow C R A, Mackrodt W C, Norgett M J and Stoneham A M 1977 *Phil. Mag.* **35** 177
- [130] Lakhlifi A 1993 *Mol. Phys.* **78** 659
- [131] Picaud S, Hoang P N M, Girardet C, Meredith A and Stone A J 1993 *Surf. Sci.* **294** 149
- [132] Chen W and Schaich W L 1989 *Surf. Sci.* **218** 518
- [133] Lakhlifi A and Girardet C 1991 *Surf. Sci.* **241** 400
- [134] Reinhardt P and Heß B A, private communication
- [135] Rittner F, Fink R and Staemmler V, to be published
- [136] Geiger A and Paschek D, private communication
- [137] Pöhlchen M and Staemmler V 1992 *J. Chem. Phys.* **97** 2583
- [138] Staemmler V 1993 *Adsorption on Ordered Surfaces of Ionic Solids and Thin Films* (Springer Series in Surface Sciences **33**) ed H-J Freund and E Umbach (Heidelberg: Springer)
- [139] Nygren M A and Pettersson L G M 1994 *J. Electron Spectrosc. Relat. Phenom.* **69** 43
- [140] Pettersson L G M 1994 *Theor. Chim. Acta* **87** 293
- [141] Pisani C, Dovesi R and Roetti C 1988 *Hartree-Fock ab initio Treatment of Crystalline Solids* (Lecture Notes in Chemistry **48**) (Berlin: Springer)
- [142] Perdew J P and Wang Y 1986 *Phys. Rev. B* **33** 8800
Perdew J P 1986 *Phys. Rev. B* **33** 8822
- [143] Becke A D 1986 *Phys. Rev. A* **33** 2786
- [144] Ziegler T 1991 *Chem. Rev.* **91** 651
- [145] Manghi F, Calandra C and Ossicini S 1994 *Phys. Rev. Lett.* **73** 3129
- [146] Fujimori A, Saitoh T, Mizokawa T and Bocquet A E 1993 *Jap. J. Appl. Phys. Suppl.* **32-3** 217
- [147] Freyria-Fava C, Dovesi R, Sanders V R, Leslie M and Roetti C 1993 *J. Phys: Condens. Matter* **5** 4793
- [148] Pisani C, Cora F, Dovesi R and Orlando R 1994 *J. Electron Spectrosc. Relat. Phenom.* **96** 1
- [149] Fahmi A and Minot C 1994 *Surf. Sci.* **304** 343
- [150] Pacchioni G, Neyman K M and Rösch N 1994 *J. Electron Spectrosc. Relat. Phenom.* **69** 13
- [151] Freitag J and Staemmler V 1994 *J. Electron Spectrosc. Relat. Phenom.* **69** 99
- [152] Zhanpeisov N U, Freitag A and Staemmler V, to be published
- [153] Nygren M A, Pettersson L G M, Freitag A, Staemmler V, Gay D H and Rohl A L *J. Phys. Chem.* accepted for publication
- [154] Causà M, Dovesi R, Pisani C and Roetti C 1986 *Phys. Rev. B* **33** 1308
- [155] Causà M, Dovesi R, Pisani C and Roetti C 1986 *Surf. Sci.* **175** 551
- [156] Rösch N R, Neyman K M and Birkenheuer U 1993 *Adsorption on Ordered Surfaces of Ionic Solids and Thin Films* (Springer Series in Surface Sciences **33**) ed H-J Freund and E Umbach (Heidelberg: Springer)
- [157] Zhanpeisov N U, Pelmenschikov A G and Zhidomirov G M 1990 *Kinet. Catal.* **31** 563
- [158] Fahmi A, Minot C, Silvi B and M Causà 1993 *Phys. Rev. B* **47** 11717
- [159] Kobayashi H and Yamaguchi M 1989 *Surf. Sci.* **214** 466
- [160] Groh D J, Pandey R and J M Recio 1994 *Phys. Rev. B* **50** 14860
- [161] Janssen G J M and Nieuwpoort W C 1988 *Phys. Rev. B* **38** 3449
- [162] Boussard P, Siegbahn P E M and Wahlgren U 1993 *Adsorption on Ordered Surfaces of Ionic Solids and Thin Films* (Springer Series in Surface Sciences **33**) ed H-J Freund and E Umbach (Heidelberg: Springer)
- [163] Bagus P S, Pacchioni G and Parmigiani F 1993 *Chem. Phys. Lett.* **207** 569
- [164] Klüner T, Freund H-J, Freitag J and Staemmler V, to be published
- [165] Fujimori A, Minami F and Sugano S 1984 *Phys. Rev. B* **29** 5225
- [166] Fujimori A and F Minami 1984 *Phys. Rev. B* **30** 957
- [167] Janssen G J M and Nieuwpoort W C 1988 *Int. J. Quantum Chem. Symp.* **22** 679
- [168] Pacchioni G, Cogliandro G and Bagus P S 1991 *Surf. Sci.* **255** 344

- [169] Pacchioni G and Bagus P S 1992 *Cluster Models for Surface and Bulk Phenomena (NATO ASI Series, Series B: Physics, vol 283)* ed G Pacchioni, P S Bagus and F Parmigiani (New York: Plenum) p 305
- [170] Pacchioni G, Cogliandro G and Bagus P S 1992 *Int. J. Quantum Chem.* **42** 1115
- [171] Blyholder G 1964 *J. Phys. Chem.* **68** 2772
- [172] He J-W, Estrada C A, Corneille J S, Wu M-C and Goodman D W 1992 *Surf. Sci.* **261** 164
- [173] Zhanpeisov N U, Staemmler V and Bearn M 1995 *J. Mol. Catal. A: Chem.* **101** 51
- [174] Bredow T and Jug K 1995 *J. Phys. Chem.* **99** 285
- [175] Barandiarán Z and Seijo L 1988 *J. Chem. Phys.* **89** 5739
- [176] Seijo L and Barandiarán Z 1991 *J. Chem. Phys.* **94** 8158
- [177] Nygren M A, Pettersson L G M, Barandiarán Z and Seijo L 1994 *J. Chem. Phys.* **100** 2010
- [178] Mejias J A and Sanz J F 1995 *J. Chem. Phys.* **102** 327
- [179] Mejias J A, Oviedo J and Sanz J F 1995 *Chem. Phys.* **191** 133
- [180] Shen Z-X, Shi C K, Jepsen O, Spicer W E, Lindau I and Allen J W 1990 *Phys. Rev. Lett.* **64** 2442
- [181] Brooks N B, Law D S, Warburton D R, Wincott P L and Thornton G 1989 *J. Phys: Condens. Matter* **1** 4267
- [182] Hüfner S, Steiner P, Sander I, Neumann M and Witzel S 1991 *Z. Phys. B* **83** 185
Hüfner S and Wertheim G 1973 *Phys. Rev. B* **8** 4857
- [183] Hüfner S, Hullinger F, Osterwalder J and Riesterer T 1984 *Solid State Commun.* **50** 83
- [184] Lundquist B I 1967 *Phys. Kond. Mat.* **6** 193, 203; 1968 **7** 117; 1969 **9** 2236
- [185] Freund H-J, Eberhardt W, Heskett D and Plummer E W 1983 *Phys. Rev. Lett.* **50** 768
- [186] Kevan S D (ed) 1992 *Studies in Surface Science and Catalysis (Angle Resolved Photoemission, vol 74)* (Amsterdam: Elsevier) ch 4, 5
- [187] Cox P A and Williams A A 1985 *Surf. Sci.* **152-3** 791
- [188] Kemp J P, Davies S T P and Cox P A 1989 *J. Phys: Condens. Matter* **1** 5313
- [189] Fromme B, Schmitt M, Kisker E, Gorschlüter A and Merz H 1994 *Phys. Rev B* **50** 1874
- [190] Wu M-C and Möller P J 1990 *Surf. Sci.* **235** 228
- [191] Gorschlüter A and Merz H 1994 *Phys. Rev. B* **49** 17293
- [192] Mohamed M H, Sadeghi H R and Henrich V E 1988 *Phys. Rev. B* **37** 8417
- [193] Göpel W, Anderson J A, Frankel D, Jaehnic M, Phillips K, Schäfer J A and Rucker G 1984 *Surf. Sci.* **139** 333
- [194] Newman R and Chrenko R M 1959 *Phys. Rev.* **114** 1507
Powell R J 1967 *Stanford Electronics Laboratory Report* No 5220-1 (unpublished)
Adler D and Feinleib J 1970 *Phys. Rev. B* **2** 3112
- [195] Propach V, Reinen D, Drenkhahn H and Müller-Buschbaum H 1978 *Z. Naturforsch. B* **33** 619
- [196] Woodruff D P and Bradshaw A M 1994 *Rep. Prog. Phys.* **57** 1029
- [197] Haßel M, Kühlenbeck H, Freund H-J, Shi S, Freitag A, Staemmler V, Lütkehoff S and Neumann M 1995 *Chem. Phys. Lett.* **240** 205
Shi S and Staemmler V *Phys. Rev. B*, accepted for publication
- [198] Pratt G W Jr and Coelho R 1959 *Phys. Rev.* **166** 281
- [199] Wu M-C, Estrada C A and Goodman D W 1991 *Phys. Rev. Lett.* **67** L910
Wu M-C, Truong Ch and Goodman D W 1993 *Adsorption on Ordered Surfaces of Ionic Solids and Thin Films* (Springer Series in Surface Science **33**) ed H-J Freund and E Umbach (Heidelberg: Springer)
- [200] Hollas J M 1982 *High Resolution Spectroscopy* (London: Butterworth)
- [201] Cappus D, Xu C, Ehrlich D, Dillmann B, Ventrice C A, Al-Shamery K, Kühlenbeck H and Freund H-J 1993 *Chem. Phys.* **177** 533
- [202] Vureno G A, Salmeron M B and Somorjai G A 1988 *Surf. Sci.* **201** 129
- [203] Kim Y-J and Fadley C S, private communication
- [204] Rohr F *PhD thesis* Ruhr-Universität Bochum, in preparation
Wirth K 1993 *Diploma thesis* Ruhr-Universität Bochum
- [205] Egersdörfer B and Papp H, private communication
- [206] Ignatiev A, Lee B W and VanHove M A 1977 *Proc. 7th Int. Vac. Congr. and 3rd Int. Conf. Sol. Surf. (Vienna, 1977)* p 1733
- [207] Mays R B and Roberts M W 1977 *J. Catal.* **49** 216
- [208] Haßel M 1995 *PhD thesis* Ruhr-Universität Bochum
- [209] Neuhaus E 1994 *Diploma thesis* Ruhr-Universität Bochum
- [210] Pignocco A J and Pellisier G E 1967 *Surf. Sci.* **7** 261
- [211] Leygraf C and Ekelund S 1973 *Surf. Sci.* **40** 609
- [212] Langell M and Somorjai G A 1982 *J. Vac. Sci. Technol.* **21** 858

- [213] Masuda S, Harada Y, Kato H, Yagi K, Kometa T, Miyano T, Onchi M and Sakisaka Y 1988 *Phys. Rev. B* **37** 8088
- [214] Smentkowski V S and Yates J T Jr 1990 *Surf. Sci.* **232** 113
- [215] Portele F 1969 *Z. Naturforsch. A* **24** 1268
- [216] Pirug G, Broden G and Bonzel H P 1980 *Surf. Sci.* **94** 323
- [217] Brundle C R 1978 *IBM J. Rev. Develop.* **22** 235
- [218] Muan A 1958 *Am. J. Sci.* **256** 171
- [219] Migano T, Sakisata Y, Komeda T and Onchi M 1986 *Surf. Sci.* **169** 197
- [220] Haßel M 1991 *Diploma thesis* Ruhr-Universität Bochum
- [221] Al-Shamery K, Beauport I, Freund H-J and Zacharias H 1994 *Chem. Phys. Lett.* **222** 107
- [222] Kennett H M and Lee A E 1972 *Surf. Sci.* **33** 377
- [223] Michel P and Jardin C 1973 *Surf. Sci.* **36** 478
- [224] Ekelund S and Leygraf C 1973 *Surf. Sci.* **40** 179
- [225] Foster L S 1990 *Chem. Rev.* **90** 331
- [226] Allos T I Y, Birss R R, Parker M R, Ellis E and Johnson D W 1977 *Solid State Commun.* **24** 129
- [227] Schawlow A L, Wood D L and Clogston A M 1959 *Phys. Rev. Lett.* **3** 271
- [228] Kühlenbeck H 1994 *Appl. Phys. A* **59** 469
- [229] Samuelsen E J, Hutchings M T and Shirane G 1970 *Physica* **48** 13
- [230] Riesen H and Güdel H U 1987 *Mol. Phys.* **60** 1221
- [231] Pacchioni G, Minerva T and Bagus P S 1992 *Surf. Sci.* **275** 450
- [232] Pacchioni G 1993 *Surf. Sci.* **281** 257
- [233] Pacchioni G and Bagus P S 1993 *Adsorption on Ordered Surfaces of Ionic Solids and Thin Films* (Springer Series in Surface Science **33**) ed H-J Freund and E Umbach (Heidelberg: Springer)
- [234] Neyman K M and Rösch N 1992 *J. Chem. Phys.* **168** 267; 1993 *Surf. Sci.* **297** 223; 1993 *Chem. Phys.* **177** 561
- [235] Pisani C, Dovesi R, Nada R and Tamiro S 1989 *Surf. Sci.* **216** 267
- [236] Zaki M I and Knözinger H 1989 *J. Catal.* **119** 311
Little L H 1966 *Infrared Spectra of Adsorbed Species* (London: Academic) p 84
- [237] Haßel M and Freund H-J 1995 *Surf. Sci.* **325** 163
- [238] Xu C and Goodman D W *Handbook of Heterogenous Catalysis* ed G Ertl, H Knözinger and J Wertkamp (Weinheim: Verlag Chemie) ch 4.6 (in press)
- [239] Sandos H E, Gardner P, King D A and Morris M A 1994 *Surf. Sci.* **304** 159
- [240] Yoshinobu J, Ballinger T H, Xu Z, Jänsch H J, Zaki M I, Xu J and Yates J T Jr 1991 *Surf. Sci.* **255** 295
- [241] Vesecky S M, Xu X and Goodman D W 1994 *J. Vac. Sci. Technol. A* **12** 2114
Wu M C, Truong C M and Goodman D W 1993 *J. Phys. Chem.* **97** 4182
Truong C M, Wu M C and Goodman D W 1993 *J. Am. Soc.* **115** 3647
He J W, Corneille J S, Estrada C A, Wu M C and Goodman D W 1992 *J. Vac. Sci. Technol. A* **10** 2248
Wu M C, Estrada C A, Corneille J S and Goodman D W 1992 *J. Chem. Phys.* **96** 3892
- [242] Henzler M, Stock A and Böhl M 1993 *Adsorption on Ordered Surfaces of Ionic Solids and Thin Films* (Springer Series in Surface Science **33**) ed H-J Freund and E Umbach (Heidelberg: Springer)
- [243] Heidberg J, Cabigon L, Kampshoff E, Kandel M, Kühnemuth R, Meine D, Redlich B, Schönekas O, Suhren M, Weiss H and Wetter D 1993 *Adsorption on Ordered Surfaces of Ionic Solids and Thin Films* (Springer Series in Surface Science **33**) ed H-J Freund and E Umbach (Heidelberg: Springer)
- [244] Weiß H 1995 *Habilitationsschrift* University of Hannover, unpublished
- [245] Heidberg J, Meine D and Bunsenges Ber 1993 *Phys. Chem.* **97** 211
- [246] Zecchina A, Scarano D, Bordiga S, Ricchiardi G, Spoto G and Geobaldo F IR-Studies of CO and NO adsorbed on well characterized oxide single microcrystals, to be published
- [247] Marchese L, Coluccia S, Martra G and Zecchina A 1992 *Surf. Sci.* **269** 135
- [248] Escalona Platero E, Coluccia S and Zecchina A 1985 *Langmuir* **1** 407
- [249] Escalona Platero E, Coluccia S and Zecchina A 1986 *Surf. Sci.* **171** 465
- [250] Escalona Platero E, Fubini B and Zecchina A 1987 *Surf. Sci.* **179** 404
- [251] Freund H-J and Neumann M 1988 *Appl. Phys. A* **47** 3
- [252] Blyholder G 1974 *J. Vac. Sci. Technol.* **11** 865
- [253] Stöhr J 1992 *NEXAFS Spectroscopy* (Springer Series in Surface Sciences **25**) (Berlin: Springer)
- [254] Fink K and Staemmler V, to be published
Pacchioni G and Bagus P S, private communication
- [255] Schmeisser D, Greuter F, Plummer E W and Freund H-J 1985 *Phys. Rev. Lett.* **54** 2095
- [256] Jacobi C, Astaldi C, Geng P and Bertolo M 1989 *Surf. Sci.* **223** 569

- [257] Lassetre E N 1969 *Canad. J. Chem.* **47** 1733
- [258] Huber K P and Herzberg G 1979 *Molecular Spectra and Molecular Structure, IV: Constants of Diatomic Molecules* (New York: Van Nostrand Reinhold)
- [259] Homann K, Jaeger R M and Kuhlbeck H 1993 *J. Electr. Spectrosc. Rel. Phen.* **62** 273
- [260] Wu M C, Møller P J 1989 *Surf. Sci.* **221** 250
Møller P J and Wu M C 1989 *Surf. Sci.* **224** 265
Wu M C and Møller P J 1990 *Surf. Sci.* **235** 228
- [261] Wu M C and Møller P J 1991 *The Structure of Surfaces III* ed S Y Tong, M A van Hove, K Takayanagi and X D Xider (Berlin: Springer) p 652
- [262] Wu M C and Møller P J 1990 *Surf. Sci.* **250** 179
- [263] Guo Q and Møller P J 1990 *Vacuum* **41** 1114
Møller P J and Guo Q 1991 *Thin Sol. Films* **201** 267
- [264] Møller P J and Nerlov J 1993 *Surf. Sci.* **307-9** 591
- [265] Ge O and Møller P J *Appl. Surf. Sci.* **82-3** 305
- [266] Guo Q and Møller P J *Surf. Sci. Lett.* in press
- [267] Ludviksson A, Ernst K H, Zhang R and Campbell C T 1993 *J. Catal.* **141** 380
- [268] Ernst K H, Ludviksson A, Zhang R and Campbell C T 1993 *Phys. Rev. B* **47** 13782
- [269] Altman E I and Gorte R J 1988 *Surf. Sci.* **195** 392; 1988 *J. Catal.* **113** 185
- [270] Cordatas H, Buulnesin T and Gorte R J 1995 *Surf. Sci.* **323** 219
- [271] Altman E I and Gorte R J 1989 *Surf. Sci.* **216** 386
- [272] Pan J-M, Maschhoff B L, Diebold U and Madey T E 1993 *Surf. Sci.* **291** 381
- [273] Diebold U, Pan J-M and Madey T E 1993 *Phys. Rev. B* **47** 3868
- [274] Pan J-M and Madey T E 1993 *J. Vac. Sci. Technol. A* **11** 1667
- [275] Steinrück H-P, Pesty F, Zhang L and Madey T E 1995 *Phys. Rev. B* **51** 2427
- [276] Duviez C, Henry C R and Chapon C 1991 *Surf. Sci.* **253** 190
- [277] Henry C R, Chapon C, Duriez C and Giorgio S 1991 *Surf. Sci.* **253** 177
- [278] Henry C R, Chapon C, Goyhenex C and Monot R 1992 *Surf. Sci.* **272** 283
- [279] Légaré P and Bilwes B R 1992 *Surf. Sci.* **279** 159
- [280] Légaré P, Finck F, Roche R and Maire G 1989 *Z. Phys. D* **12** 19
- [281] Gillet E and Matolin V 1991 *Z. Phys. D* **19** 361
- [282] Ealet B and Gillet E 1993 *Surf. Sci.* **281** 91
- [283] Ogawa S and Ichikawa S 1995 *Phys. Rev. B* **51** 17231
- [284] Gota S, Gantier M, Donillard L, Thromat N, Durand J P and Le Févre P 1995 *Surf. Sci.* **323** 163
- [285] Bender M, Al-Shamery K and Freund H-J 1994 *Langmuir* **10** 3081
- [286] Ehrlich D, Bender M, Yakovkin I and Freund H-J, to be published
Ehrlich D 1995 *PhD thesis* Ruhr-Universität Bochum
- [287] Kittel C 1971 *Introduction to Solid State Physics* 4th edn (New York: Wiley)
- [288] Raether H 1965 *Ergebnisse der exakten Naturwissenschaften* **38** 84